Control of Power Electronic Interfaces for Photovoltaic Power Systems

Kazi Nazmul Hasan

B. Sc. in Electrical and Electronic Engineering,
Bangladesh University of Engineering and Technology, 2006

A thesis submitted in fulfillment of the
requirements for the Degree of

Master of Engineering Science (Research)

School of Engineering

University of Tasmania

August, 2009

Statement of Originality and Authority of Access

I hereby declare that this thesis is my own original work. It contains, to the best of my knowledge, no material previously published or written by another person. There is also no material which has been accepted for the award of any other degree or diploma of a university or other institute of higher education, except where due acknowledgment is made in the text.

This thesis may be made available for loan. Copying of any part of this thesis is prohibited for two years from the date this statement was signed; after that limited copying is permitted in accordance with *the Copyright Act 1968.*

Nazmul 26/08/2009

Kazi Nazmul Hasan

Acknowledgments

I wish to express my deepest gratitude to my supervisors Dr. Md. Enamul Haque, Prof. Michael Negnevitsky, and A/Prof. Kashem M. Muttaqi, who supported me throughout the project. I would like to thank them for their understanding, valuable guidance, and encouragement during the difficult time of my studies.

I am grateful to the Graduate Research Unit, and School of Engineering, University of Tasmania, for providing me the graduate research scholarship during my postgraduate studies. I also would like to thank Prof. Chris Letchford, Head of School of Engineering, for his support.

Many thanks are due to all the academic staff and postgraduate students who make a friendly and helpful academic environment.

I wish to acknowledge the contribution of technical staff Mr. Steve Avery, Mr. Bernard Chenery and Mr. Hayden Honeywood for their support during my experimental work.

I would like to thank English*Assist* staff Mrs. Louise Oxley and Ms. Morag Porteous for their valuable assistance regarding English language skills and Australian academic culture.

I also express my sincere gratitude to my parents, Mr. Kazi Abul Hashem and Mrs. Aysha Akter, who are the ultimate source of my inspiration. They show me the way of life. Many thanks are also due to my sister Ms. Siddiqua Akter Shimul for her support and encouragement during my studies.

Abstract

This thesis deals with the control of power electronic interfaces for photovoltaic applications. The main objective is to develop and employ effective control algorithms and topologies that are optimally suited for photovoltaic power conversion systems. The studies, comprising of analysis, modeling, control and experimental evaluation, clearly enhance overall system performance. The major items of investigation in this thesis are power electronic converter design and modeling, current mode control, maximum power point tracking techniques, and control for energy storage systems.

The nonlinear and time varying characteristics of both the photovoltaic module and switch-mode power converters cause problems in photovoltaic systems control. The weather dependency of photovoltaic system makes these problems even more severe. As the photovoltaic source usually acts as a current source, this thesis proposes current mode control methods as a suitable control solution in photovoltaic power systems. The thesis proposes an improved algorithm, based on current mode control, to ensure an accurate tracking of the maximum power point of the photovoltaic module. In addition, four current mode control methods are investigated for the dc-dc converter controller to obtain a stable dc bus voltage. The results obtained are compared with the voltage mode control. Finally, a new control algorithm is proposed for charging and discharging of the photovoltaic battery storage system, which allows versatile power transfer among the photovoltaic source, battery and load.

Extensive simulation studies were performed based on MATLAB/Simulink/ Simpower to verify the control methods of the maximum power point tracking, dc-dc converter control and energy storage interface for a 3 KW photovoltaic power system. The current mode control methods have shown significant improvement in different aspects of the power quality, especially in case of input changes, load variations, transient responses and harmonics. A dSPACE DS1104 DSP (digital signal processor) hardware and software system was used in a prototype experimental evaluation to validate the improved performances of the current mode control of dc-dc converter for photovoltaic systems.

Contents

List of Figures

List of Tables

Chapter 1
Introduction

1.1 General

The demand for energy will continue to increase to keep pace with the advancements and living standards of the increasing human population. Conventional fossil fuel based energy sources can meet the future demand. However, they produce pollutant gases and have adverse effects on the environment. Therefore, the challenge lies in providing the additional energy from pollution free renewable energy sources while showing esteem for the environment. It is obvious that renewable power generation by itself cannot be a viable solution to the world power crisis. However, renewable based energy sources can support conventional fossil fuel based generation to mitigate the power problems as well as to reduce the environmental pollutions.

Recently, the interest in photovoltaic power systems is increasing worldwide, due to the devastating effect of climate changes, and climate friendly policies. The availability of free solar radiation and subsidised strategies also enhances the implementation of extensive use of photovoltaic solar power systems. Hence, photovoltaic power generation is experiencing an exponential growth because of its significant potential as a sustainable energy source. Fig. 1.1 shows the global annual photovoltaic installations from the year 1997 to 2007 [1]. Fig 1.2 shows the lessening amount of greenhouse gasses under the current photovoltaic power generation scenario [1]. However, one of the major concerns about the photovoltaic power system is its higher implementation cost. Nevertheless, the advancement of technology and extensive use of photovoltaic power can make this technology competitive with the fossil fuel based utility prices. Fig. 1.3 shows a comparative scenario of the utility prices and photovoltaic power costs [1].

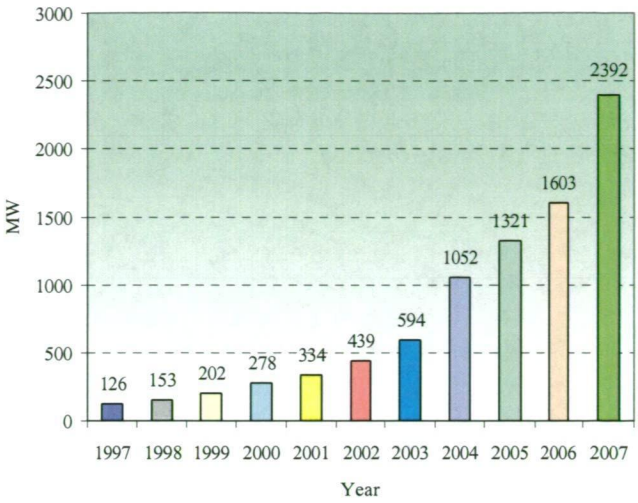

Fig. 1.1 Global annual photovoltaic power generation.

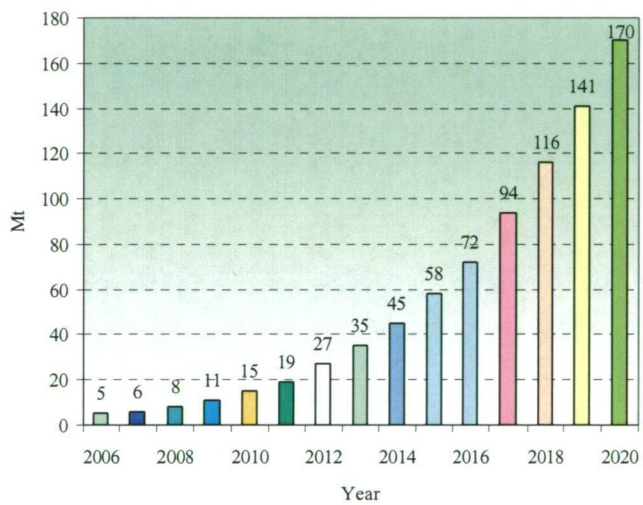

Fig. 1.2 Estimation of lessening CO_2 emission under current photovoltaic power generation scenario.

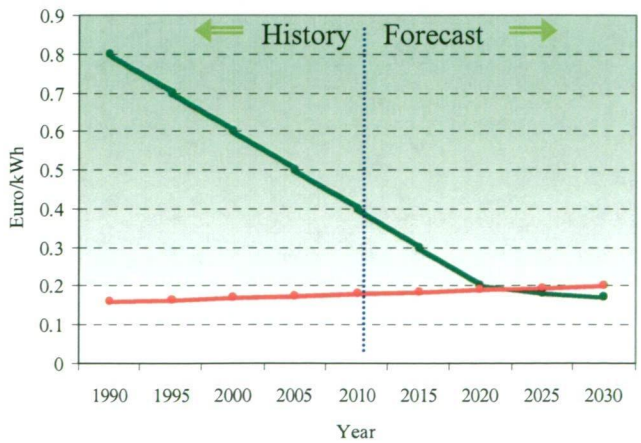

Fig. 1.3 Past and present trends of utility prices and photovoltaic power costs.

The low efficiency and irregular nature of the photovoltaic power system is the main hindrance to implementing this technology widely. That is why the efficiency increment of the renewable photovoltaic power system is now a pressing topic of research. There are several ways to increase the efficiency of the photovoltaic power systems, which include the improvement of solar cells themselves, maximum power point extraction strategies, alternative converter topologies, and employment of efficient control algorithms.

1.2 Photovoltaic Power Systems Technology

1.2.1 Electricity from Photovoltaic Module

A photovoltaic solar cell is a device which directly converts sunlight into electricity. The basic component of a photovoltaic module is the p-n junction of the semiconductor materials, which generate electricity when exposed to illumination. The materials used for photovoltaic cells are mono-crystalline silicon, multi-crystalline silicon and thin film [2]. When the photons of sunlight hit the photovoltaic cells, the electrons are knocked loose from their atoms, allowing them to flow through the materials to produce electricity. Consequently, the sunlight radiating on the photovoltaic module produces both a current and a voltage to generate electric power. The particular composition of n-type and p-type semiconductor materials in the photovoltaic solar cells produces dc power. Fig. 1.4 shows a simple demonstration of electric power generation from a photovoltaic solar cell.

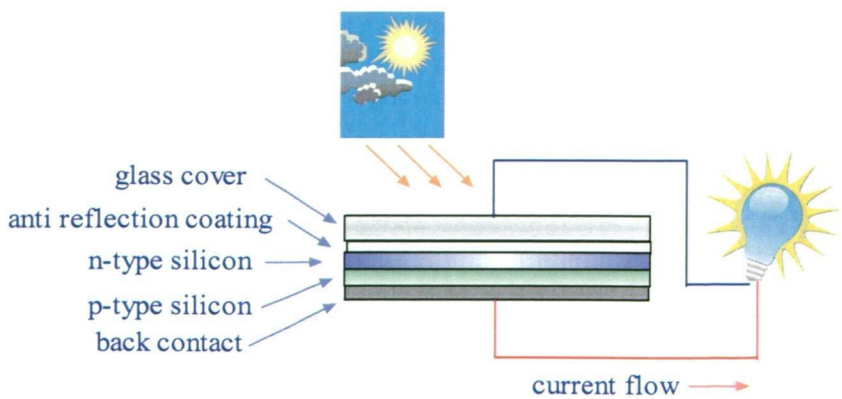

Fig. 1.4 Generation of electricity from photovoltaic module.

1.2.2 Photovoltaic Power Systems

A photovoltaic power system generally consists of photovoltaic modules and power conversion circuitry. Fig. 1.5 shows a typical photovoltaic power system. The photovoltaic module is responsible for converting the sunlight into electricity. Then the obtained solar power is processed through the power conversion circuitry. As the photovoltaic module delivers unregulated dc power, the power is then regulated using a dc-dc conversion stage. After that, the power is processed by a dc-ac conversion (inverter) stage to feed the ac loads.

Photovoltaic power systems can be categorized as small, intermediate, and large, based on the system capacity [3]. The recommended classification for small systems is 10 kW or less; intermediate systems ranges from over 10 kW up to 500 kW; and the capacity of the large systems is greater than 500 kW.

Photovoltaic power systems can work as stand-alone or grid connected systems. Stand-alone operations are viable for remote dwellings, remote sensing, satellites, spacecrafts and temporary traffic signs. A stand-alone, also known as off-grid, photovoltaic power system usually requires a storage battery. On the other hand, a grid connected photovoltaic power system usually delivers power to the grid when extra photovoltaic power generation occurs. Conversely, it takes power from the grid during low photovoltaic power generation. Nowadays photovoltaic power systems are also used as a part of a hybrid power system with wind, diesel or fuel cells.

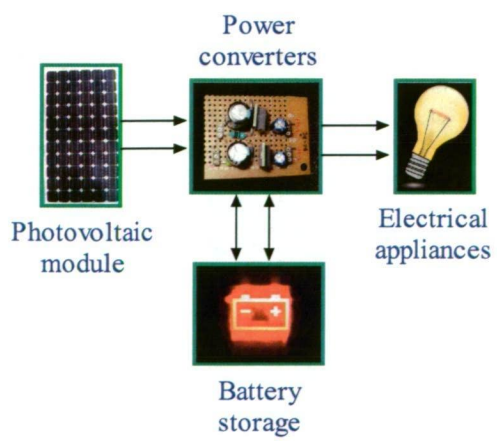

Fig. 1.5 A typical stand-alone photovoltaic power system.

1.3 Power Electronic Interfaces and Control Techniques

1.3.1 Power Converters

The efficiency and effectiveness of photovoltaic power systems mainly depends on the power electronic interfaces and control techniques. The raw power obtained from the photovoltaic module is regulated by a dc-dc converter. As the PV module voltage is usually below the utility-standard level (240V AC), the dc-dc conversion systems also need to boost the voltage level. Several alternatives are available for the dc-dc conversion interface for photovoltaic systems. Buck [4], boost [5], buck-boost [6-8], SEPIC and Cuk [9], full bridge [10], series resonant [11], push-pull [12], and flyback [13] converters are investigated in the literature. Fig. 1.6 shows a boost converter topology which is most commonly used for photovoltaic power processing.

A bidirectional converter is usually used, after the dc-dc conversion stage, to charge and discharge the battery in a stand-alone system. The voltage levels of the battery banks are usually lower then that of the dc bus, so the buck-boost operation is preferable for bidirectional converters. Hence, a bidirectional converter operates in buck mode during battery charging, and in boost mode during discharging. There are different topologies of bidirectional converters, including series buck-boost, parallel buck-boost and Cuk for battery charging and discharging [14-19].

Finally, to make the photovoltaic power usable for ac electrical appliances, an inverter stage is used along with the filters. The filters are responsible for providing a good quality of power.

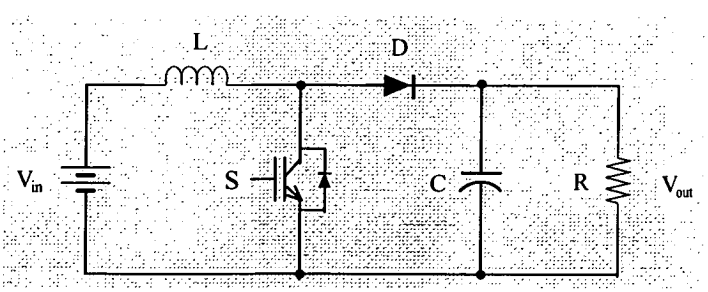

Fig. 1.6 A boost converter is mostly used in photovoltaic power processing.

1.3.2 Control Techniques

Control algorithms are the governing elements for the regulation, protection and management of the energy produced by the photovoltaic module. Proper implementation of a controller is essential in every stage of power processing and conversion of photovoltaic power systems. Different control algorithms are employed separately or jointly for maximum power point tracking, dc-dc converter control, bidirectional converter control and inverter control.

The maximum power point tracking technique is one of the fundamental concerns in photovoltaic power system. Performance of photovoltaic power systems greatly depends on the control of the maximum power point tracking techniques. Control of the maximum power point tracking techniques is also affected by environmental parameters such as temperature and irradiance.

Power converters such as dc-dc converters and dc-ac converters (i.e. inverters) are a vital part of solar power systems. These components ensure the quality of power, maximum efficiency and overall safety of the system. Moreover, the quality of the power produced by the photovoltaic power system must maintain certain standards [3], including voltage level, frequency, harmonics and power factor. A diverse range of voltage mode control and current mode control techniques is available to control the converter and inverter circuitry to enhance the efficiency and reliability of the systems. Fig. 1.7 shows a simple control-architecture for photovoltaic power systems.

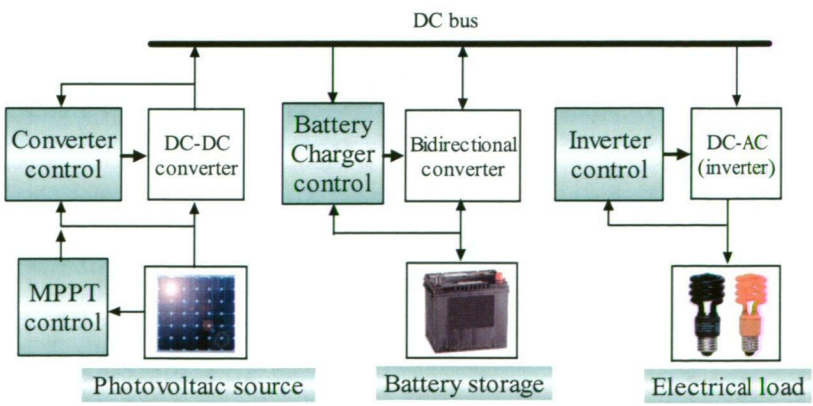

Fig. 1.7 Control of power electronic interfaces for photovoltaic power systems.

Moreover, battery back-up facilities are necessary for stand-alone PV systems, as well as, in some cases, for utility interactive systems. In battery storage systems, selection of charger characteristics and associated controls for different types of energy storage systems are important issues.

Digital Signal Processing (DSP) is one of the appropriate processors for PV systems. Control of maximum power point tracking, power converters, and the battery charger can be done with DSP hardware and software. Moreover, DSP is popular for its noise free signals, high speed, and precise real time signal processing.

1.4 Research Motivation and Objective

Renewable photovoltaic power systems are continually being improved to achieve higher efficiency and lower cost. The power electronic interfaces and control techniques can contribute a lot to make the photovoltaic power system cheaper and more efficient. The integration, interaction and matching of different components of the photovoltaic power system are also important for the optimum performance of the system.

The purpose of this study is to improve the control of the power electronic interfaces of photovoltaic power systems in order to optimize the performance of the overall system. The main idea of the project is to implement efficient controllers at the different power processing stages of the photovoltaic solar power system. Three different controllers are implemented at the different stages, these are, an MPPT controller, a dc-dc converter controller and a bidirectional converter controller.

The maximum power point tracking technique always ensures the extraction of the highest available power from the photovoltaic modules. As the photovoltaic module is operated as a current source, current control techniques are used to control the dc-dc converter. The four most popular current control techniques are also examined as the dc-dc converter controller. A newly developed control strategy is implemented as the bidirectional converter controller to ensure versatile power transfer among the PV source, the battery and the load.

The contributions of this thesis are:

- Development of a complete MATLAB/Simulink/Simpower based simulation model for a typical photovoltaic power system.
- Software implementation of an improved maximum power point tracking technique with current mode control.
- Application of current mode control methods as a suitable control solution in photovoltaic power systems.
- Implementation of a new control algorithm for the control of energy storage interface with a bidirectional converter for photovoltaic systems.
- Experimental investigation of the current mode control method as the dc-dc converter controller with dSPACE DS1104 DSP (digital signal processor) controller.

1.5 Thesis Outline

The current chapter first describes the prospects and technologies of photovoltaic power systems. The basics and importance of power electronic interfaces and control techniques for photovoltaic applications are discussed briefly. This is followed by an outline of the goals and contributions of the thesis.

Chapter 2 presents an improved maximum power point tracking technique for the photovoltaic module. Some popular maximum power point tracking techniques are reviewed first. Then, some fundamental limitations of the maximum power point tracking techniques are identified, followed by considerations of the design and control parameters of the maximum power point trackers. An improved maximum power point tracking technique with current mode control is analysed, and implemented in the MATLAB/Simulink/Simpower software system. Optimum tuning of the perturbation step size, switching frequency and sampling rates are performed in the software model.

Chapter 3 describes the current mode control of the switch-mode dc-dc converter to obtain a regulated dc output voltage. Control strategies for the dc-dc converter controllers are reviewed. Four current mode control methods are discussed. The

transfer function of the boost dc-dc converter and the core idea of current mode control are analysed. Finally, voltage mode control and four current mode control techniques are implemented in the MATLAB/Simulink/Simpower software system. Simulation results are provided, considering the effects of control algorithms, dynamic performances, input variations, load changes, external disturbances and inverter harmonics. A comparative assessment of the different control methods is also provided.

Chapter 4 proposes a control algorithm for battery storage in photovoltaic power systems. An overview of the photovoltaic energy storage is presented, including storage options, system architecture, converter topologies and control techniques. The design considerations of battery storage for photovoltaic applications are discussed. A new control algorithm is analysed, and the simulation results are presented. The control algorithm ensures the power transfer among the photovoltaic module, battery and the load.

Chapter 5 presents the experimental results of the DSP based converter controller within the prototype photovoltaic power systems. A dSPACE DS1104 hardware and controller board is used for controller implementation. The experimental results confirm the viability of the current mode control methods as a suitable solution for photovoltaic applications.

Finally, conclusions and future research directions are given in chapter 6.

1.6 Supporting Publications

This research has produced the following refereed conference publications:

[1]. K. N. Hasan, M. E. Haque, M. Negnevitsky and K. M. Muttaqi, "Output Quality Evaluation of Photovoltaic Systems with Different Current Control Methods of Switch-Mode Converters", International Conference on Harmonics and Quality of Power (ICHQP'08), University of Wollongong, NSW, Australia, 28th Sep. – 1st Oct., 2008.

[2]. K. N. Hasan, M. E. Haque, M. Negnevitsky and K. M. Muttaqi, "Performance Analysis of VMC and CMCs of Switch-Mode Converters for Photovoltaic Applications", IEEE Industrial Electronics Society Conference (IECON'08), Orlando, Florida, USA, 10^{th} – 13^{th} Nov., 2008.

[3]. K. N. Hasan, M. E. Haque, M. Negnevitsky and K. M. Muttaqi, "Control of Energy Storage Interface with a Bidirectional Converter for Photovoltaic Systems", Australasian Universities Power Engineering Conference (AUPEC'08), University of New South Wales, Sydney, Australia, 14^{th} – 17^{th} Dec., 2008.

[4]. K. N. Hasan, M. E. Haque, M. Negnevitsky and K. M. Muttaqi, "An Improved Maximum Power Point Tracking Technique of the Photovoltaic Module with Current Mode Control", Australasian Universities Power Engineering Conference (AUPEC'09), University of Adelaide, Adelaide, Australia, 27^{th} – 30^{th} Sep., 2009.

Chapter 2

Maximum Power Point Tracking of the Photovoltaic Module

2.1 Introduction

The power generated by a photovoltaic (PV) module depends on several factors such as such as solar insolation levels, temperature, shading conditions, PV cell aging and load conditions. Therefore, a solar panel is typically rated at an insolation level together with a specified temperature, such as 1000 W/m^2 at 25^0 C. The electrical power output of the photovoltaic module usually increases linearly with the insolation. Moreover, the PV module has a single operating point, where the values of the current and voltage of the cell result in a maximum power output. Fig. 2.1 shows the exponential relationship between current and voltage of the PV module, where the maximum power point (MPP) occurs at the knee of the curve. Hence, a control strategy is required to extract maximum power from the PV module.

There are several maximum power point tracking (MPPT) methods proposed in the literature [20-34], which are discussed in detail in the next section. Each of these methods has its own advantages and limitations. Generally, MPPT techniques use the power feedback method, which measures the PV module power and uses it as the feedback variable. In most cases, dc-dc converters or dc-ac inverters or both are used as power interfaces between the PV modules and electrical loads. The switching duty-cycle of these converters is the control variable of maximum power point (MPP) trackers. As the performance of the MPPT schemes is dependent on several parameters, constantly tracking the MPP is difficult. Moreover, the adjustment of the MPPT methods with the dynamic behaviour of the specific converter affects the performance of the MPPT techniques.

A version of this chapter has been accepted for publication. K. N. Hasan, M. E. Haque, M. Negnevitsky, and K. M. Muttaqi, "An Improved Maximum Power Point Tracking Technique of the Photovoltaic Module with Current Mode Control", AUPEC, Sept. 2009, Adelaide, Australia.

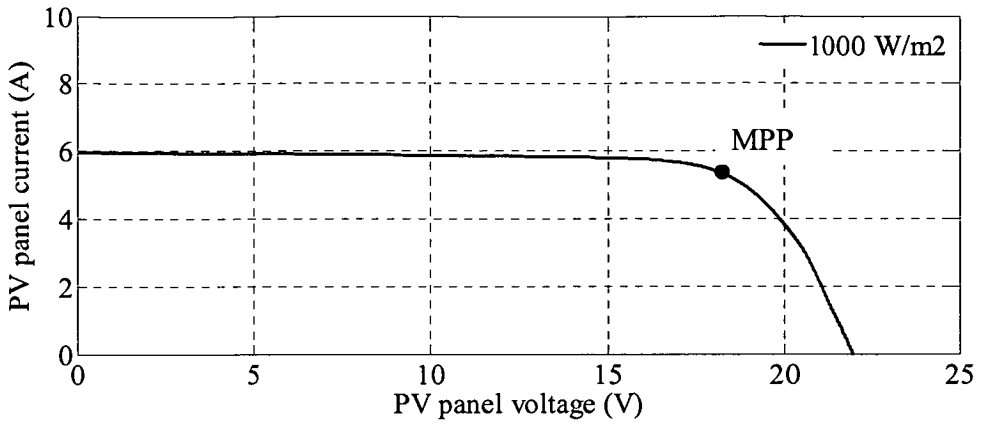

Fig. 2.1 Current-voltage characteristics of the PV module at a specified irradiance.

This chapter focuses on the investigation of maximum power point tracking (MPPT) techniques to extract the maximum available power from the PV module. A review of the existing MPPT techniques is presented first. Then, some limitations that affect the performance of the MPPT techniques are discussed followed by design considerations and control parameters of the MPP trackers. An improved MPPT technique with current mode control is proposed in this chapter. Finally, the proposed MPPT algorithm is verified through extensive simulation results.

2.2 Review of MPPT Techniques

The nonlinear 'current-voltage' and 'power-voltage' characteristic of the PV module, as shown in Fig. 2.2, results in a unique maximum power point at which the PV module can deliver the highest amount of power. The reason behind the decrease of current beyond the MPP can be explained from the device properties point of view. As the photovoltaic solar panels are made of silicon p-n diode, that shows the same electrical characteristics as p-n junction diode. The electrical characteristic of the p-n junction diode is shown Fig. 2.3(a). When the curve shown in Fig. 2.3(a) is shifted by the short circuit current of the photovoltaic solar cell, the curve looks like as shown in Fig. 2.3(b). Again, the diode is used as load; on the other hand, photovoltaic (PV) solar cell is used as the source. So, the characteristic curve of photovoltaic solar cell is shifted to the first quadrant, which then can be presented as shown in Fig. 2.3(c). This is the well known PV characteristic curve.

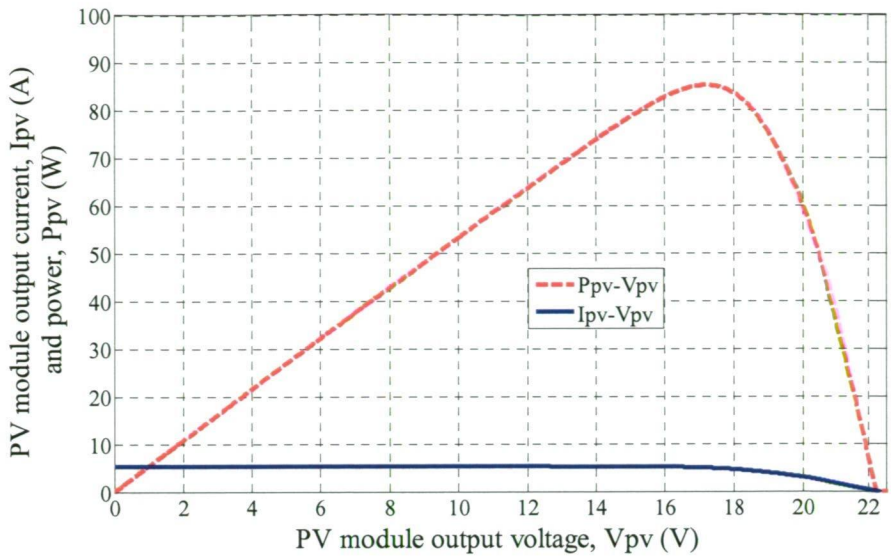

Fig. 2.2 Current-voltage and power-voltage characteristics of the PV module at a constant temperature and a specified irradiance.

As can be seen from Fig. 2.3(c) that the photovoltaic current decreases sharply beyond the maximum power point, and the voltage increases slightly. As a result, the photovoltaic power decreases beyond the maximum power point.

The matter is further been complicated due to the dependence of these characteristics on solar irradiation and temperature. In order to achieve a viable solution to the MPPT problems, several methods are proposed. The ultimate goal of every method is to operate the switch-mode converter in such a way that the current and voltage of the PV module is to be set in a specified range, so that maximum power can be obtained from the PV module.

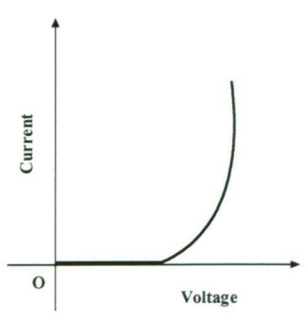

(a) Diode (p-n junction) characteristics

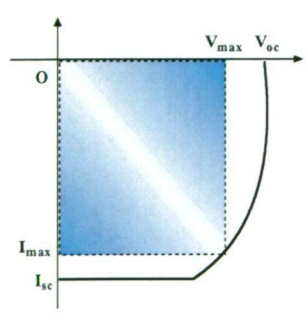

(b) Current vs voltage (I-V curve) for an illuminated pn-junction solar cell

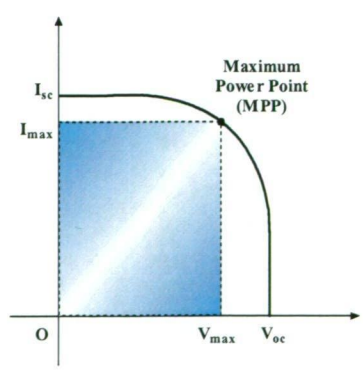

(c) I-V curve reflected into the first quadrant

Fig. 2.3 PV characteristics from the device properties point of view.

The existing MPPT methods vary according to the different aspects including the use of the sensor, speed of response, accuracy of tracking, ease of implementation, cost, PV module parameter dependency, steady-state and transient response. Some methods use voltage sensors, some use current and some use both types. Several methods offer high speed though they are not very accurate. On the other hand, accurate methods are slow. In the following subsection, some popular MPPT techniques are reviewed and their pros and cons are investigated.

2.2.1 Perturb and Observe Method

The perturb and observe method [20-24] involves a control in the voltage of the switch-mode converter observing the slope of the p-v characteristics of the photovoltaic module. As can be seen from Fig. 2.4, an increase in voltage increases the power while the PV module is operating on the left of the MPP, and decreases the power while on the right of the MPP. The process is repeated periodically until the MPP is reached. The system then oscillates around the MPP. The oscillation can be minimized by reducing the perturbation step size. However, a smaller perturbation size slows down the MPPT.

The notable characteristics of this method are less dependency on the PV array parameters, both voltage and current sensing, and mutual analog and digital computation. This is considered to be the most popular method due to its simpler implementation, moderate accuracy in tracking MPPT and suitability for all environmental conditions.

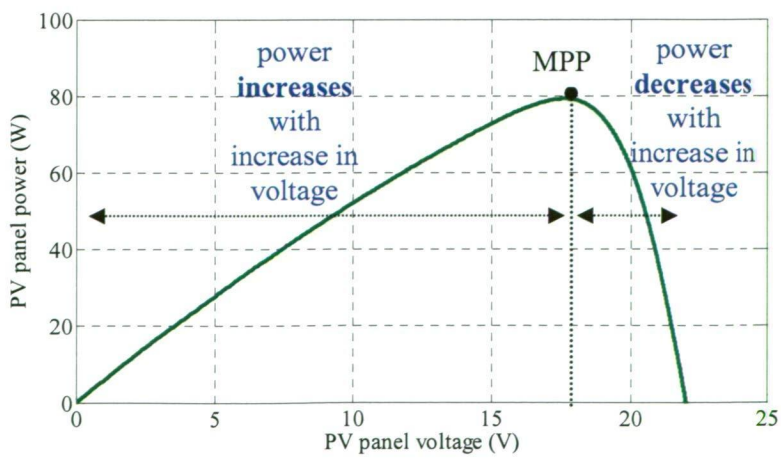

Fig. 2.4 Simple representation of the perturb and observe MPPT technique.

The demerits [22, 23] of the perturb and observe method are higher transient tracking time, slower speed, very small tracking step, lower energy tracking factor (E_{TF}) and failure to operate in rapidly changing environmental conditions. Energy tracking factor is,

$$E_{TF} = \frac{Energy\ extracted\ by\ a\ given\ MPPT\ scheme\ during\ \tau_{max}}{Maximum\ energy\ available\ during\ \tau_{max}}$$

where, τ_{max} = maximum transient tracking time taken by the slowest MPPT scheme.

2.2.2 Incremental Conductance Method

The incremental conductance method [20, 22-23, 25-28] tracks the MPP by comparing the instantaneous conductance (I/V) with the incremental conductance ($\Delta I/\Delta V$). This method is based on the fact that the slope of the PV module power curve is zero at the MPP, positive on the left and negative on the right of the MPP, as given by

- $\frac{dP}{dV} = 0$ at the MPP
- $\frac{dP}{dV} > 0$ left of the MPP
- $\frac{dP}{dV} < 0$ right of the MPP

Since,

$$\frac{dP}{dV} = \frac{d(IV)}{dV} = I + V\frac{dI}{dV} = I + V\frac{\Delta I}{\Delta V} \tag{2.1}$$

So, the incremental conductance method searches the true MPP using the following steps,

- If $\frac{\Delta I}{\Delta V} > -\frac{I}{V}$, incrementing the duty-cycle
- If $\frac{\Delta I}{\Delta V} < -\frac{I}{V}$, decrementing the duty-cycle
- If $\frac{\Delta I}{\Delta V} = -\frac{I}{V}$, keeping the previous value of the duty-cycle

The noteworthy characteristics of the incremental conductance method are high-quality performance in rapidly changing environmental conditions along with PV array independency, medium implementation complexity. Another significant characteristic of this method is the digital computation only. This method ensures moderate accuracy in tracking MPPT, and is suitable for all environmental conditions. The drawbacks [22, 23] of this method are the highest transient tracking time, the slowest speed, very small tracking steps and the lowest energy tracking factor (E_{TF}).

2.2.3 Ripple Correlation Control Method

This method [22, 23, 29-31] senses PV module voltage and current and hence calculates the power of the PV module. The high frequency ripple in voltage and power is then captured to compute dP/dV. Then a decision is taken depending whether $(dP/dt)\times(dV/dt)$ is positive or negative. If $(dP/dt)\times(dV/dt)$ is positive, the operating point of the PV module lies on the left of MPP, and vice versa.

During this process, an integrator is used to generate the reference voltage, which is then compared with the actual PV voltage in order to generate the corresponding error. The error is used to suitably alter the duty ratio of the converter. The whole circuit consists of the sensing circuits, gate pulse generator, boost circuit and the control loop. The ripple correlation control method uses inverting amplifiers, high pass filters and integrators.

The Ripple correlation control method is PV array independent, having low implementation complexity and analog computation. This method has the fastest tracking speed, the highest E_{TF}, and is suitable for fast changing environmental conditions [22, 23]. The disadvantages of this method are that it is not so accurate, and hence has lower tracking capability, is unsuitable for high switching frequency, and has the highest power ripple in steady-state near MPPT.

2.2.4 Modified Hill Climbing Method

In the modified hill climbing method [23, 30], an automatic tuning parameter 'a' is introduced. This parameter decides the step length, whose value depends on the change in power. The automatic tuning parameter 'a' will be large during the transient stage and will be small during steady-state. Consequently, it can reduce the power loss at steady-state and can track quickly during rapidly changing environmental conditions. This method uses the equation,

$$a(k) = C\frac{\Delta P}{a(k-1)} \tag{2.2}$$

where C is a constant, ΔP is the change in power, k and $k-1$ are the two consecutive iterations.

When the power changes in a large range, the tuner changes the value of 'a' to a large scale which satisfies the fast response requirement during the transient stage. When the power change is small, the controller assumes that the system has entered the steady-state stage and the value of 'a' becomes small to keep smooth control over the slowly changing power.

The significant characteristic of the modified hill climbing method is the variable step size. This method requires on-line computation of the tuning parameters. The merits of this method are very accurate tracking, moderate tracking speed, good dynamic and steady-state performance and the lowest power ripple in steady-state near MPPT. One notable demerit of this method is its dependency on PV module configurations [22, 23].

2.2.5 β Method

This algorithm [23, 33] works in two stages. In the first stage, using large iterative steps, operating point can be quickly driven to close proximity to MPP of the PV module. In the second stage, the exact MPP can be found by using small iterative steps. The control parameter β is calculated by the equation

$$\beta = \ln(I_o \times c) \tag{2.3}$$

where I_o reverse saturation is current and 'c' is a diode constant. Again

$$c = \frac{q}{\eta k T N_s} \tag{2.4}$$

Where q is the electronic charge, η is the ideality factor, k is the Boltzmann constant, T is the temperature in Kelvin and N_s is the no. of series connected cells in the PV module.

The β method senses the PV array voltage and current, and then calculates a suitable β for the specific PV system. After that the calculated β is compared with the actual β, which depends on the actual PV parameter of that particular condition. Afterwards, the computation of the error is performed followed by the use of the error to fix the duty-cycle.

This technique uses variable step size and is especially suitable for fast changing environmental conditions. The superiority of this method lies in the fast tracking speed, good accuracy and suitability for all environmental conditions [22, 23]. The main drawbacks of this method are the dependency on PV module characteristics and high implementation complexity.

2.2.6 Constant Voltage Method

Constant voltage method [23, 34] is based on the fact that the ratio of the MPP-voltage to a reference voltage is nearly a constant. With a change in temperature, the MPP of the photovoltaic array changes accordingly. This method uses the physical fact that the temperature characteristic of the p-n junction diode is very similar to that of the solar array.

The forward voltage drop in the p-n junction mounted on the bottom of the PV array is used as the reference voltage. The sensed PV array voltage is compared with the reference voltage to generate an error signal. The error is used to suitably alter the duty ratio of the converter. This method follows the steps below to find the maximum power point of the PV module:

- Senses the voltage V_s of the solar array

- Takes the reference voltage V_{ref} from the p-n junction diode
- Calculates the error, $e = V_{ref} - V_s$
- Updates the duty ratio

The major characteristics of the constant voltage method are its voltage sensing and low cost. The advantages of this method are simple implementation, moderate tracking speed and good performance in stable environmental conditions. This technique is not as accurate as other methods discussed before [22, 23].

2.3 Problems Associated with MPPT Techniques

There are some common problems involved with MPPT techniques which can greatly reduce the performance, and hence result in a considerable amount of power loss. Those problems which restrict the attainable performance of MPPT are described below.

2.3.1 Matching with Converter Topologies

Generally, the MPPT controller drives a dc-dc converter, whose duty-cycle is modulated in order to track the instantaneous MPP of the PV module. Studies [4-5, 11-12] show that converter topology alters the performance of MPPT techniques. As both the PV module and converter shows non-linear and time-varying characteristics, perfect matching between them is necessary for the optimum performance of the whole system.

Among the basic dc-dc converter topologies, the boost converter is the most promising solution as a photovoltaic MPPT interface. The continuous inductor current and discontinuous output current makes it superior in PV applications [5]. Additionally, the boost topology offers cheaper implementation and better dynamic response when compared to other basic dc-dc converters. The boost converter also has advantages over the buck converter, mostly at low insolation levels, while it can always track the maximum power point [4].

2.3.2 Changing Environmental Conditions

The PV module is characterized, normally, in laboratory test conditions. In contrast, real environmental phenomena changes abruptly. This can adversely affect the performance of the MPPT techniques. It is well known that the change in solar irradiation largely influences the true MPP. Fig. 2.5.a and b show the PV current-voltage and power-voltage characteristics at different insolation levels. The change in temperature also reallocates the operating point of the MPP. The problem of finding the MPP becomes severe during rapidly changing environmental conditions. Several recent research publications have highlighted this issue [21, 26, 28, 33].

2.3.3 Non-Optimal Conditions

There are some non-ideal conditions which impede the MPPT techniques' ability to harvest the maximum available power. Partial shading, low solar insolation, dust assemblage and PV module aging are in this category. Partial shading is the most severe among these problems. Studies [5, 35] suggest that partial shading can cause a significant reduction in PV power output even in minor shading occurrences. An experimental investigation [5] reveals that the MPP power degrades by about 28% when 1 of the 72 photovoltaic cells is shaded. The shading effect lowers the module output because the current of the series-connected cells is affected by the shaded cell. Nevertheless, the cells are connected in series to get a specific output voltage.

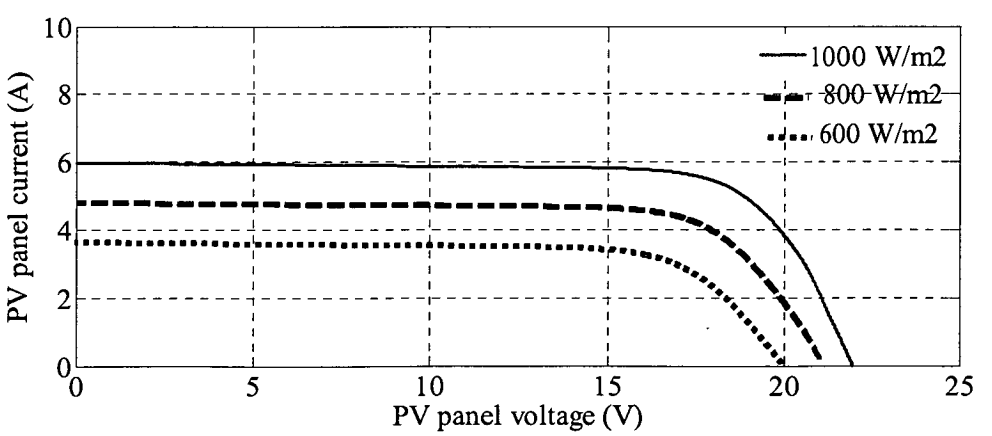

(a) *i-v* characteristics

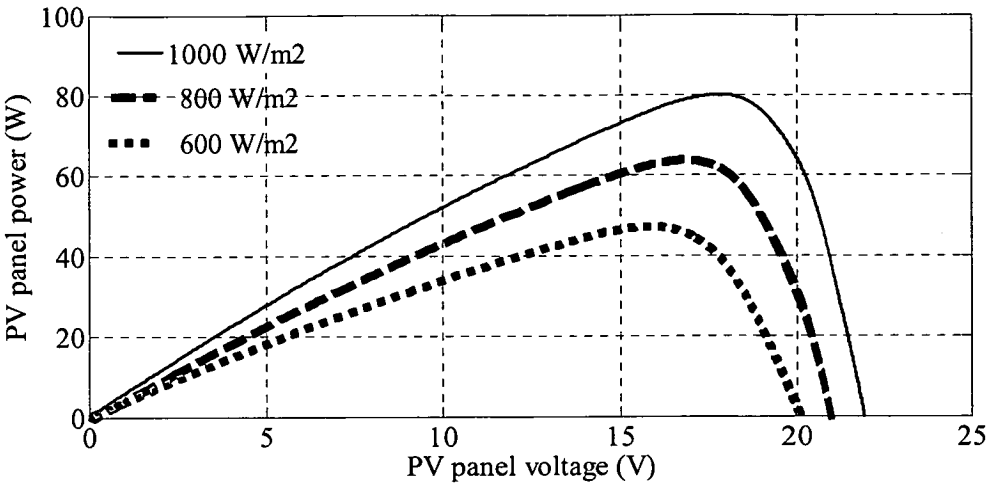

(b) *p-v* characteristics

Fig. 2.5 PV module (a) *i-v* and (b) *p-v* characteristics at different solar insolation levels.

2.4 Design Considerations of MPPT Techniques

Usually, the operating voltage and current are sensed and fed to the control circuit for the computation of the control parameters corresponding to the optimum instantaneous operating point. When studying MPPT techniques, several factors are to be considered which affect the performance of that particular MPPT technique. These are:

- Tracking speed
- Tracking accuracy
- Costs
- Dependency on PV array
- Analog or digital or both
- Stability
- Steady-state error
- Implementation: simple or complex
- Sensors: voltage or current or both
- Ripple in the PV power
- Energy tracking factor
- Response to environmental change
- Dynamic response

Apart from the control circuitry, the sampling interval (T_s) and perturbation step size (d_{step}) of the MPPT algorithm need to be considered carefully [36-39]. These

parameters, i.e. (T_s) and (d_{step}) have a significant effect on the performance of the MPPT. A poor choice of these parameters can easily lead to instability or inefficient tracking. The optimal choice of sampling rate and duty-cycle has to be customized with the dynamic nature of the specific converter adopted. Another point is that, during steady-state condition the sampling and signal processing can create unnecessary losses as there is less need of frequent sampling. Conversely, frequent sampling should be done during rapidly changing atmospheric conditions to offer a fair transient response.

2.4.1 Perturbation Step Size

The perturbation step size needs to be higher for fast tracking of the MPP. Conversely, the perturbation step size is to be lower to minimize the oscillation around the MPP. Lowering the 'duty-cycle perturbation' reduces the steady-state losses caused by the oscillation, as the operating point can stay very close to MPPT; though it makes the algorithm less efficient during rapidly changing environmental conditions.

2.4.2 Sampling Interval

The sampling interval is to be set higher than a threshold value to avoid oscillations around MPP in steady-state and to reduce the instability of the MPPT algorithm. The rate of sampling must ensure that after each duty-cycle perturbation, the system reaches the steady-state before the next sample of PV voltage or current is taken. In fact, in order to allow the MPPT algorithm to make a correct interpretation of the effect of a duty-cycle step perturbation on the corresponding steady-sate variation of the array output power, it is necessary for the time between two consecutive sampling to be long enough to allow the power to reach its steady-state value.

Theoretical analysis, simulation study and experimental results reveal an optimal choice of perturbation step size $d_{step} = 0.05$ and the sampling interval $T_s = 20ms$ for a 1.5 kW boost-converter based MPPT systems [36].

2.5 Control Parameters of MPPT Techniques

MPPT techniques employ control circuits those operate the PV module in a manner that allows the module to deliver, and the power converter to extract, the maximum available power from a particular PV module. Generally, the MPPT algorithm sets a reference value of one variable controlling the power converter that interfaces the PV module to load. The reference is chosen so that the converter draws the current or gets the voltage so that the PV module operates at or near the MPP for the existing irradiance and temperature.

The PV module voltage and/or current are used as control parameters of MPPT techniques. The voltage and/or current are set to a reference value and online sensing of the PV module parameters is performed to follow the reference.

To track the maximum power point, it is enough to follow either the voltage or current at or near the MPP. As the change of voltage is less than the change in current in response to the solar irradiation change, it is preferable to use the PV module voltage as the MPPT control variable [5]. The reason behind this is that the photovoltaic current exhibits fast dynamic behaviour in response to the rapidly moving clouds. Moreover, the PV module MPP voltage usually bounded to 70% - 82% of the open circuit voltage while the current varies within 'zero Ampere' to the 'short circuit current' range. In this case, the use of voltage as the MPP control variable allows a short tracking range. The MPPT tracker based on the voltage reference is shown in Fig. 2.6.

The control structure shown in Fig. 2.6 is applicable for both the dc-dc converter and dc-ac inverter based MPPT module. The MPP tracker sets a reference voltage to follow. This reference is continuously tracked and updated by the MPPT tracker.

As the PV module current is directly linked with solar insolation changes, the MPPT techniques based on current reference can achieve a fast response and accurate holding of the MPP under rapidly changing environmental conditions [40-42]. Fig. 2.7 shows an MPPT control structure based on current reference.

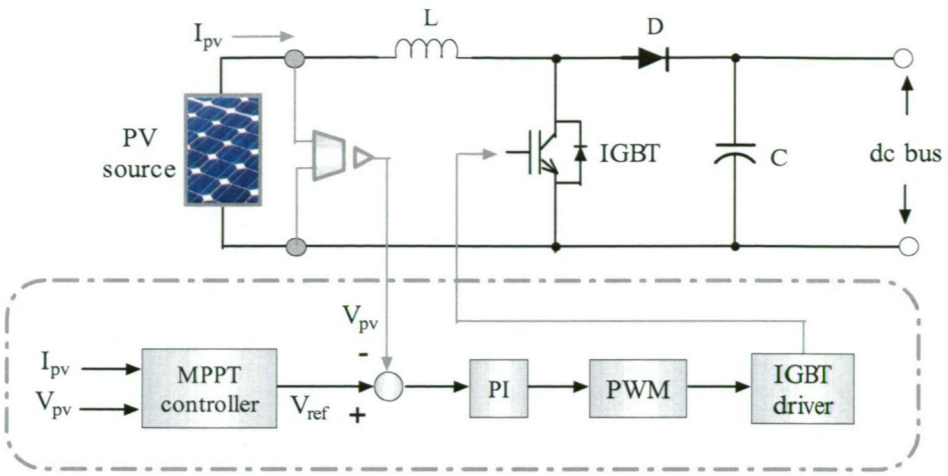

Fig. 2.6 Control mechanism of MPPT based on the reference voltage.

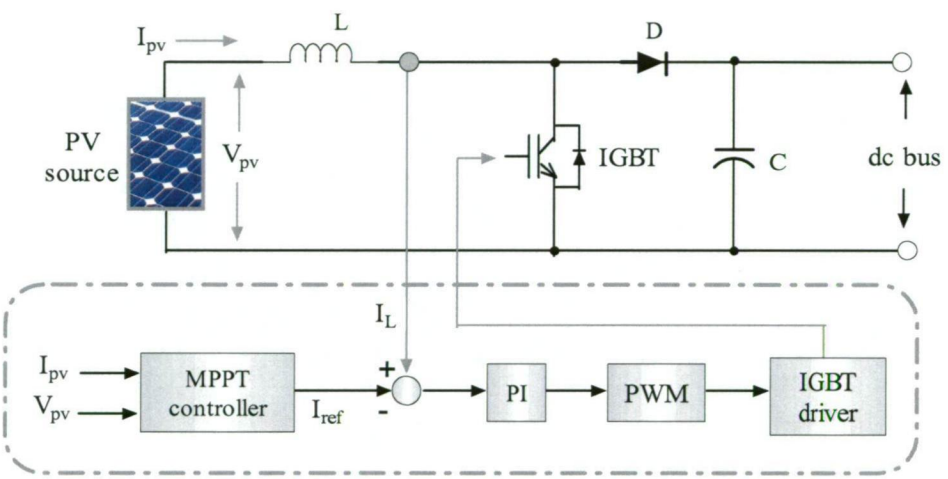

Fig. 2.7 Control mechanism of MPPT based on the reference current.

It can be seen from the PV module characteristic equation, as shown in eq. 2.5 that the short circuit current is proportional to the solar insolation.

$$I_{pv} = I_{LG} - I_{sat}\left(e^{\frac{q}{nkT}(V_{pv}+I_{pv}R_s)} - 1\right) - \frac{V_{pv}+I_{pv}R_s}{R_{sh}} \qquad (2.5)$$

where, I_{pv} (A) is PV module output current, I_{LG} (A) is the light generated current, I_{sat} (A) is the PV module saturation current, R_{sh} (Ω) is the shunt resistance, R_s (Ω) is the series resistance, T (K) is the PV module temperature and k is Boltzmann constant.

Additionally, there is a linear relationship between the MPP current and the short circuit current, [22, 42] which can be represented as,

$$I_{mpp} = K_c I_{sc} \tag{2.6}$$

where I_{mpp} is the current at MPP, I_{sc} is the short circuit current, and K_c is the current factor. This correlation reveals that the current could be used as the control variable to track the true MPP. A fast-acting current loop can adjust the duty-cycle of the converter to follow the reference current calculated by the MPPT tracker.

Nevertheless, a proper value of the duty-cycle calculated by the MPP tracker can adjust the converter duty-cycle to extract maximum available power from the PV module [36-39, 43]. Hence, the duty-cycle perturbation step size is to be chosen carefully for improved performance of the MPPT. Fig. 2.8 shows a typical system where duty-cycle is linked with instantaneous PV power.

In duty-cycle based design [38], the duty-cycle perturbation at the time $(t+1)$ is planned according to the sign of the difference between the power drawn from PV array at time t and the power drawn at time $(t+1)$. So the next duty-cycle perturbation step can be decided on the basis of the following relationship:

$$d(t+1) = d(t) + \left[d(t) - d(t-1)\right] \times sign\left[P(t+1) - P(t)\right] \tag{2.7}$$

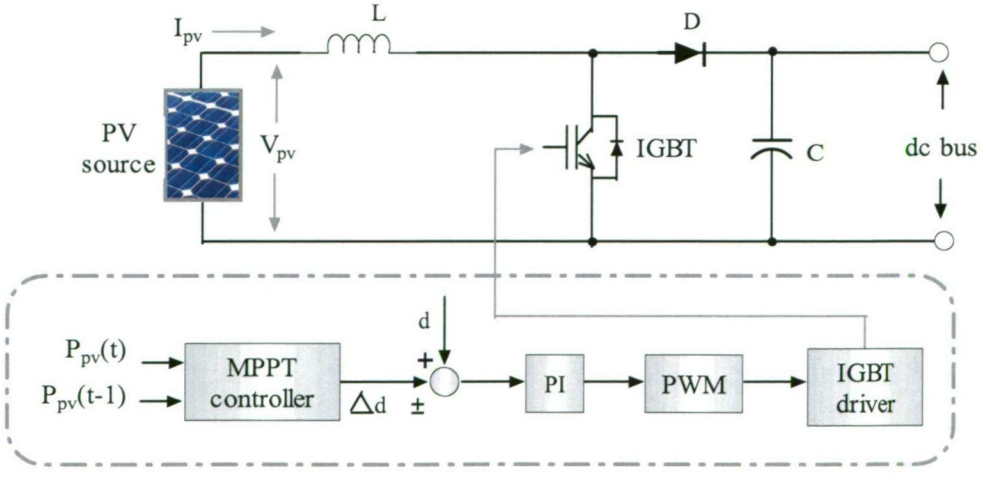

Fig. 2.8 Control mechanism of MPPT based on the duty-cycle perturbation.

2.6 Improved MPPT with Current Mode Control

An improved version of the MPPT technique with current-mode control [40-42] is presented here. The proposed MPPT tracker produces a reference current which is then compared with the inductor current of the dc-dc boost converter. Subsequently the error current goes through a PI controller to generate the PWM switching signal.

The algorithm of the improved current mode control MPPT technique is shown in Fig. 2.9. A MATLAB function block is used to calculate the desired switching pulses and fed to the IGBT of the dc-dc converter.

A variable perturbation step size is set for the reference current. The perturbation step size is defined based on the PV power difference in response to the change in solar insolation. The perturbation step, dI is added or subtracted with the reference current at each iteration of the algorithm, presented by,

$$I_{ref}(t) = I_{ref}(t-1) + dI \tag{2.8}$$

where $I_{ref}(t)$ is the latest reference current value, $I_{ref}(t-1)$ is the reference current value of previous iteration and dI is the perturbation step size of the reference current. dI is calculated based on the following equation:

$$dI = K\frac{dP_{pv}}{P_{pv}(t)} \tag{2.9}$$

$$dP_{pv} = P_{pv}(t) - P_{pv}(t-1) \tag{2.10}$$

where K is the slope of the power-voltage curve of the PV module, dP_{pv} is the change in power, $P_{pv}(t)$ is the latest power output of the PV module, $P_{pv}(t-1)$ is the power output of the PV module at previous iteration.

The effectiveness of the improved MPPT technique lies in the employment of the variable perturbation step size. Most importantly, the variable perturbation step size depends on the PV power difference which changes with the change in solar insolation and temperature. The perturbation step size is repeatedly modified according to the PV power difference, as shown in the eq. 2.9. Hence, a large change in solar insolation produces a large change in power difference which is then automatically updated by the larger perturbation step size.

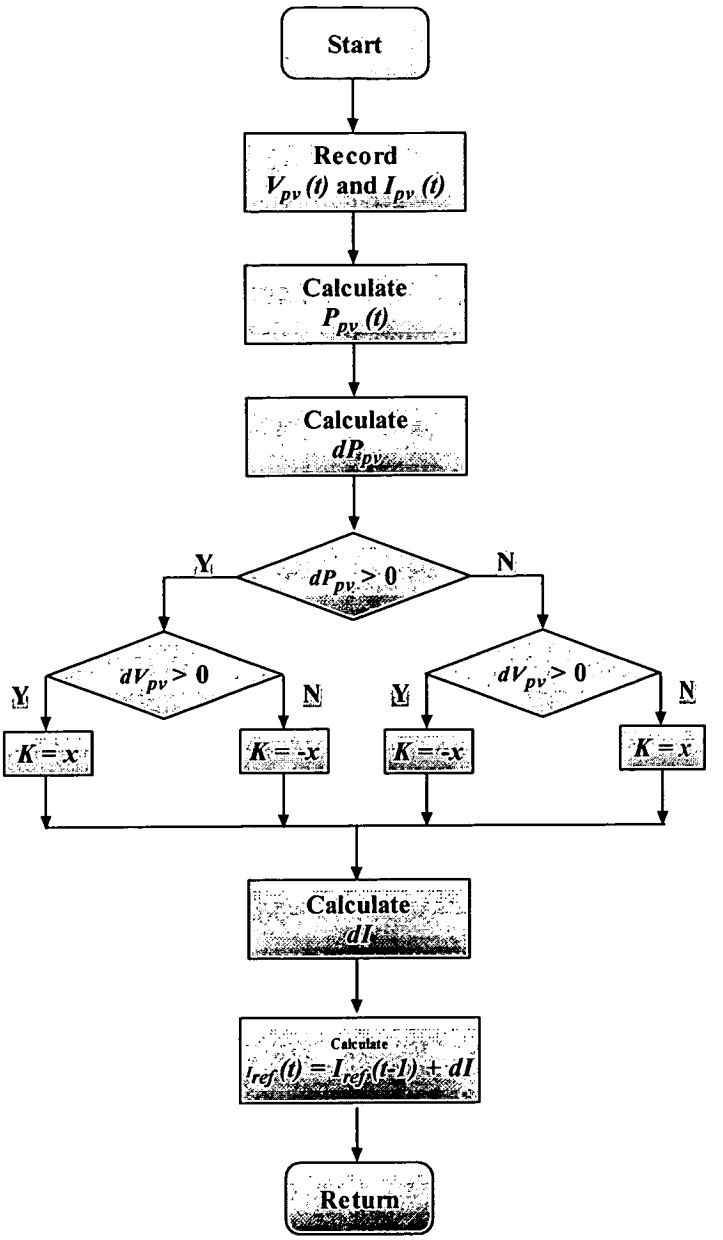

Fig. 2.9 Flowchart of improved MPPT technique with current mode control.

The variable perturbation step size may cause abrupt oscillation before the steady-state condition is reached. This instability problem can be minimized by the current reference. As the PV characteristic is governed by the PV current under changes of solar insolation, controlling the inductor current reduces the oscillation in PV power during the transient state, at rapidly changing atmospheric conditions.

2.7 Simulation Results and Discussion

2.7.1 System Configuration

Fig. 2.10 shows the block diagram of the improved MPPT with current mode control. The PV module power is processed by the dc-dc converter and inverter to feed the load. The dc-dc MPPT module tracks the MPP of PV module and delivers power to the dc bus. Afterwards, the inverter transforms the power from dc to ac and supports the ac load, with controlled voltage and frequency.

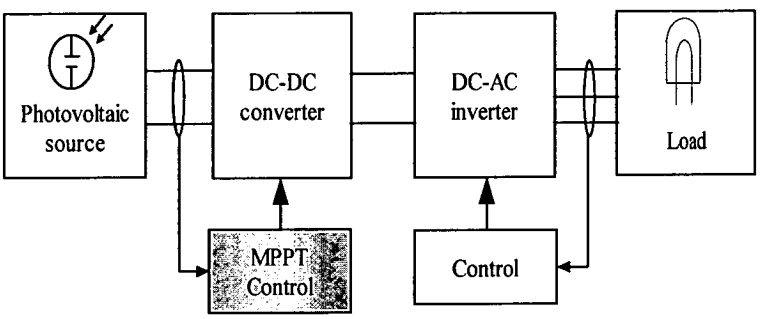

Fig. 2.10 Block diagram of improved MPPT technique with current mode control.

2.7.2 Simulation Model

A simulation model has been developed using MATLAB/Simulink dynamic system simulation software. A Simulink model of the photovoltaic module is used as the PV source. This model takes solar irradiance and PV module current as input and gives PV module voltage and power as output. Different parameters of the circuit, such as short circuit current, open circuit voltage, current and voltage at maximum power point can also be set in the model. Table 2.1 shows the specification of the PV panel. A classical boost converter is used as the dc-dc conversion interface. The utility ac voltage is usually 230V and thus requires a dc voltage of about 400V at the output of the dc-dc converter. Since the voltage of PV module is usually below this level, the system raises the voltage level using the boost converter. The simulation model is designed according to the system power capability requirements.

Table 2.1 Specifications of the PV module

Parameter	Value
Maximum power	80W
Open circuit voltage	22V
Short circuit current	6A
MPP voltage	17.8V
MPP current	5.5A

The PV model takes the insolation data and conventional current data to produce PV module voltage and power, which together give PV module characteristics. The power is then processed by the boost converter. In this case, PV module voltage, power and the input inductor current of the boost converter are monitored continuously. A reference current is generated by the MPPT controller. The inductor current of the boost converter follows that reference value.

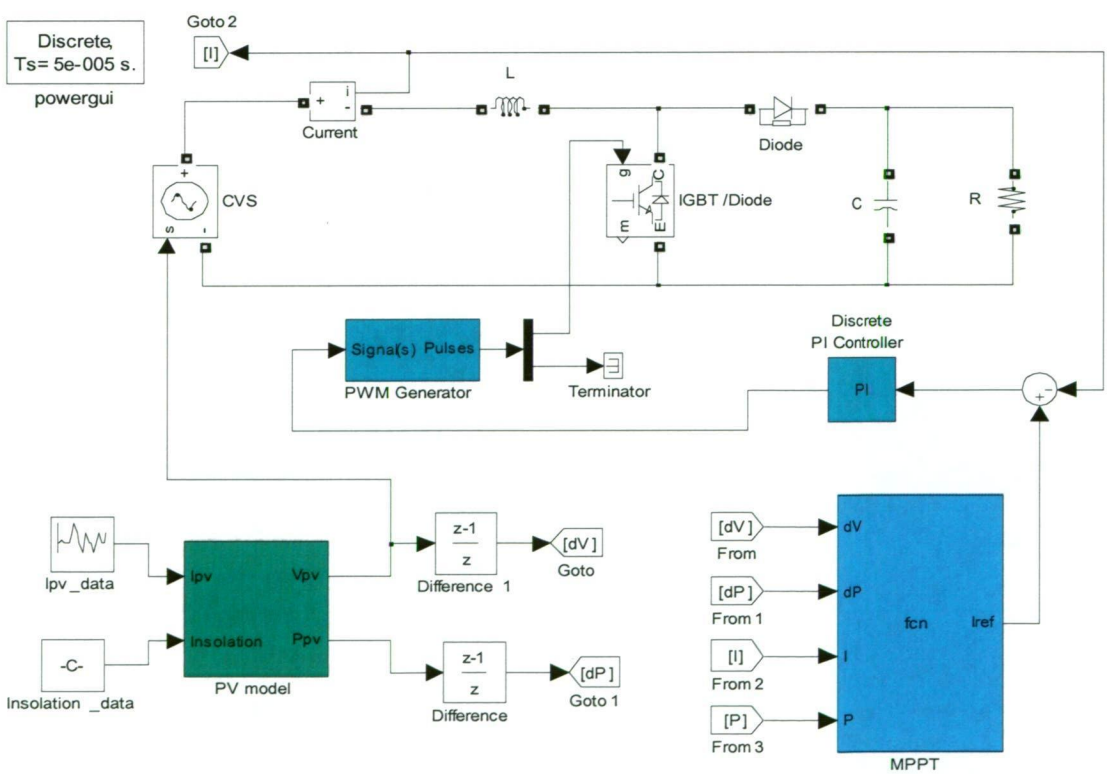

Fig. 2.11 Simplified representation of simulation model of MPPT technique with current mode control (the inverter and the load is not shown here).

A MATLAB function block receives the required current, voltage and power information to calculate the reference current. The calculation uses the methods described in section 2.6 and the eqs. 2.8 to 2.10. The reference current is then compared with the input inductor current of the boost converter and calculates an error. Afterwards, the error current is passed through a PI controller to enhance the stability of the controller. The modified error is then fed by the PWM generator to generate the switching signal to drive the IGBT of the boost converter. Fig. 2.11 shows the simulation model of the MPPT technique with current mode control.

2.7.3 Results and Discussion

2.7.3.1 Tracking Performance of Reference Current

The tracking performance of the MPPT algorithm with variable step-size is presented in Fig. 2.12. The reference current, I_{ref} generated by the algorithm and the PV module current, I_{pv} is shown in the figure. The step-size changes quickly with the change in PV power to track the MPP. Initially, the level of solar irradiation is 400Wm^{-2}. Then at 0.4s, it changes to 700Wm^{-2}. At this time, the current level goes up. Afterwards, the irradiation level changes again at 0.8s, from 700Wm^{-2} to 1000Wm^{-2}. There are also two consecutive changes at 1.2s and 1.6s. In every case of changing irradiations, the reference current forces the PV module current to extract maximum power.

2.7.3.2 Effect of Irradiance Change

To verify the improved MPPT with current mode control, the PV system is simulated with a series of values of solar irradiance. The simulation results are shown for the solar irradiance of 400 Wm^{-2}, 700 Wm^{-2} and 1000 Wm^{-2}. It is observed from the photovoltaic panel p-v curve as shown in Fig. 2.13 that the operating point oscillates around the true MPP and moves along the locus of the MPP as the solar irradiance changes. In each step, the MPP is accurately identified and therefore optimum use of PV module power is ensured.

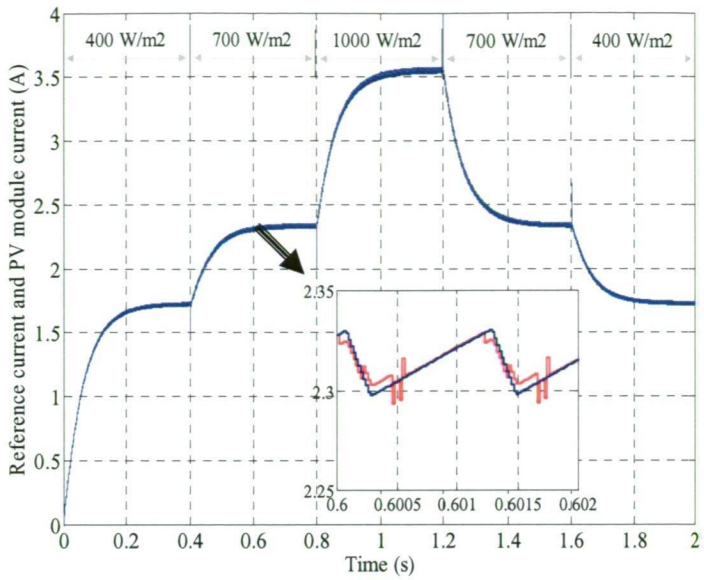

Fig. 2.12 The reference current and PV module current at a series of values of solar irradiance.

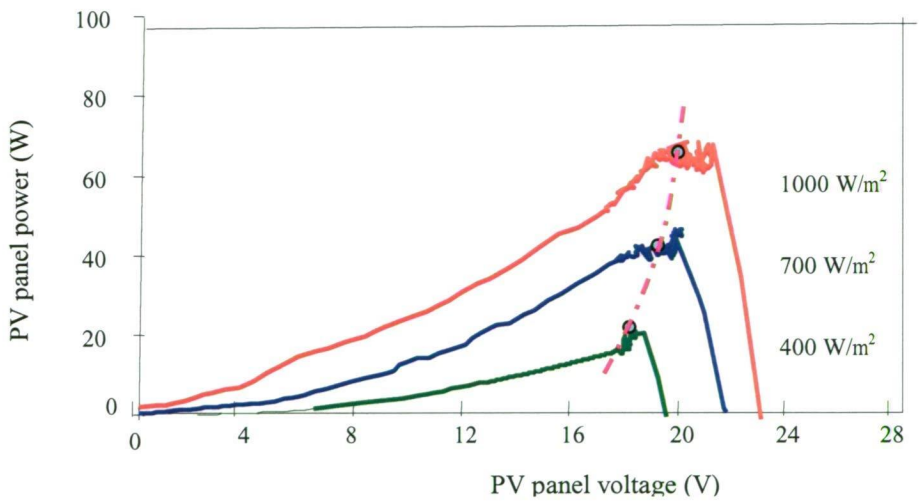

Fig. 2.13 PV module power vs voltage at a series of values of solar irradiance with improved MPPT with current mode control.

2.7.3.3 Effect of Perturbation Step-Size

Duty-cycle perturbation step-size has high influence on the performance of the MPPT techniques. Fig. 2.14 shows the effect of perturbation step-size on the power extraction of improved MPPT with current mode control. The perturbation step-size varies with different values of x, according to the eq. 2.9. The higher values of x can track the MPP quickly, but it fluctuates more around the MPP, which results in more loss of power. The value of $x = 50$, as shown in the simulation results of Fig. 2.14, causes more loss of power having more oscillation around the true MPP.

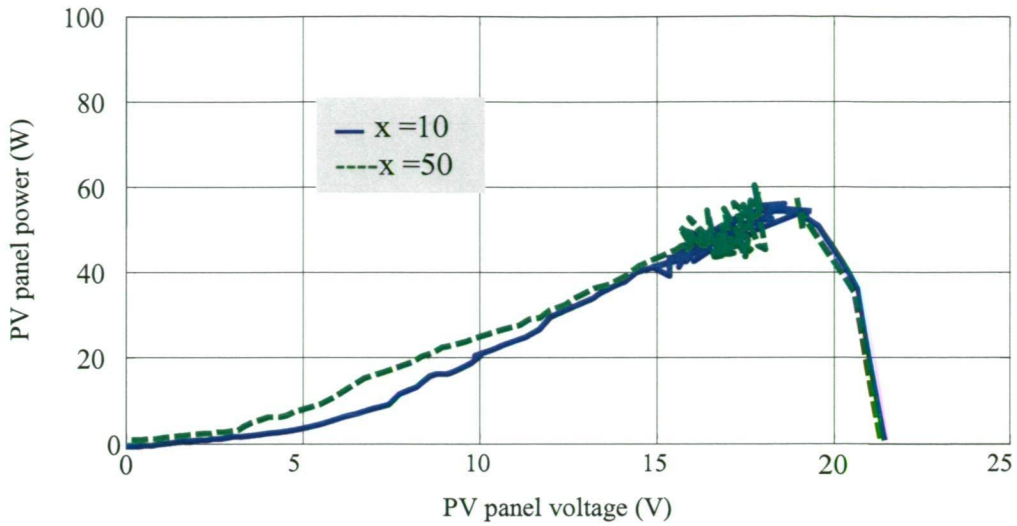

Fig. 2.14 PV module power vs voltage at different values of perturbation step size with improved MPPT with current mode control.

2.7.3.4 Effect of Switching Frequency

Fig. 2.15 shows the p-v characteristics of the photovoltaic panel at different switching frequency of the dc-dc converter. The simulation result shows that the performance in 10 kHz is better as the MPPT technique can track the true MPP more efficiently than at 5 kHz. Less power can be obtained in 5 kHz switching frequency for the specified system.

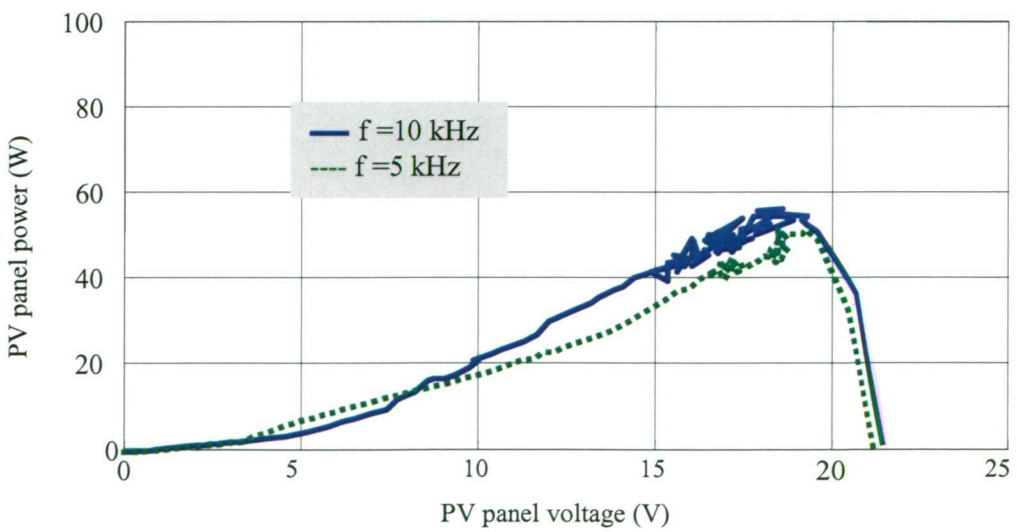

Fig. 2.15 PV module power vs voltage at different frequencies with improved MPPT with current mode control.

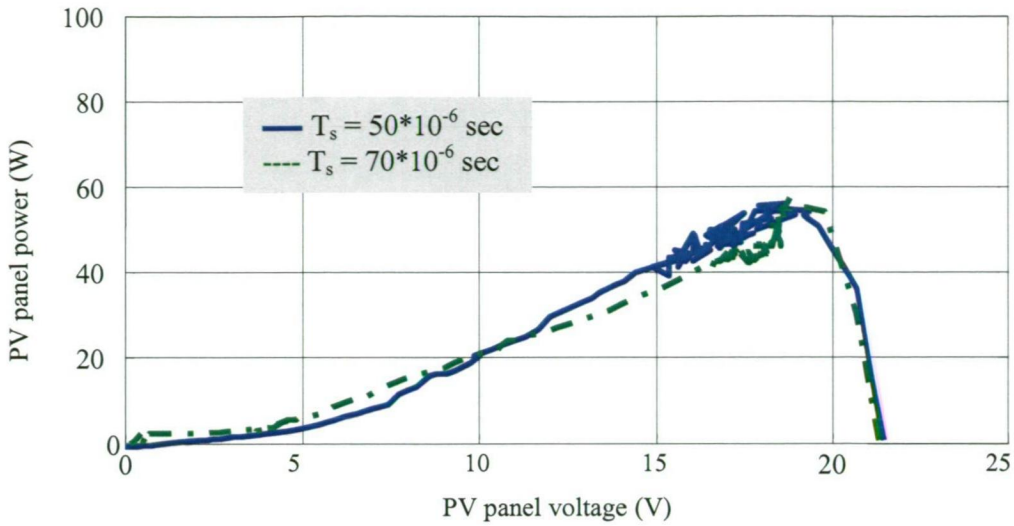

Fig. 2.16 PV module power vs voltage at different sampling rates with the improved MPPT with current mode control.

2.7.3.5 Effect of Sampling Rate

The effect of sampling rate on the improved MPPT technique with current mode control can be seen in Fig. 2.16. As the sampling rate changes from 50×10^{-6} s to 70×10^{-6} s in the MATLAB based Simulink/Simpower software simulation system, the changes in power harvesting by the MPPT technique is obvious. The power extracted by the MPP tracker reduces with the decrease in the sampling rate.

2.8 Conclusions

This chapter focuses on the maximum power point tracking techniques of photovoltaic power systems. The study summarizes the existing MPPT techniques, and their merits and demerits. Some important limitations that affect the performance of MPPT techniques are identified. Afterwards, design considerations and control parameters which recognize the vital significant issues for designing MPPT algorithms are discussed.

The results show that the improved MPPT technique with current mode control can track the MPP at different solar insolation. Especially, the generation the reference current with the change in solar irradiation is noticeable. The effect of perturbation

step size, switching frequency and sampling time is also noticeable from the simulation results. A higher perturbation step size enhances more oscillation around the true MPP. A lower switching frequency lessens the harvesting amount of PV power from the PV panel. On the other hand, the MPP is less efficiently tracked with fewer sampling data. Nevertheless, a proper optimization of several parameters is essential for the optimal performance of the MPPT techniques. The simulation study confirms that the improved MPPT technique with current mode control can extract maximum power under varying weather conditions.

Chapter 3

Current Mode Control of Switch-mode DC-DC Converters

3.1 Introduction

In photovoltaic power systems, a dc-dc conversion stage followed by a dc-ac conversion stage is used to make the photovoltaic (PV) module power suitable for ac loads. The dc-dc converter is responsible for boosting the voltage and ensuring maximum utilization of the PV array power. Most importantly, in PV systems, the function of a dc-dc converter is to supply a regulated dc output voltage irrespective of the load variations and input fluctuations. The utility ac voltage is usually 230V, and thus requires a dc voltage of around 400V at the output of the dc-dc converter. As the PV module voltage is usually below this level, the system boosts up the voltage level using the dc-dc conversion stage. Since the photovoltaic current, and hence the voltage, is subjected to rapid and random changes, the dc-dc converter topology and control strategy requires a robust regulation. Different converter topologies highlight different aspects of viability in PV applications. There are several alternatives available for the control strategy of PV converters. For closed-loop control of converters, two fundamental mechanisms, voltage mode control or current mode control, are generally employed. Depending on the operating conditions, dc-dc switch-mode converters may operate either in continuous or discontinuous conduction mode. For switching techniques, dc-dc switch-mode converters usually use the PWM technique.

This chapter analyzes the current mode control of dc-dc converters for photovoltaic applications. A review of the control techniques of the dc-dc converter will be carried out first. Then a comparative evaluation of the voltage mode control and current

---

A version of this chapter has been published. K. N. Hasan, M. E. Haque, M. Negnevitsky and K. M. Muttaqi, "Performance Analysis of VMC and CMCs of Switch-Mode Converters for Photovoltaic Applications", IECON, Nov. 2008, Florida, USA.

K. N. Hasan, M. E. Haque, M. Negnevitsky and K. M. Muttaqi, "Output Quality Evaluation of Photovoltaic Systems with Different Current Control Methods of Switch-Mode Converters", ICHQP, Sep. – Oct. 2008, Wollongong, Australia.

mode control will be carried out, followed by analysis of the dc-dc converter together with control techniques. The simulation model of the photovoltaic power system with current mode control will then be presented, considering input fluctuations and load variations. Steady-state analysis and dynamic responses of photovoltaic systems will also be investigated, and harmonic analysis will be performed. Finally, simulation results and discussions will be provided.

3.2 Review of Control Strategies for DC-DC Converter

The function of a dc-dc converter is to provide a regulated dc output voltage irrespective of the change in input parameters and load. Hence, the control of the output voltage is usually performed in a closed-loop manner using the negative feedback principle. Fig. 3.1 presents the fundamental concepts of the closed-loop feedback control of dc-dc converters.

Commonly used closed-loop principles for PWM dc-dc converters are voltage mode control and current mode control. The working principles of the voltage mode and the four most popular current control methods are briefly explained below.

3.2.1 Voltage Mode Control

The voltage mode control senses the output voltage of the dc-dc converter and compares it with a reference voltage. The comparator calculates the error. Then the compensator generates the input to the PWM modulator to provide the switching pulses. An important advantage of this method is the ease of implementation and simplicity [44-46]. Fig. 3.2 shows the voltage mode control method for the control of converter.

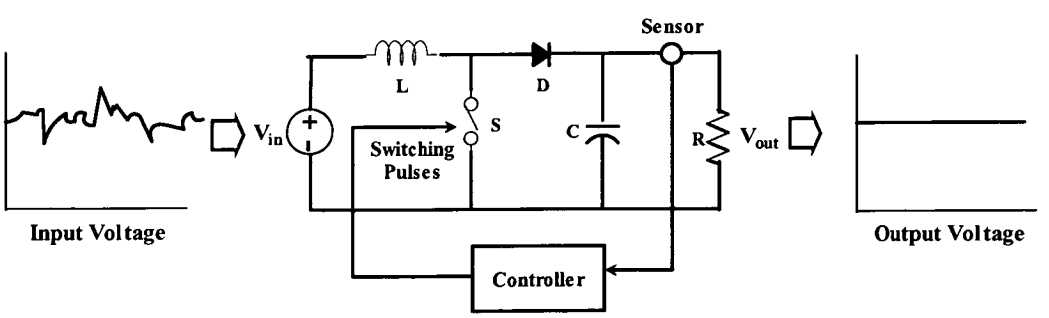

Fig. 3.1 Basic working principle of a dc-dc converter.

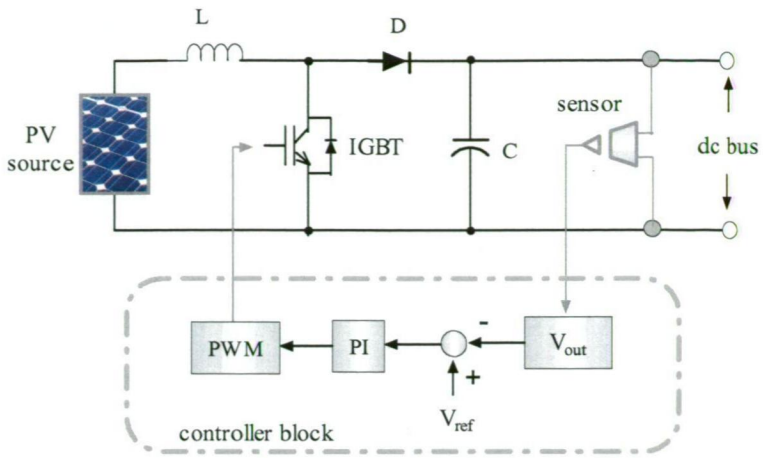

Fig. 3.2 Voltage mode control method for the control of converter.

The error amplifier reacts to change the converter output voltage. Thus, the voltage mode control provides good load regulation. Nevertheless, the line regulation of voltage mode control is comparatively slower, as the change in input must first be sensed as the change in output voltage before any action is taken.

Generally, the slower response of voltage mode control makes it redundant in PV applications. Any change in the PV system source or load is first sensed as an output change, and then gets corrected by the feedback loop. The loop gain of the voltage mode control also varies with the change in input voltage.

3.2.2 Current Mode Control

The current control method employs a current feedback loop in addition to the voltage feedback loop. A current mode control technique generally uses the current from an inductor or a switch, as well as the output voltage error signal. Subsequently, it generates input to the PWM modulator or gate pulses as switching signals. Several methods are proposed for the control of the input current of dc-dc converters [44-48]. Generally, the solar module is modelled as a current source. So, the converter is responsible for active control of the current waveform. Several approaches are available to obtain the required dc voltage by the use of the effective control of the dc-dc converter. A short review of the four methods examined in the research is presented here.

3.2.2.1 Average Current Control

The average current control method measures the input current and compares it with a reference voltage. A comparison of the sensed voltage, (which is proportional to the input current), with feedback voltage, produces an error signal to drive the controller and the PWM modulator [48-51]. Fig. 3.3 shows the average current control method.

The average current control method employs the sensed input current to follow the output reference waveform. To obtain the input current which is supposed to be proportional to the input voltage, the reference voltage is derived from the sensed input voltage waveform. Hence, the sensed input current is proportional to the input voltage.

This method performs well in both continuous and discontinuous conduction mode. It also works well over a wide range of input voltages and load power. The average current control method uses the feed-forward as well as a feed-back signal. This allows the system to obtain a stable dc voltage by cancelling the source side disturbances. Feed-forward signals can cause the converter dc output voltage to be less sensitive to the variations in the source voltage.

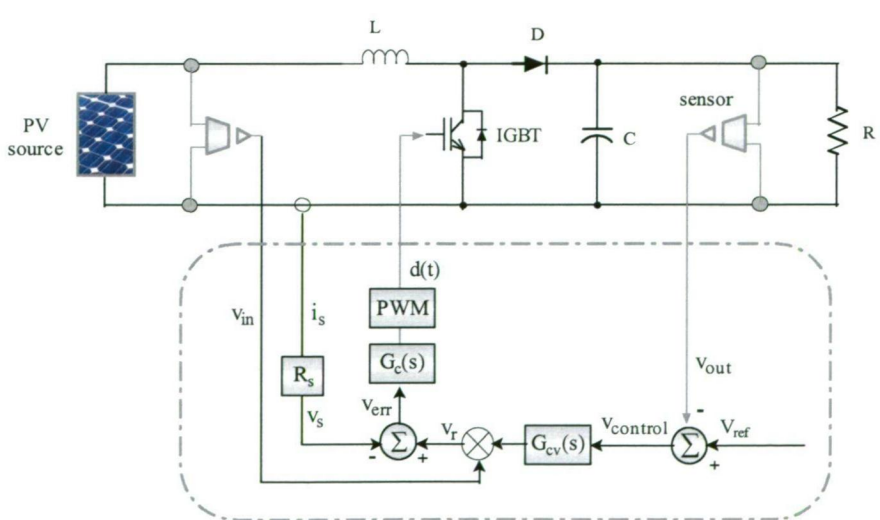

Fig. 3.3 Average current control method for the control of boost converter.

The input current passes through a sensor resistor. The voltage across the sensor resistor is then taken through an amplifier circuit. The output voltage of the amplifier circuit is proportional to the average value of the input current, defined by the equation,

$$v_s(t) = R_s \left| i_s(t) \right|_{T_s} \tag{3.1}$$

This voltage is compared to the reference voltage $v_r(t)$. Consequently, an error signal is produced which is used to drive the compensator network and the PWM driver. The reference, $v_r(t)$, used in this stage, comes from the following formula,

$$v_r(t) = k_x v_{in}(t) v_{control}(t) \tag{3.2}$$

The emulated resistance can be obtained as,

$$R_e = \frac{v_{in}(t)}{i_s(t)} = \frac{\dfrac{v_r(t)}{k_x v_{control}(t)}}{\dfrac{v_s(t)}{R_s}} \tag{3.3}$$

Hence,

$$R_e = \frac{R_s}{k_x v_{control}(t)} \tag{3.4}$$

As can be seen in the block diagram and eq. 3.3, a multiplier is used to adjust the emulated resistance and average power flow.

In this control scheme, average power flow and output voltage are regulated by the variation of the emulated resistance R_e. The control loop continually adjusts R_e to maintain the balance of the average converter power and the load power, such that the following relation is obeyed,

$$P_{av} = \frac{{v_{in}}^2{}_{rms}}{R_e} = P_{load} \tag{3.5}$$

3.2.2.2 Current Programmed Control

In this method, the converter switch current (i_{sw}) is measured and compared with the control current. The control current comes from the feedback loop. The comparator output drives a latch [48, 52, 53]. The current programmed control is shown in Fig. 3.4.

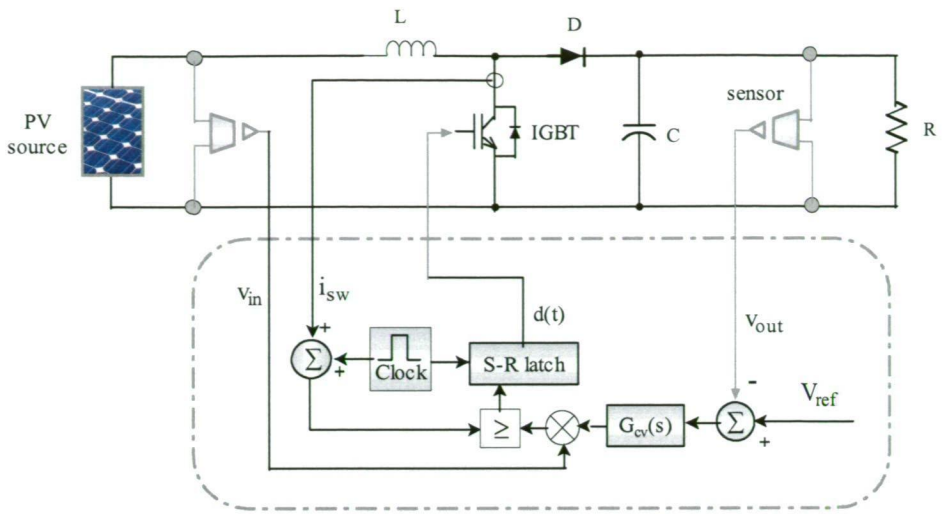

Fig. 3.4 Current programmed control method for the control of boost converter.

The current program control method employs a programmed current which is proportional to the input voltage. The control signal is used to stabilize the output voltage magnitude. In the conventional current programmed control scheme, the control current ($i_{control}$) is simply proportional to the input voltage by the following relationship,

$$i_{control}(t) = \frac{v_{in}(t)}{R_e} \tag{3.6}$$

This method ensures that the converter output is controlled by choice of the peak switch current. The peak switch current follows the control current, and a simple control network turns the switches ON or OFF. Consequently, the switching duty cycle depends on the control current, converter inductor current, capacitor voltage and input voltage.

An artificial ramp with sufficiently large slope m_a is necessary to stabilize the current programmed boost converter. There is a minimum value of the artificial ramp at all static operating points. Erickson et. al. [48] propose a value for the artificial ramp which can be expressed as,

$$m_a = \frac{V}{2L} \tag{3.7}$$

3.2.2.3 Hysteretic Current Control

The hysteretic current control method works with a variable frequency within a given limit. The hysteretic controller provides the gate signal for switching 'ON-OFF' as necessary to maintain a waveform within a set limit [48, 54-56]. Fig. 3.5 shows the hysteretic current control method.

The switch is in either the on or off position according to the response of the zero current detectors. A zero current detector is used to sense the inductor current (i_L). Consequently, the zero current detector sets a latch, turns the switch ON and initiates a switching cycle. As expected, the inductor current increases when the switch is ON, and decreases when the switch is OFF. Meanwhile, the switch current is also monitored, and is compared with a reference voltage $v_r(t)$ that is proportional to the applied input voltage $v_{in}(t)$. When the sensed current is equal to the reference, the latch is reset and the switch is turned OFF.

In the hysteretic current control system, the converter power stage is to be designed carefully, as the switching frequency can vary over a wide range according to system design.

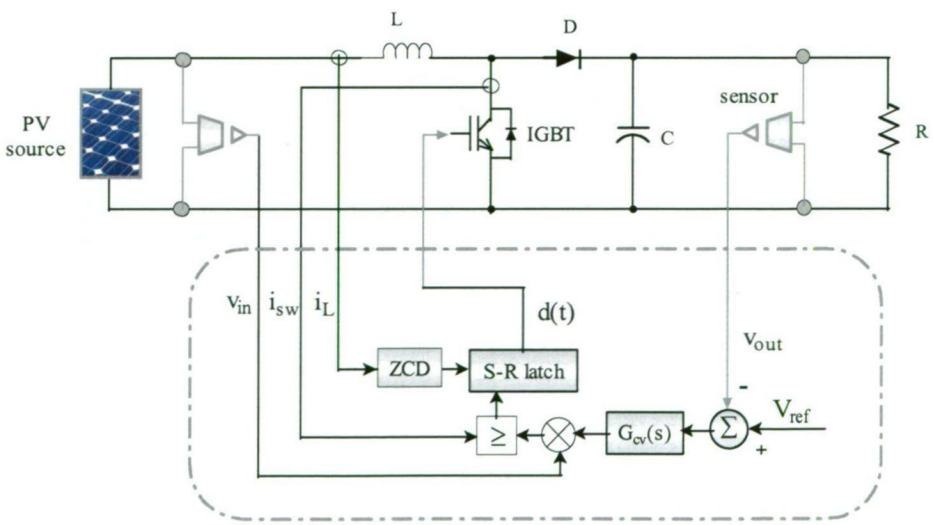

Fig. 3.5 Hysteresis current control method for the control of boost converter.

3.2.2.4 Nonlinear Carrier Control

The nonlinear carrier control method uses a current transformer to obtain the switch current (i_{sw}), which is then integrated. The output of the integrator is compared with the output of the nonlinear carrier generator. The carrier voltage is generated from the double integration of the feedback voltage. The output of the comparator then goes to the latch which generates gating pulses [48, 57, 58]. The nonlinear carrier control method is shown in Fig. 3.6.

The nonlinear carrier controller is inherently stable and free from stability problems. In this method, the switch current is controlled. Hence the switch current is sensed and integrated. The integration offers the advantage of improved noise immunity. A simple way to generate the parabolic carrier waveform uses two integrators, as illustrated in Fig. 3.7.

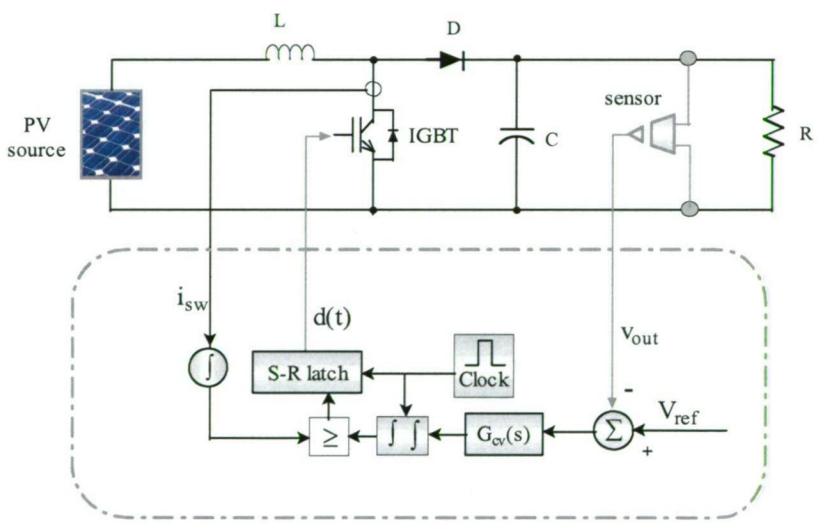

Fig. 3.6 Nonlinear carrier control method for the control of boost converter.

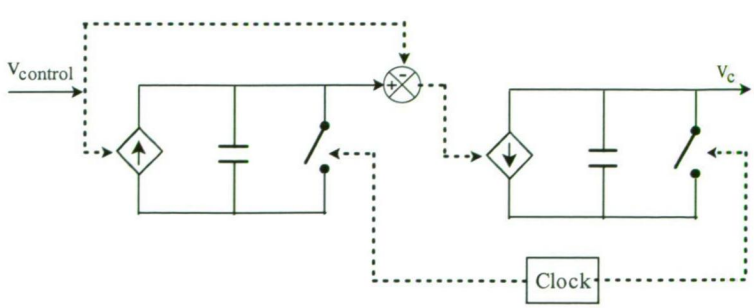

Fig. 3.7 Generation of parabolic carrier waveform by double integration.

The slowly varying control voltage ($v_{control}$) is integrated, to obtain a ramp waveform whose peak amplitude is proportional to ($v_{control}$). The dc component of this waveform is removed, and then integrated again. The output of the second integrator is the parabolic carrier (v_c). Both integrators are reset to zero before the end of each switching period by the clock generator. The amplitude of the parabolic carrier, and hence the emulated resistance, can be controlled by the variation of ($v_{control}$).

3.3 Voltage Mode vs Current Mode Control

In the voltage mode control, one stage of comparison is made, followed by compensation. Whereas, in the current mode control, two stages of comparison are performed before compensation. Voltage mode control uses only the feedback signal, while current mode control uses both the feedback and feed-forward signals to make a stable output voltage. Consequently, in voltage mode control, any change in the PV system source or load is first sensed as an output change, and then corrected by the feedback loop. On the other hand, current mode control can sense the input change quickly, as it uses feed-forward control. Figs. 3.8 (a) and (b) show the voltage mode control and current mode control techniques, respectively as block diagrams.

The voltage mode control senses the output voltage of the converter and compares it with a reference voltage. The comparator calculates the error. Then the compensator forms the input to the PWM modulator to provide the switching pulses [59]. Generally, the voltage mode control has a slow response, which makes the VCM redundant in PV applications. The loop gain of the voltage mode control also varies with the change in input voltage [44].

In contrast, the current mode control uses a pair of nested loops. The outer loop compares the output voltage with a reference voltage whereas the inner loop derives an error signal from the difference of the feed-forward current and the compared resultant voltage of the outer loop. Thus, the error provides the gate signals for switching pulses [59]. The current mode control is usually adopted because it exhibits, in general, better safety, better stability and faster response [45, 60-64]. The

current mode control has higher control to output gain and crossover frequency in comparison with the voltage mode control. The closed-loop phase response of the current mode control is smoother than that of the voltage mode control. The current mode control has a faster response in case of very high speed load transients [45]. Furthermore, no additional circuitry is needed to sense the inductor current as it is already in place from the current feedback loop [62]. Some characteristics of the voltage control and current control methods are listed in table 3.1.

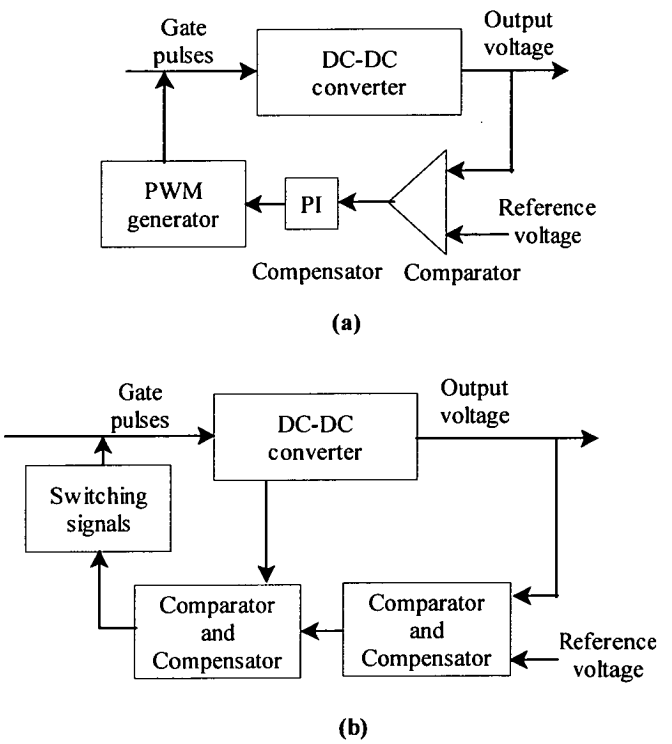

Fig. 3.8 Conventional (a) voltage and (b) current mode control techniques.

Table 3.1 Notable characteristics of the voltage and current mode control methods

Voltage mode control method	Current mode control method
o Easier to design and analyze	o Easy compensation
o Good noise margin	o Effective control of input current
o Better for multiple output	o Better control over input voltage
o Feasible for high power applications	o Faster response
o Wide input and output voltage range	o Better safety

Current mode control methods are recommended for the systems natured with current source power supply, where faster dynamic response is needed. Current mode control is also suitable to eliminate delayed response and gain variation with changes in input voltages. Considering the facts mentioned above, it seems that current control method can be a good solution for photovoltaic power control.

3.4 Analysis

3.4.1 Boost Converter Analysis

A switch-mode power supply consists of the power stage and the control circuit. The power stage performs the basic power conversion while the control circuit employs a method to stabilize the converter.

One popular method to simplify the converter analysis procedure is to represent the converter through a PWM switch model [48, 65, 66]. The result of the PWM switch analysis is a simple small-signal model which replaces just the nonlinear switching elements of the PWM converter. The simple form of the PWM switch model is shown in Fig. 3.9. Terminal a (active) and p (passive) connects to the active and passive switch respectively. Terminal c (common) is common to both the active and passive switches. The PWM switch model is useful for determining the dc operating point and ac transfer function of a power stage.

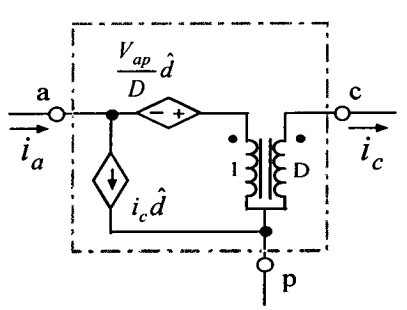

Fig. 3.9 PWM switch model for continuous-conduction-mode small signal analysis.

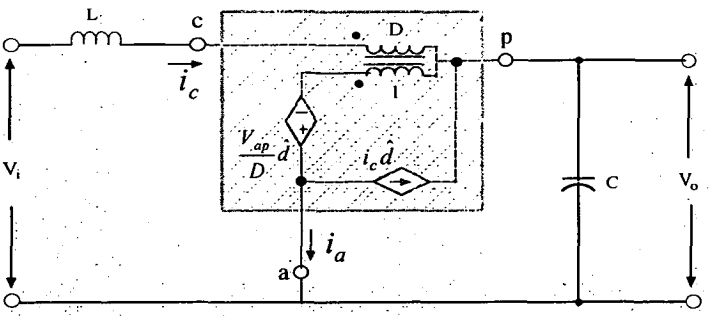

Fig. 3.10 Boost power stage with PWM switch model for continuous-conduction-mode small signal analysis.

The boost converter with inserted PWM switch model into the power stage circuit is shown in Fig. 3.10. The dc analysis and ac small-signal analysis are presented below. For dc analysis, $\hat{d}$ is zero, L is short, and C is open. Then a simple loop equation gives:

$$-V_i + R_L i_c + V_{cp} + V_o = 0 \tag{3.8}$$

$$\Rightarrow -V_i + R_L i_c + V_{ap} D + V_o = 0$$

$$\Rightarrow -V_i + R_L i_c - V_o D + V_o = 0 \tag{3.9}$$

Since,

$$I_o = \frac{V_o}{R}$$

$$\Rightarrow I_c - I_a = \frac{V_o}{R}$$

$$\Rightarrow I_c - I_c D = \frac{V_o}{R}$$

$$\Rightarrow I_c = \frac{V_o}{R} \times \frac{1}{1-D} \tag{3.10}$$

Substituting the value of I_c in eq. 3.9, and after rearranging,

$$V_o - V_o D + R_L \times \frac{V_o}{R} \times \frac{1}{1-D} = V_i$$

$$\Rightarrow V_o \left[1 - D + \frac{R_L}{(1-D)R} \right] = V_i$$

$$\Rightarrow V_o \left[(1-D)\left(1 + \frac{R_L}{(1-D)^2 R} \right) \right] = V_i$$

$$\Rightarrow V_o = \frac{V_i}{1-D} \times \frac{1}{1+\frac{R_L}{(1-D)^2 R}} \tag{3.11}$$

To derive the control-to-output transfer function, superposition principle is used here. First, we set the V_i source to zero. This shorts the input to the 1: D transformer. Further, we push the inductor through the transformer. The resultant boost power stage is shown in Fig. 3.11.

Fig. 3.11 contains two dependent sources. The transfer function can be expressed as a superposition terms arising from these two sources. When the current source is set to zero, the output can be expressed as,

$$V_o = \frac{V_{ap}}{D}\hat{d} \times \frac{R \| C}{\frac{L}{D^2} + (R \| C)} \tag{3.12}$$

When the voltage source is set to zero, the output voltage can be expressed as,

$$V_o = i_c \hat{d} \times \left(\frac{L}{D^2} \| R \| C \right) \tag{3.13}$$

The transfer function is the sum of eqs. 3.12 and 3.13:

$$G_{dv} = \frac{V_o}{d} = \frac{V_{ap}}{D} \times \frac{R \| C}{\frac{L}{D^2} + (R \| C)} + i_c \times \left(\frac{L}{D^2} \| R \| C \right) \tag{3.14}$$

By algebraic manipulation, the control-to-output transfer function for the boost power stage can be expressed as eq. 3.15,

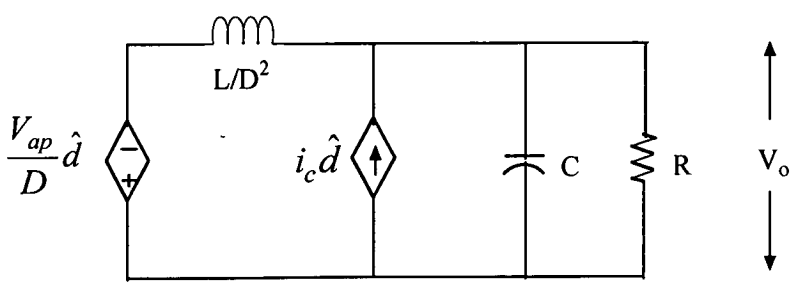

Fig. 3.11 Manipulation of boost equivalent circuit to find the control-to-output transfer function.

$$G_{dv} \approx K \frac{\left(1+\frac{s}{\omega_1}\right)\left(1-\frac{s}{\omega_2}\right)}{1+\frac{s}{\omega_0 Q}+\frac{s^2}{{\omega_0}^2}} \tag{3.15}$$

$$K = \frac{V_i}{(1-D)^2} = \frac{{V_o}^2}{V_i} \tag{3.16}$$

$$\omega_1 = \frac{1}{C} \tag{3.17}$$

$$\omega_2 \approx \frac{(1-D)^2 R}{L} = \frac{R}{L}\left(\frac{V_i}{V_o}\right)^2 \tag{3.18}$$

$$\omega_o \approx \frac{1}{\sqrt{LC}}\sqrt{\frac{(1-D)^2 R}{R}} = \frac{1}{\sqrt{LC}}\frac{V_i}{V_o} \tag{3.19}$$

$$Q \approx \frac{\omega_o}{\frac{1}{L}+\frac{1}{RC}} \tag{3.20}$$

Boost converter small-signal transfer function from the duty cycle of the switch to the boost converter output in continuous conduction mode contains a gain term, double pole, one LHP zero and one RHP zero. As boost converter has RHP-zero, it is more difficult to stabilize a boost converter when it is running in CCM. The boost converter's double pole and RHP-zero are dependent on the input voltage, output voltage, load resistance, inductance, and output capacitance.

The simulated circuit, where $L = 100mH$, $C = 500\mu F$, $R = 30\Omega$, $V_i = 200V$ and $V_o = 400V$ leads to the control-to-output transfer function,

$$G_{dv} \approx \frac{-26s^2 - 5000s + 4000000}{s^2 + 77s + 5000} \tag{3.21}$$

Eq. 3.21 gives the bode plot as shown in Fig. 3.12,

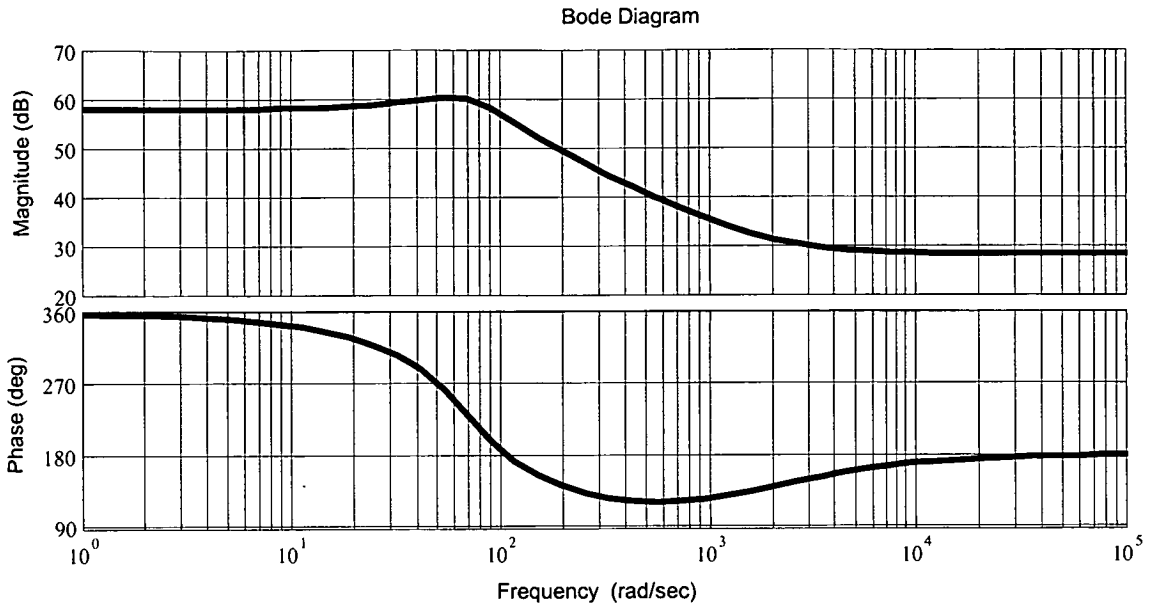

Fig. 3.12 Bode plot of control-to-output transfer function of boost converter.

3.4.2 Current Mode Control Analysis

There are some factors to be considered for the current mode control techniques. Those are modulator gain, slope compensation and the suitable slope of the compensating ramp. The slope compensation depends on the relation of average current to the value of the current at the time the sample is taken [48, 66, 67].

Control-to-output gain of a boost converter can be expressed as,

$$\frac{V_{out}}{V_c} = K_m \times \frac{R_{out}}{R_{out} + (K_m \times R_l)} \tag{3.15}$$

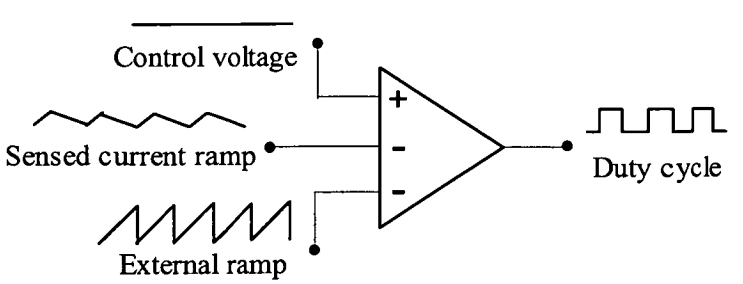

Fig. 3.13 General implementation of the current mode control modulator.

where, the current sense gain, $R_1 = G_1 \times R_s$, the current sense amplifier gain, G_1, the resistance of the series resistor, R_s, the modulator voltage gain,

$$K_m = \frac{1}{(0.5 - D) \times R_1 \times \frac{T}{L} + V_{SL}/V_{out}} \tag{3.16}$$

and the fixed slope,

$$V_{SL} = S_E \times T \tag{3.17}$$

The dominant pole of the transfer function appears at,

$$\omega_p = \frac{1}{C_{out}} \times \left(\frac{1}{R_{out}} + \frac{1}{K_m \times R_1} \right) \tag{3.18}$$

The inductor pole appears when the impedance of the inductor equals the current loop gain,

$$\omega_L = \frac{K_m \times R_1}{L} \tag{3.19}$$

An optimal compensating slope can ensure the stability of the current loop, by damping the tendency of sub harmonic oscillation. The optimum slope of the ramp presented in the modulating comparator input is equal to the sum of the absolute value of the inductor up-slope and down slope scaled by the current sense gain.

Hence, the current mode slope compensation is,

$$\frac{V_{ramp}}{T} = V_{in} \times \frac{R_1}{L} \tag{3.20}$$

Ramp slope for the boost converter can be expressed as,

Up-slope,

$$V_{in} \times \frac{R_1}{L} \tag{3.21}$$

Down-slope,

$$(V_{out} - V_{in}) \times \frac{R_1}{L} \tag{3.22}$$

The type of control has been analyzed here uses the instantaneous value of the inductor current once in every switching cycle to control either the turn-on or turn-off of the power switches. Fig. 3.14 shows the basic implementation of the current mode control techniques.

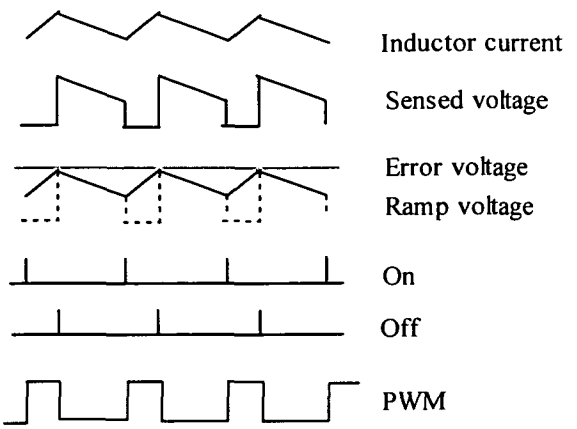

Fig. 3.14 General concept of current control method for the control of the converter.

3.5 Simulation Model

The simulation model has been developed using Matlab/Simulink dynamic system simulation software. A Simulink model of PV module is used as the PV source [68]. This model takes solar irradiance and PV module current as input and gives PV module voltage and power as the output. Different parameters of the circuit, such as short circuit current, open circuit voltage, current and voltage at MPP can also be set in the model. The PV module is designed for 3kW output power which can support a typical residential system. The dc-dc converter of the system is designed for 200V dc input voltage, which can be boosted up to 400V dc. The inverter output provides a 230 V, 50 Hz voltage while 2 kW, 3 phase parallel RLC load is fed by the PV system. The simulation model is designed according to the system power capability requirements. All of the PI and PID controller parameters of the control loops are tuned using Zeigler-Nichols tuning method and have chosen the optimum values for the system specifications. Table 3.2 shows the specifications of the system. The parameters are chosen on trial and error basis to support the specified loads.

3.6 Simulation Results and Discussion

The responses of PV power conversion systems with different current control techniques are obtained through simulations. Figs. 3.15-3.19 show the simulation results of PV power conversion systems using the four current control techniques as discussed earlier. System stability, transient response and power quality issues are also investigated.

Table 3.2 System specifications

Input voltage	180 ~ 220 V
Switching frequency	25 kHz
Converter mode	VMC, CMC
Inductor value	10 mH
Capacitor value	500 μF
Converter output voltage	380 V dc
Inverter output voltage	230 V ac

3.6.1 Effect of Control on Converter Output Voltage

Fig. 3.15 shows the output voltage responses of the dc-dc boost converters for PV applications simulated with four different current mode control techniques. The average current control and current programmed control have a very high percentage of overshoot, at 81% and 95%, respectively. The hysteresis current control method offers a low overshoot and small fluctuations at the output voltage. The nonlinear carrier control method also has no overshoot though it contains some ripple at the output voltage. It is noted that, the average current control (395V), current programmed control (398V) and nonlinear carrier control (405V) can support the desired 400V output voltage level at the converter output, while the hysteresis current control (373V) is far below this level.

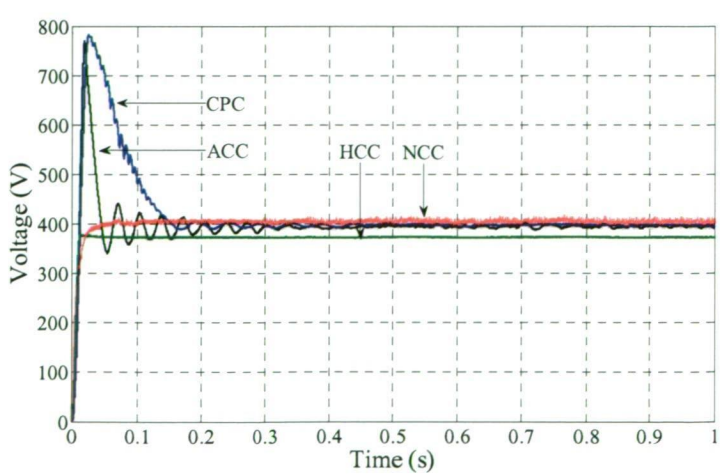

Fig. 3.15 Output voltage of photovoltaic boost converter with different CCMs.

3.6.2 Effect of Control on Dynamic Performances

Dynamic responses of the current mode control techniques are presented in Fig. 3.16. To investigate the dynamic performances, loads are disconnected at a time instant of 0.6 sec. and then reconnected at the time instant of 0.7 sec. By this time, the average current control offers a voltage fluctuation of 29% below and 34% above its steady state value. For the current programmed control, the voltage goes down by 33% and rises to 53% of average dc level. The hysteresis current control (27% below and 40% above) and nonlinear carrier control (53% below and 15% above) also suffer significant fluctuations in the output voltage during dynamic response analysis.

3.6.3 Effect of Input Variations on Control Schemes

The simulation platform is designed for the photovoltaic system with 200V input to the dc-dc converter. Fig. 3.17 shows the output voltage of the converter for a ± 10% input variation from the specified limit. The hysteresis current control (HCC) offers the best performance for input variations. For a ± 10% input voltage variation, the output voltage of the dc-dc converter changes by 2% for the average current control (ACC) and by 3% for the current programmed control (CPC). The output voltage of the hysteresis current control changes by 1.5% and for the nonlinear carrier control (NCC) it is 2.6% with ripples.

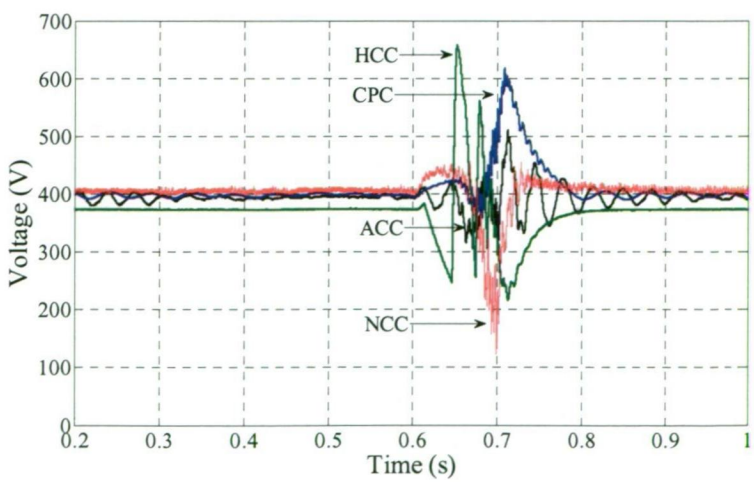

Fig. 3.16 Dynamic response of converter with different CCMs.

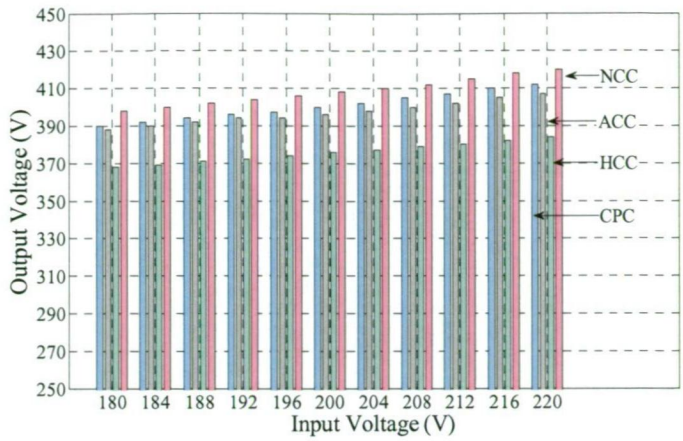

Fig. 3.17 Effects of input variations on converter with different CCMs.

3.6.4 Effect of Load Changes on Control Schemes

To investigate the impact of load variations on the performance of the control strategy of dc-dc converter for PV systems, the load is changed from 1kW to 3 kW (Fig. 3.18). Initially, a 3 kW load is fed by the PV system. Then, at 0.4 sec., a 1.5 kW load is connected to the system. At this time, the voltage level rises by 20% for both the HCC and NCC. For the ACC and CPC, some fluctuations occur at the output voltage. At the time of 0.6 sec, a 1 kW load is connected to the system. There is no significant change of voltage at this load variation. At the time of 0.8 sec., the system returns to supply a 3 kW load. The simulation result suggests that the HCC and the NCC is the most responsive with load changes. On the other hand, the CPC shows the best performance with load fluctuations. The ACC also performs well with load variations.

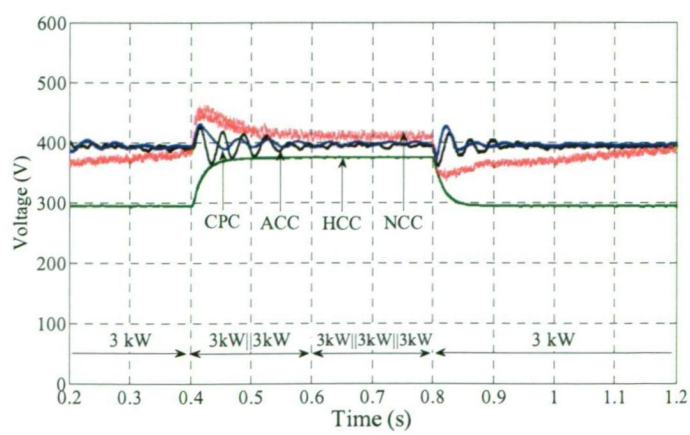

Fig. 3.18 Effects of load changes on converter with different CCMs.

3.6.5 Effect of External Disturbances on Control Schemes

The disappearance of sunlight for a short time due to cloud is a common event. With sudden external disturbances, such as the input voltage falls to zero and then recovers, the CPC (345V-440V) offers the best result, as shown in Fig. 3.19. In this case, the NCC (80V-430V) shows the worst performance. The performance of the ACC (180V-580V) and the HCC (215V-374V) are also not satisfactory.

3.6.6 Effect of Control on Inverter Harmonics

The total harmonic distortion (THD) is an important factor of the PV power systems since switching actions and power electronic interfaces are associated with these systems. Simulation study reveals (Fig. 3.20) that the simulated system offers THD below the IEEE standard recommended limits (THD<5%) [69]. The HCC shows the best performance regarding THD whereas the ACC has the highest THD among all of the observed current control methods.

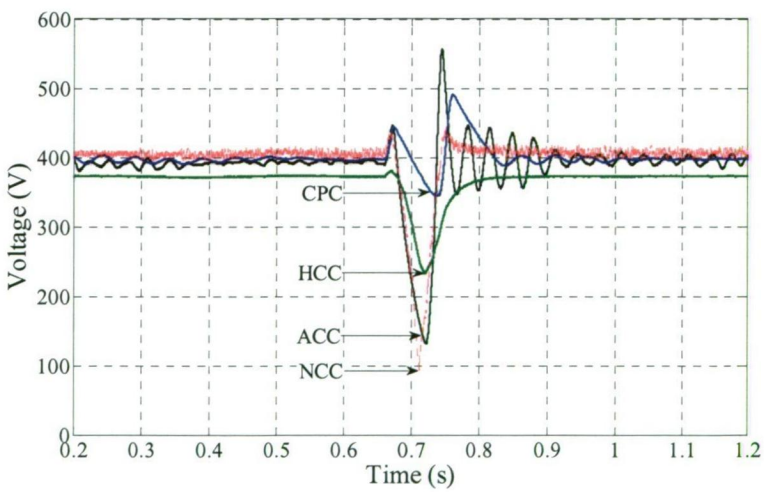

Fig. 3.19 Effects of external disturbances on converter with different CCMs.

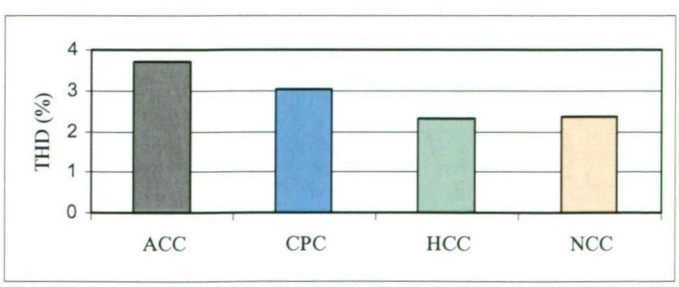

Fig. 3.20 THD at the output of the inverter with different CCMs.

3.7 Comparative Assessment of Different Control Methods

Table 3.3 represents different response of PV systems associated with voltage mode control (VMC) and four different current mode control techniques. It is shown that the VMC has the highest settling time and high overshoot. Transient response of the VMC is also not satisfactory. The ACC has very high overshoot and the highest THD. This control method performs well during transient response and in case of sudden load changes. The ACC and NCC provides high ripple (6%) in converter output voltage. The ACC has the highest settling time (0.45 s) while the NCC reaches very fast to its final steady state value. The CPC shows good performance in case of input variations, load changes and external disturbances. Overshoot is very high for the CPC. It offers the worst dynamic performance. On the other hand, the HCC provides very low percentage of overshoot. The HCC also shows a promising result regarding input variations. The response of the HCC is the worst with load changes. The NCC is not suitable for input variations, load changes and external disturbances. The NCC performs well concerning parameter sensitivity. Table II reveals that the output voltage of inverter is within the desired band limit for all of the current control methods. Simulation results demonstrate that the THD remains within acceptable limits for all four methods although the HCC provides the best performance (2.33%).

Table 3.3 Comparative assessment of different control methods

Criterion ⇩ / Control ⇨	VMC	ACC	CPC	HCC	NCC
Converter output (V)	396	395	398	373	405
Converter output ripple (V)	8	6	2	1.5	6
Delay time (sec)	0.04	0.008	0.009	0.006	0.0045
Rise time (sec)	0.06	0.009	0.011	0.011	0.025
Settling time (sec)	0.50	0.45	0.17	0.12	0.04
% Overshoot	15	25	42	0.8	no
Inverter output (V)	233	234	230.7	233.4	236.7
THD of inverter (%)	4.5	3.69	3.04	2.33	2.35

3.8 Conclusions

The performances of different control methods of dc-dc converter controller for PV power systems in various operating conditions are investigated in this chapter. A photovoltaic system is modeled and different controllers are implemented using MATLAB/ Simulink. The performances of the average current control, current programmed control, hysteresis current control, and nonlinear current control techniques have been analyzed and compared. Transient response and power quality issues of the PV systems operated with different current controllers at different working conditions have been investigated. Effects of input variations, load fluctuations and external disturbances have also been analyzed. It is evident from the simulation study that none of the control method can offer an ideal solution. The control techniques can be selected based on the working conditions.

Chapter 4

Control of Battery Storage with a Bidirectional Converter

4.1 Introduction

In photovoltaic power systems, a photovoltaic module produces irregular and fluctuating electric power, and therefore requires energy storage to supply continuous power to loads. Generally, a stand-alone photovoltaic power system uses energy storage to support inadequate solar irradiation. Fig. 4.1 shows the discrepancy between the available photovoltaic power and the demand of the electric load connected to the photovoltaic power system. An energy storage system can store excess energy when ample photovoltaic power generation occurs, especially, at midday. Additionally, the storage system can support the load for periods of low photovoltaic power generation, particularly, at night. So, in photovoltaic power applications, an energy storage system acts as a complementary source with the photovoltaic source. There are several alternatives available for energy storage devices, such as battery, supercapacitor, hydrogen electrolyzer, flywheel, pumped hydro, compressed air and hybrid storage. The most common technology used in photovoltaic energy storages is the battery storage, due to its availability, low cost and simple technology. The bidirectional converter which is used to charge and discharge the battery plays an important role in energy storage systems. The control algorithms and controller implementations involve a high level of complexity. Another noticeable consideration is the capacity of the energy storage as it is related to the cost and reliability.

This chapter focuses on control strategies for the energy storage of photovoltaic systems. An overview of photovoltaic energy storage systems will be presented first. Different alternatives for the storage elements, system configurations, converter

---

A version of this chapter has been published. K. N. Hasan, M. E. Haque, M. Negnevitsky and K. M. Muttaqi, "Control of Energy Storage Interface with a Bidirectional Converter for Photovoltaic Systems", AUPEC, Dec. 2008, Sydney, Australia.

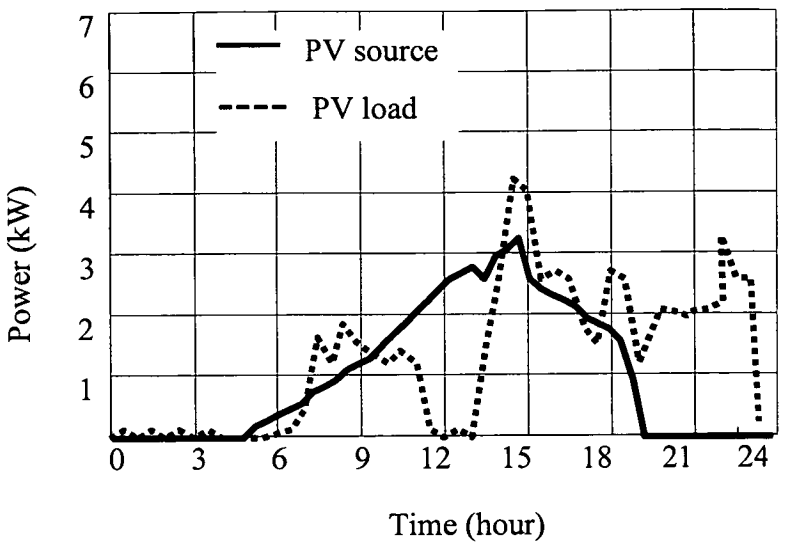

Fig. 4.1 The discrepancy between the generated PV power and load.

topologies and control techniques will be discussed. A novel control technique for battery charger control is proposed in this chapter. A simulation model of the proposed control algorithm for a photovoltaic energy storage system is analysed. Finally, the proposed control algorithm is verified through simulation studies based on MATLAB/Simulink/Simpower.

4.2 Overview of Photovoltaic Energy Storage Systems

The integration of photovoltaic power systems and energy storage schemes is one of the most significant issues in renewable power generation technology. Optimal design of an energy storage system for photovoltaic power applications requires consideration of storage options, system configurations, converter topologies and control techniques.

4.2.1 Storage Options

4.2.1.1 Battery

Batteries are the most commonly used energy storage systems over a wide range of ratings and applications. A battery bank is usually used in photovoltaic energy storage systems due to its high round-trip efficiency, wide availability, low cost and

easiness in charging and discharging [70, 71]. A battery consists of electrochemical components. Charging a battery causes a reaction in the compounds, in order to store the electrical energy in chemical form. The reverse chemical reaction releases the electrical energy from the battery upon demand. A battery storage system can be located almost anywhere and can be installed easily.

4.2.1.2 Hydrogen/ Fuel Cell

Hydrogen energy storage systems are another promising storage option for photovoltaic applications. In this scheme, the excess energy produced with respect to the load, is sent to the electrolyzer for hydrogen production. When energy produced from the PV module becomes insufficient, the stored hydrogen is fed to the fuel cell to produce electricity [70]. This type of energy storage system is suitable for long-term energy storage. The problems associated with this type of storage system are the high initial cost, and complexity in the control system. Moreover, a hydrogen-based storage system would include more components including an electrolyzer, storage tanks and fuel cells. Additionally, the hydrogen storage system cannot respond to emergency and momentary power needs [72, 73].

4.2.1.3 Supercapacitor or Ultracapacitor

Supercapacitor-battery hybrid energy storage systems for stand-alone photovoltaic systems are presented in [71]. The supercapacitor contains a higher power density than the battery, which allows the supercapacitor to provide more power over a short period of time. Conversely, the battery has a higher energy density to store more energy and release that over a long period of time. The supercapacitor-battery hybrid energy storage system integrates the advantages of both technologies. The supercapacitor can supply high peak power requirements, such as for motor start-up, whereas the battery can supply low power requirements [72].

4.2.1.4 Compressed Air

Compressed air energy storage systems use photovoltaic power to compress air, and store the compressed air at high pressure in an underground reservoir, when excess energy is generated from the photovoltaic module. During peak demand, the compressed air is then released and combined with other fuels to drive a turbine-generator set [72-75]. Compressed air energy storage systems utilize two-third less fuel then conventional units and are able to start up within tens of minutes [76]. The drawbacks of these systems are the need for special arrangements, equipments and very large reservoirs.

4.2.1.5 Flywheels

Flywheel energy storage systems store energy in a rotor spinning at extremely high velocities. It can produce electrical power on demand from the stored energy. Flywheel energy storage systems have the ability to respond quickly to tens of thousands of cycles per year with high durability [77]. These systems are more suitable to enhance the power quality of the grid than to support the load for a long time.

4.2.1.6 Pumped Hydro

Pumped hydro storages can also be used in photovoltaic energy storage systems. During off peak hours, the surplus power is used to pump water from a lower reservoir to a higher reservoir. Then during peak demand, the water is released to turn the turbine ON and produce electrical energy. The drawback of this technology is the requirement of large reservoir and suitable geographic location. Additionally, pumped hydro storage is costly and takes a long time to plan and build [72].

The choice of energy storage system depends on several factors including load requirements, system demand, geographic location, storage capacity and cost. Table 4.1 compares the six most widely used energy storage devices considering their efficiency and maximum capacity [72-74].

Table 4.1 Comparison of energy storage options

Storage Components	Efficiency (%)		Maximum capacity	
	Individual	System	Power	Hours
Battery	75	60-80	10 MW	4
Fuel Cell	40	60-85	50 MW	-
Supercapacitor	95	85-95	-	-
Compressed Air	70	90	350 MW	26
Flywheel	90	80-85	100 KW	3
Pumped Hydro	90	70-80	1000's MW	Days

4.2.2 System Architecture

Proper orientation and integration of different components are key issues for the optimal operation of battery storage systems. Hence, system architecture plays a great role in photovoltaic energy storage systems. Alternative configurations place different system components at different positions. A residential photovoltaic energy storage system as shown in Fig. 4.2 has been proposed in [78]. In this arrangement, the photovoltaic power is transferred to the load through a unidirectional and a bidirectional converter, and a considerable amount of power loss occurs in each conversion stage. Hence, system efficiency deteriorates with an increasing number of power conversions. These disadvantages arise from the fact that both of the converters in the system process the photovoltaic power.

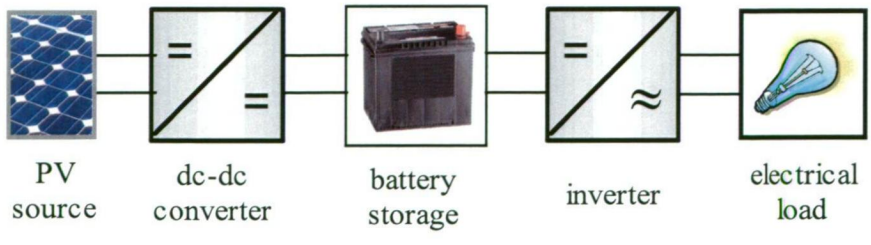

Fig. 4.2 A photovoltaic battery storage system with series connected components.

If the system is designed for dc loads, the components are to be connected as shown in Fig. 4.3. This is a very simple structure which is especially suitable for portable small photovoltaic systems and telecommunication equipment [79]. Depending on the availability of photovoltaic power, the converter used in this architecture operates as boost or buck for charging the battery and supporting the load. Hence, the converter designed for this configuration is complicated.

In some system configurations [70, 80-82], the battery-bank is directly connected to the dc bus without a bidirectional converter. This configuration requires more battery stacks and reduces the system efficiency. Also, the battery life is degraded without proper control of charging and discharging of the battery. Though series strings of storage batteries provide high voltage, a slight mismatch or temperature difference can cause charge imbalance if the series string is charged as a unit [83]. Such high voltage batteries are expensive and produce more arcing on the switches than low voltage batteries. Another problem with higher voltage batteries is the possibility of one cell failing. A faulty cell would produce lower voltage, however, in an extreme case; one open cell could break the current flow [84].

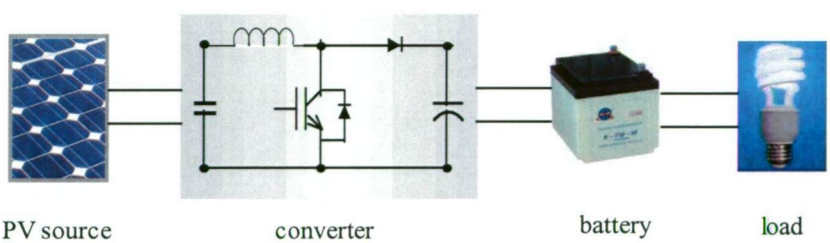

Fig. 4.3 A photovoltaic battery storage system suitable for portable dc applications.

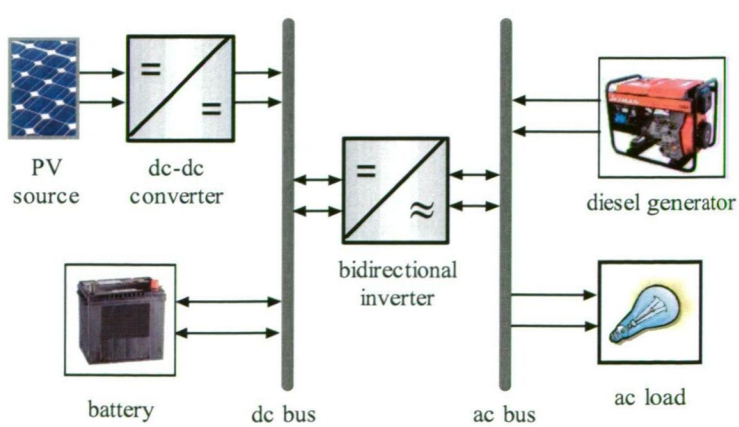

Fig. 4.4 A photovoltaic system with energy storage.

Another system architecture of the photovoltaic energy storage, as shown in Fig. 4.4, is proposed in [81]. The diesel generator employed in the system enhances reliability. But, in addition to the bidirectional inverter, another bidirectional converter is needed in this configuration to charge and discharge the battery, which increases the system complexity, resulting in complicated control.

4.2.3 Converter Topologies

Bidirectional converters are very important considerations in battery storage systems. The number of switches and others components are the main concerns for converter selection. The Cuk bidirectional converter has continuous input and output current. It needs less filtering and features reduced electromagnetic interference [85]. At nominal power, the Cuk topology offers half of the maximum current as compared with the flyback bidirectional converter [86]. Moreover, bidirectional converters based on Cuk topology, as shown in Fig. 4.5 have only two switches and two diodes.

An isolated full-bridge bidirectional converter is shown in Fig. 4.6. Here, the low voltage side is the current-fed full-bridge, and the high voltage side is the voltage-fed full-bridge. In this topology, the additional auxiliary circuit and active clamping circuit, consist of auxiliary switch, S_{aux} and clamping capacitor, C. These facilitate the zero-voltage-zero-current-switching for voltage fed side and zero-voltage-switching for current fed side. Furthermore, the resonant current between the clamping capacitor C, and the leakage inductance L_l is limited, which improves the overall performance [87].

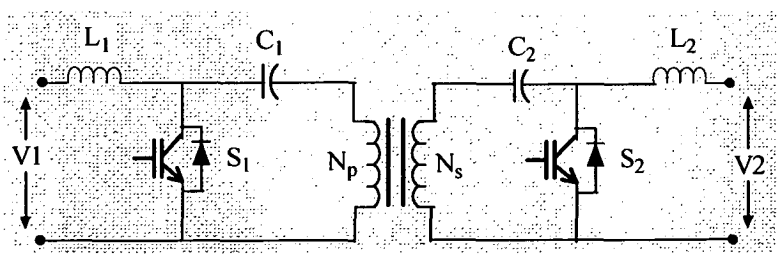

Fig. 4.5 Bidirectional dc-dc converter based on Cuk topology.

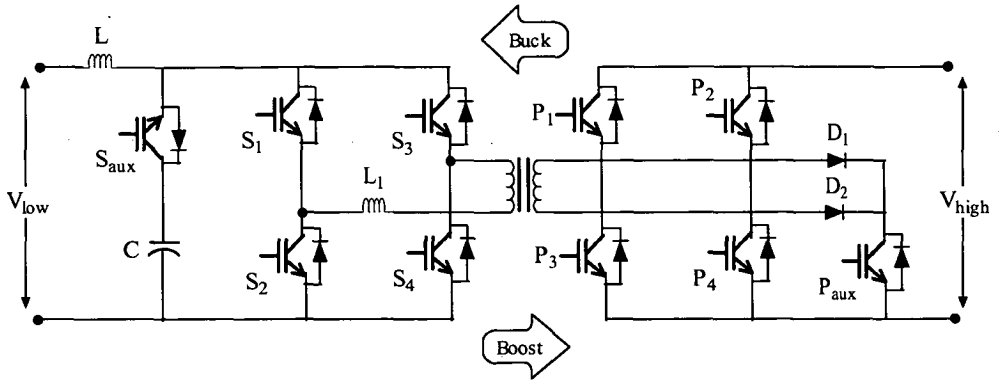

Fig. 4.6 Isolated full-bridge bidirectional dc-dc converter.

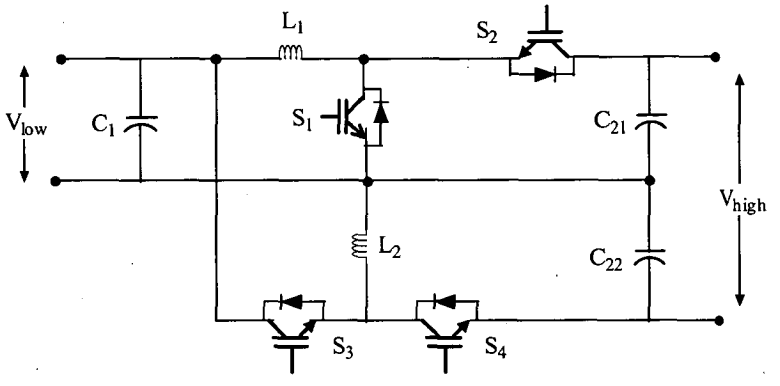

Fig. 4.7 Boost and buck-boost bidirectional dc-dc converter.

As buck and boost are basic operations needed for bidirectional converters, topologies based on buck and boost circuits are most popular. Fig. 4.7 shows a boost and buck-boost bidirectional dc-dc converter. This circuit consists of a boost and a buck-boost converter. Two converters are connected in parallel on the low voltage side, and connected in series on the high voltage side. This circuit offers zero voltage switching which reduces switching losses. This circuit is very efficient, especially for photovoltaic applications [88].

4.2.4 Control Techniques

The control technique is a vital component in photovoltaic energy storage systems. In earlier photovoltaic energy storage applications, time based energy scheduling is used to manage the mode of operation [78]. The controller employed in these methods turns the switch 'ON' to charge the battery at daytime based on the time setting. But due to overcast weather, battery charging may be disrupted.

Nowadays, the most common method of regulation and control of batteries are based on estimation of the state-of-charge of the battery. Different algorithms exist to measure the state-of-charge of the battery. Some algorithms rely on records of battery history and characteristics. Other algorithms are based on online monitoring and measurements. Usually, the charging is stopped at a specific high voltage disconnect point, chosen to allow a limited amount of gassing, charge equalization and electrolyte agitation, without excessive loss of electrolyte. Similarly, discharge is stopped at a specific low voltage disconnect point, chosen to maintain a reasonable battery life.

Common approaches to determining when the batteries are fully charged rely on measuring battery terminal voltage by direct measurement of the battery voltage, or determining the dV/dt, or measuring the battery impedance changes with charging.

Moreover, when the battery approaches to the full state-of-charge, the temperature begins to rise sharply. So a thermistor can detect the charge termination when dT/dt (where T is the temperature of the battery) is above a threshold value, meaning, charge is halted when the slope of the temperature curve rises above a threshold value. Temperature based detection is considered more accurate than voltage-based detection because the detection usually happens at the full state-of-charge. As can be seen in Fig. 4.8, the voltage method leads the cell to overcharging for a certain time until the voltage drop is detected [82].

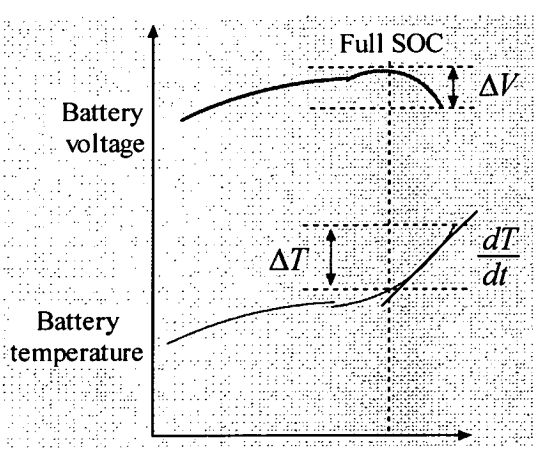

Fig. 4.8 Voltage and temperature profile of a battery for detecting SOC.

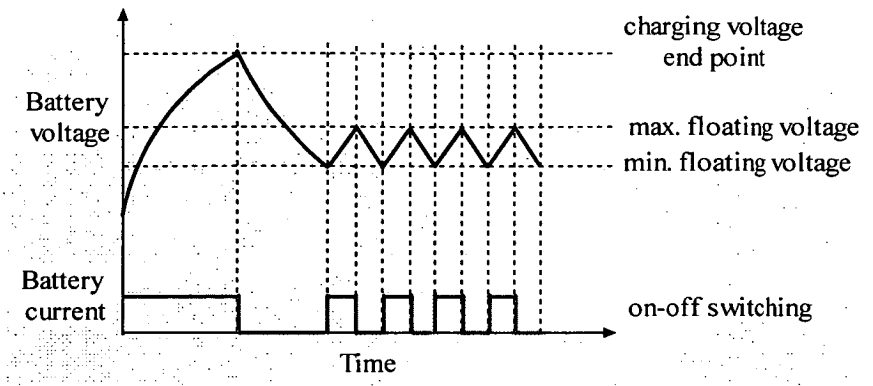

Fig. 4.9 Battery charging based on on-off control.

A battery charging approach is presented in [89] based on on-off control as shown in Fig. 4.9. The PV current is supplied to the battery and the battery voltage is regulated within a floating voltage level. A disadvantage of this method is that during the off time of the controller, no energy is transferred to the battery which lengthens the charging process.

An algorithm based on ampere-hour measurement is proposed in [81]. In this algorithm the battery SOC is estimated as:

$$SOC_{k+1} = SOC_k + \frac{\sum_t (I_{bat}(t) - I_{gas})\Delta t}{C} \tag{4.1}$$

where, SOC_k and SOC_{k+1} are the battery state of charge at steps k and $k+1$ respectively, I_{bat} is the battery current, I_{gas} is the battery losses and Δt is the time interval and C is the nominal capacity in ampere-hour.

Batteries can be charged in several different manners. These are float charging, intermittent charging, multiple rates charging, and interrupted charging.

A. Float Charging

Float charging is performed with constant voltage applied continuously to the battery throughout its lifetime, and the battery is allowed to draw as much current as required. This method is very common in standby power applications [90].

B. Intermittent Charging

In this method of charging, the battery voltage is monitored to reach a threshold value. When the battery reaches the upper voltage threshold, charging is stopped and the battery is kept in open circuit. The battery voltage is monitored until it drops to the lower voltage threshold, when charging begins again [91].

C. Three Stage Charging

Three state charging, delivers power to the battery in three steps. The first step is bulk charging. The battery is charged at maximum current until it reaches its final charging voltage. This step replaces 70-80 % of the battery's capacity at the fastest possible rate. The battery is kept in this mode until the charge voltage reaches the upper voltage threshold. The charging current is steadily decreased while the battery voltage is maintained at the absorption voltage. The final stage is float charging. A small current is supplied to the battery to maintain the battery voltage [92].

D. Interrupted Charging

Another battery charging algorithm is interrupted charging. This method charges the battery in four modes. At first, the battery is charged with constant current with a charge rate of 0.1C to an upper threshold, and then left in open circuit until the lower threshold limit is reached. The battery is then pulse charged with a charge rate of 0.05C until the upper voltage limit is reached again. These are the charge rates chosen for optimum operation. The battery is then left in open circuit and is at full capacity [92, 93].

4.3 Proposed Control Technique

The proposed battery charger algorithm, as shown in Fig. 4.10, uses the data obtained from the dc bus power and the battery state of charge. Depending on the system operating conditions, the operation mode controller generates the control signal. To balance the power flow in the system and to achieve power conditioning compatibility, this controller operates readily. The battery state-of-charge is adjusted to match the power demand of the load. For this reason, the inner power loop works with the outer battery state-of-charge to adjust the charging algorithm.

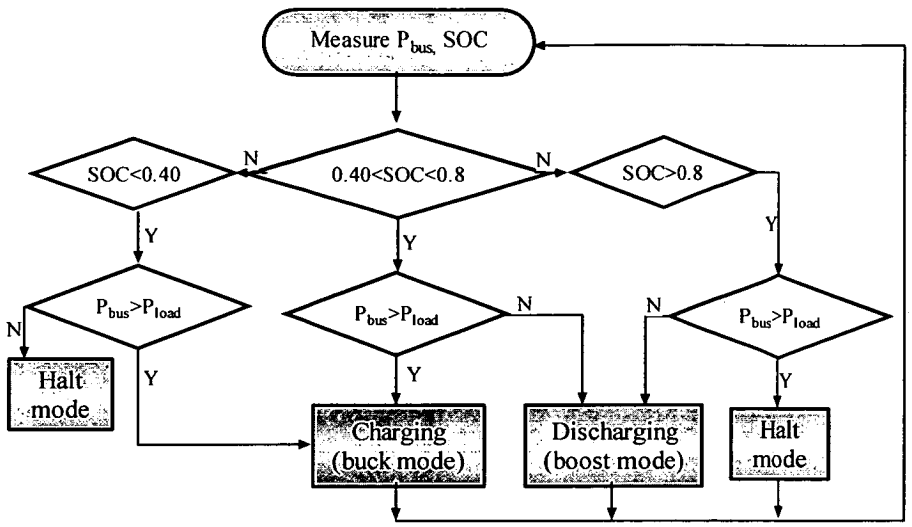

Fig. 4.10 Bidirectional converter (battery charging/discharging) control algorithm.

If the battery state-of-charge is below 80% and the dc link has sufficient power from the PV module to charge the battery, then the bidirectional converter acts as a buck converter and charges the battery. On the other hand, if the battery state-of-charge is above 40% and the load needs support from the battery, then the bidirectional converter acts as a boost converter and delivers power from the battery to the load. Whenever the battery is overcharged or has no sufficient charge to deliver, then it automatically goes to the halt mode.

Control of the bidirectional converter is the key factor of the power management. To manage the energy exchanges between the dc link, the PV module and the storage device, three operating modes are employed which are charging, discharging and halt mode.

4.4 System Configuration

4.4.1 Power Management

The purpose of the power management is to satisfy the load power demand and to maintain the state of charge of the battery bank within a specified limit to prevent blackouts and to extend the battery life. The power management block diagram is

presented in Fig. 4.11. As there are two energy sources in the system, it requires managing the sources to ensure reliability, optimal operation and cost effectiveness. In this case, the photovoltaic generation profile, the residential load profile and the battery storage profile needs to be considered. The concept of energy transfer is achieved by using a novel control algorithm incorporated with the bus power and battery state-of-charge.

4.4.2 Controller Implementation

The control strategy used here consists of three parts. First part is the converter controller for voltage regulation, the second part is the battery charging and discharging controller using the bidirectional converter, and the third part is the inverter controller for obtaining ripple-free power. The block diagram of the control mechanism is shown in Fig. 4.12.

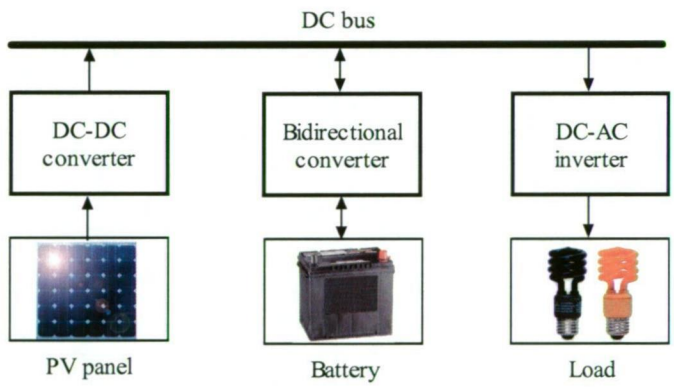

Fig. 4.11 Power management of the photovoltaic energy storage system.

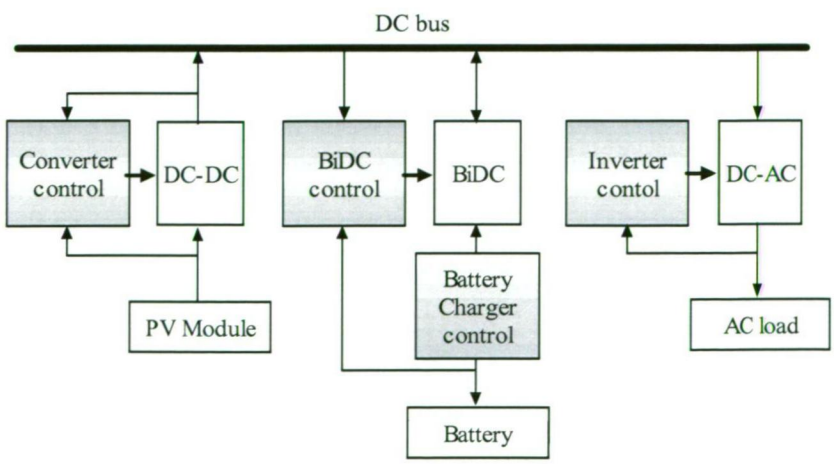

Fig. 4.12 Control circuit of the photovoltaic system, with energy storage.

4.4.3 Bidirectional Converter Control

The efficiency, reliability and dynamic performance of the system relies on the operation of the bidirectional converter under different modes of operation, so that individual parts of the system can operate properly. A buck-boost type high performance bidirectional converter, as shown in Fig. 4.13, is used to charge and discharge the battery [94]. This bidirectional converter has following properties, which enhance its performance: a) power flow with large voltage diversity, b) high step-up and step-down ratio, c) soft switching and zero voltage switching, d) reduced switching losses due to fewer switches, e) less conduction losses, f) synchronous rectification, g) no transformers, h) no magnetizing current saturation, i) less weight and volume.

The voltage gain of the bidirectional converter in the buck state can be expressed as [94],

$$G_{V1} = \frac{V_L}{V_H} = \frac{d_3(1-d_3)}{N(1-d_3)+1} \tag{4.2}$$

and the voltage gain of the bidirectional converter in the boost state can be represented as,

$$G_{V2} = \frac{V_H}{V_L} = \frac{2+N}{1-d_1} \tag{4.3}$$

where, V_L and V_H are the battery terminal voltage and dc link voltage respectively. d_3 and d_1 are the duty cycle of switch S_3 and S_1 respectively. N is the turn ratios of the coupled inductor L_P and L_S, as shown in Fig. 4.13.

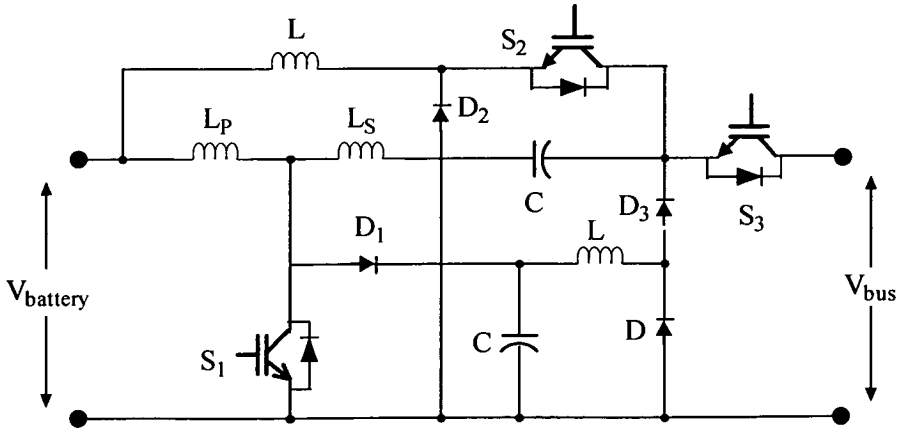

Fig. 4.13 Bidirectional converter circuit diagram.

4.4.3.1 Charging Operation

The bidirectional converter operates in buck mode during charging the battery. Three switches are used during charging operation. The circuit operation at different modes of one switching cycle is shown in Fig. 4.14. During mode 1, the switches S_1 and S_2 are OFF, and the switch S_3 is ON. In this mode, the current flows through the diode D_2 to charge the battery. In mode 2, all switches are OFF. For the period of mode 3, the switch S_2 is ON, and the switches S_1 and S_3 are OFF. Again, in mode 4, all switches are OFF. During mode 5, the switches S_1 and S_3 are ON, and the switch S_2 is OFF. Finally, in mode 6, the switches S_1 and S_2 are OFF, and the switch S_3 is ON. Fig. 4.15 shows the switching pulses goes to the different switches at different modes of operation.

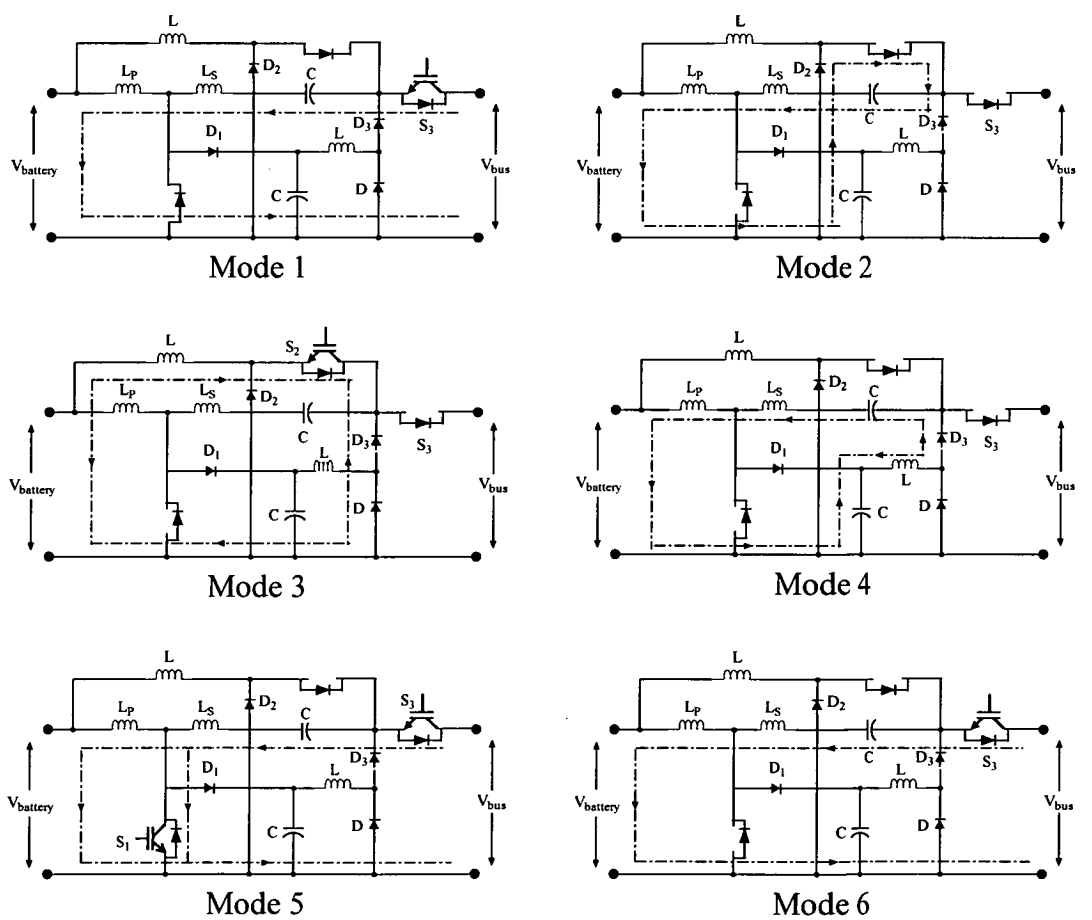

Fig. 4.14 Bidirectional converter operations in charging mode.

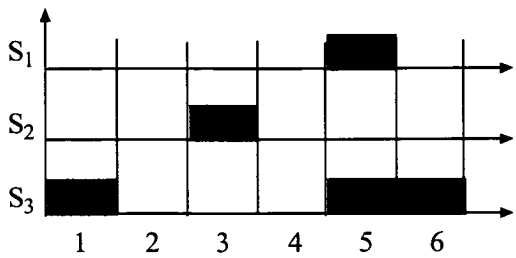

Fig. 4.15 Charging switch state.

4.4.3.2 Discharging Operation

The bidirectional converter operates in boost mode while discharging the battery. Two switches, S_1 and S_3, are used during discharging operation. The circuit operation at different modes of one switching cycle, and the state of different switches are shown in Fig. 4.16. During mode 1, the switch S_1 is ON, and the switch S_3 is OFF. In mode 2, the switch S_1 is OFF, and the switch S_3 becomes ON. For the period of mode 3, the switches S_1 and S_3 are OFF. Again, in mode 4, the switch S_1 is OFF, and the switch S_3 becomes ON. During mode 5, the switches S_1 and S_3 are ON.

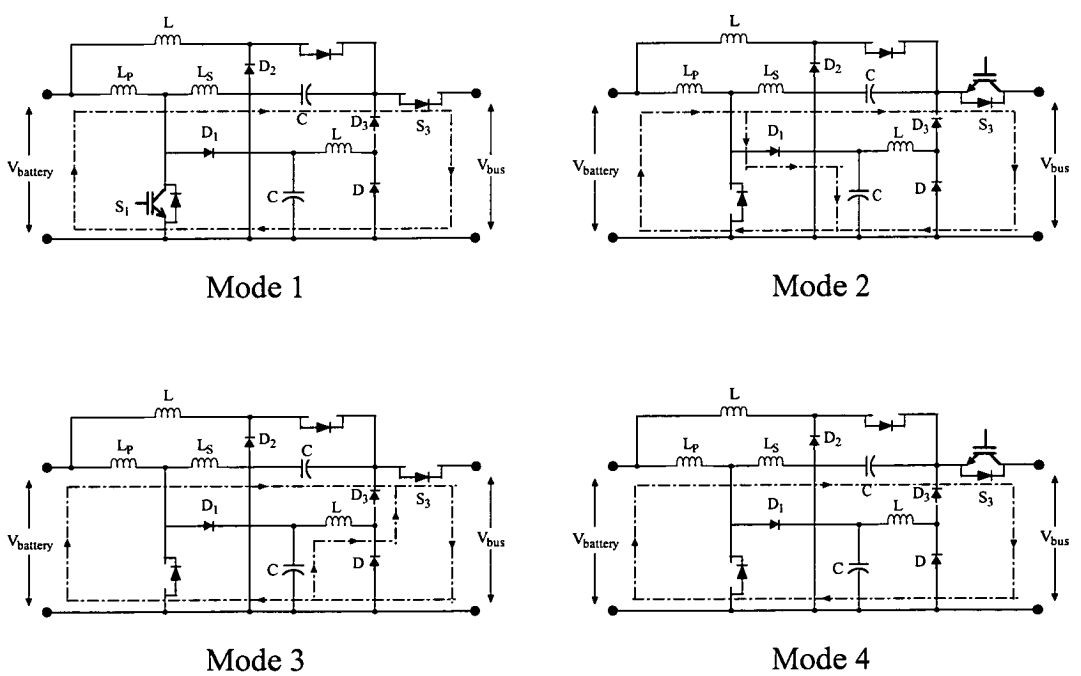

Mode 1 Mode 2

Mode 3 Mode 4

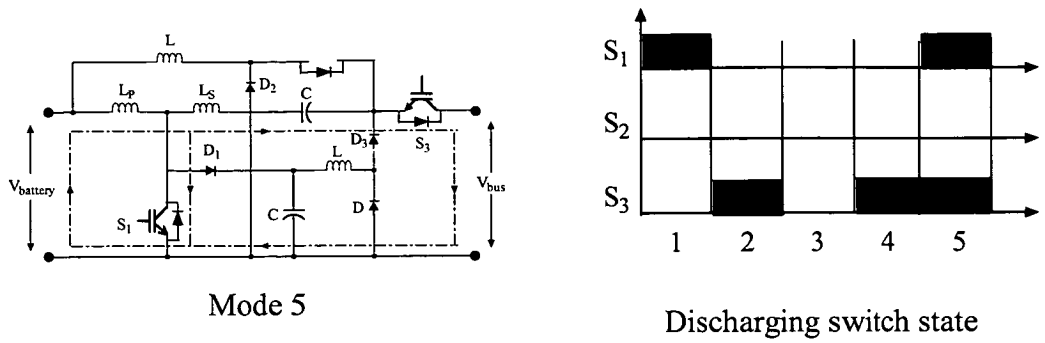

Mode 5

Discharging switch state

Fig. 4.16 Bidirectional converter operations in discharging mode.

4.4.4 Battery Model

A lead-acid battery model is used as per the system power requirements. The rated capacity of the battery model is set at 500 Ah. This rated capacity can support 2kW loads for approximately 32 hours according to Peukerts law defined by the equation,

$$C = I^P t \tag{4.4}$$

where, C is the battery capacity (Ah), I is the discharge current (A), P is the Peukert's constant and t is the discharge time (hour). For lead-acid battery, the value of P is between 1.1 and 1.3.

Battery type, initial state of charge and discharge characteristics can be set in this model. The lead-acid battery has discharging characteristics without exhibiting memory effect and superior life-cycle costs for the PV power system applications [95-97]. The charger regulates the state of charge of the battery within 40% to 80%, as the overcharging and deep-discharging of the battery may degrade the capacity and shorten the battery life-cycle. Infrequent or inadequate recharging can also cause over discharging symptoms called sulfation. The choice between using more batteries operating at shallower discharge rates to extend the life of the batteries vs. using fewer batteries with deeper discharge rates and the correspondingly lower initial cost is considered carefully [98].

Table 4.2 System specifications of the photovoltaic energy storage system

Subsystems	Specifications
PV module	3kW (peak), I_{sc}=5.45A, V_{oc}=22.2V
DC-DC converter	Boost, V_{in} = 180 ~220V, V_{out}= ~380V, Hysteresis current control switching, f_s=25kHz
Bidirectional converter	V_{low}= 48V, V_{high}=380V, Buck-Boost, PWM switching
Battery	48 V, 500 Ah, Lead-acid
Inverter	PWM IGBT, V_{in}= 380V dc, V_{out}= 230V rms, 50 Hz
Load	2kW

4.5 Simulation Results and Discussion

Simulation results show the voltages and currents at the different stages of the PV simulation system. Fig. 4.17 shows the current and voltage of the output of the dc-dc converter. The dc-dc converter gives the output voltage of around 380V at the dc link which is either processed by the inverter to support the load or fed through the bidirectional converter to charge the battery. As can be seen from the Fig. 4.17, at the time of charging the battery, the dc link voltage goes down as more loads are imposed on the dc link. At this time, however, the voltage falls by 5% from the stable level. The hysteresis current control technique works well to stabilize the dc link voltage. Here, the current through the converter is about 5A though it contains a high percentage of ripples. The limit of the converter current is important as it is used to estimate the rating of the switches and the values of the other parameters which are used in the converter circuit.

The terminal voltage and the state of charging and discharging of the lead-acid battery are shown in Fig. 4.18. The battery voltage remains almost constant at 48V

during the discharging mode of operation. In the charging mode, however, it goes up to 60V. The battery charging and discharging is done uniformly within the specified limit of the state of charge. The charging and discharging of the battery depends on the battery capacity and the load demands. As the battery capacity is set to a higher value and the load is set to a lower value then it takes more time for the charging the battery than the discharging, and vice versa. The charger regulates the state of charge of the battery within 40% to 80%, as the overcharging and deep-discharging of the battery may degrade the capacity and shorten the life span of the battery.

As it is discussed earlier, the bidirectional converter acts as a buck-boost converter. During the charging time, it converts 380V of dc bus voltage to the battery terminal voltage of 48V. Whereas during the discharging time, the bidirectional converter boosts the 48V of battery terminal voltage to the 380V of dc link voltage. Fig. 4.19 shows the battery terminal voltage and dc bus voltage. The current through the low and high voltage side of the bidirectional converter is shown in Fig. 4.20. The direction of the current through the bidirectional converter shows the charging and discharging modes of operation.

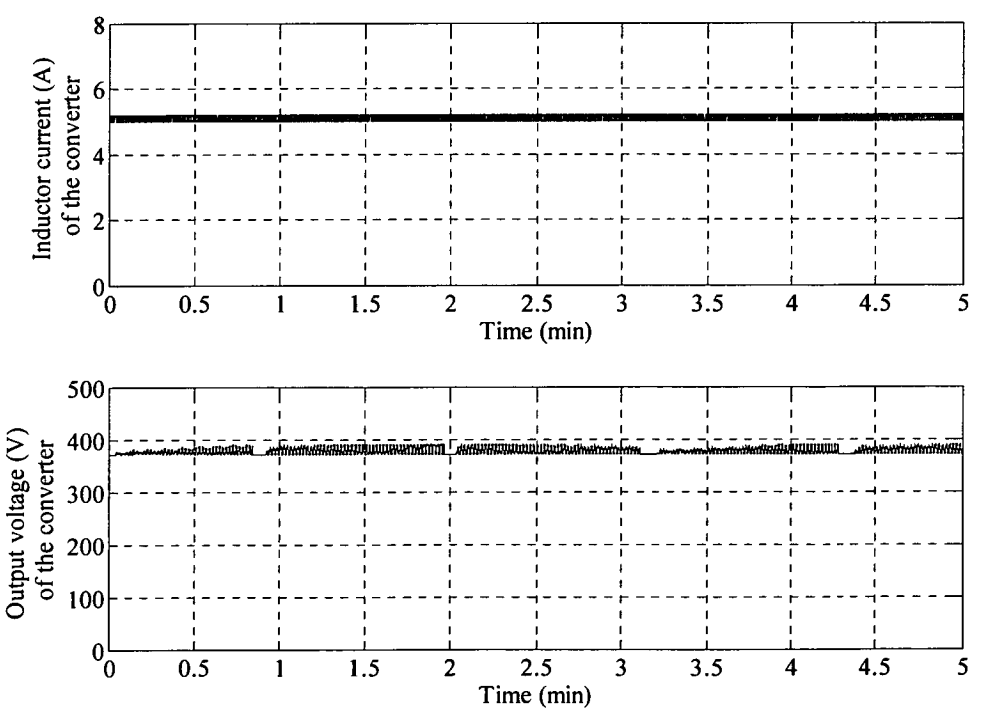

Fig. 4.17 Current and voltage at the dc bus.

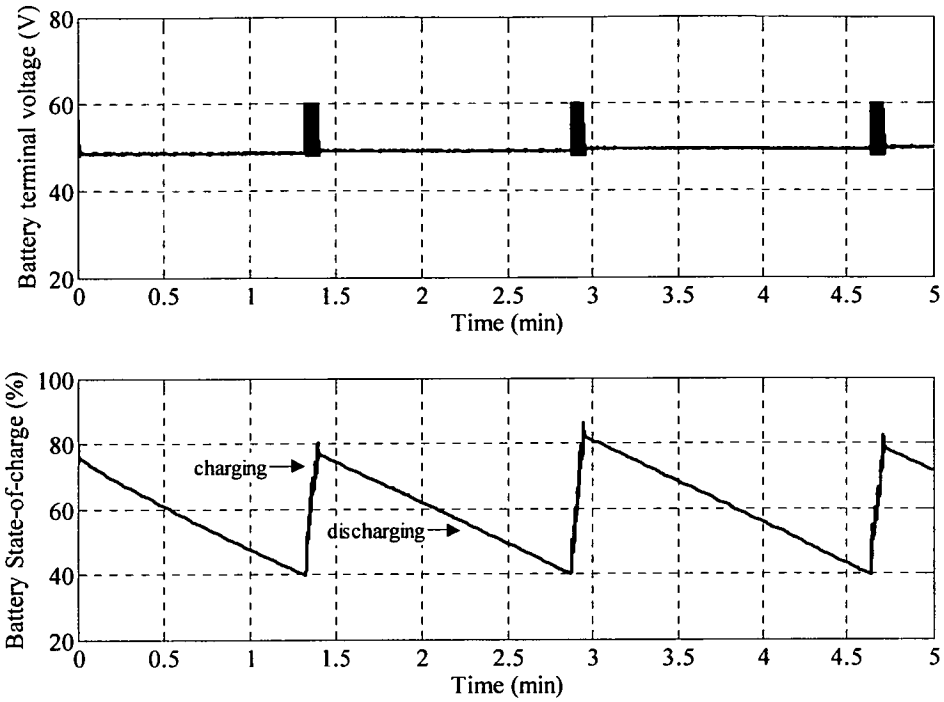

Fig. 4.18 Voltage and state of charge of the lead-acid battery.

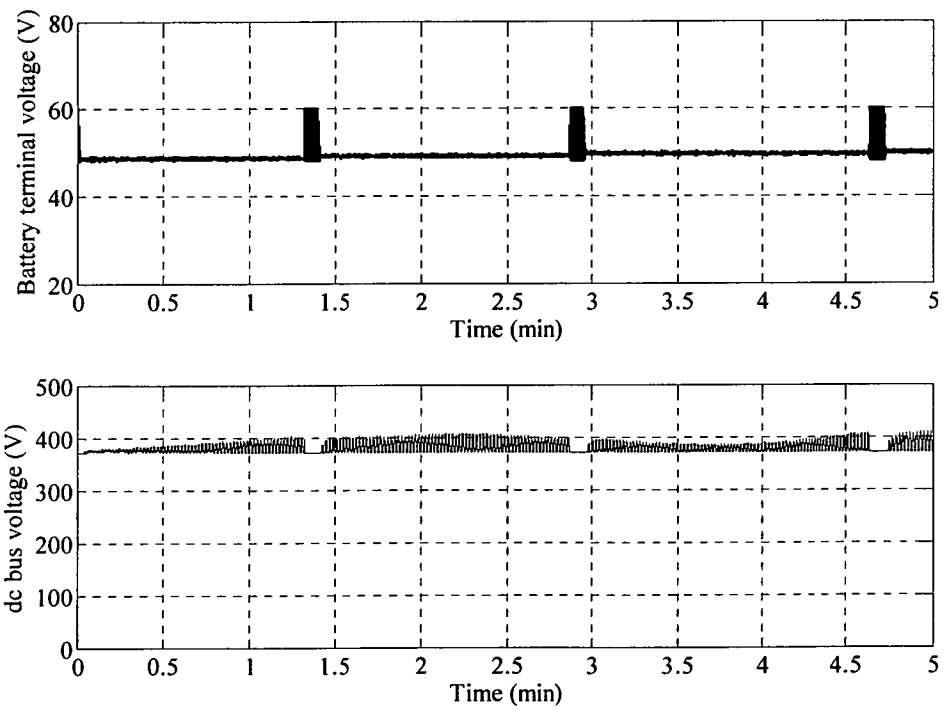

Fig. 4.19 Battery terminal voltage and dc bus voltage.

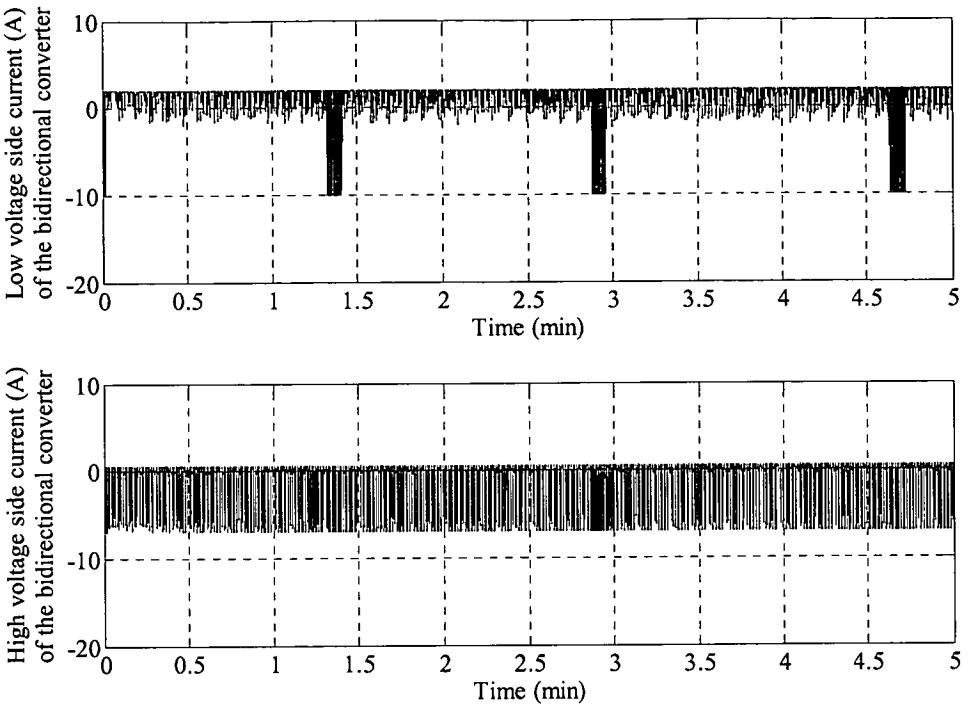

Fig. 4.20 Current in the bidirectional converter at low and high voltage side.

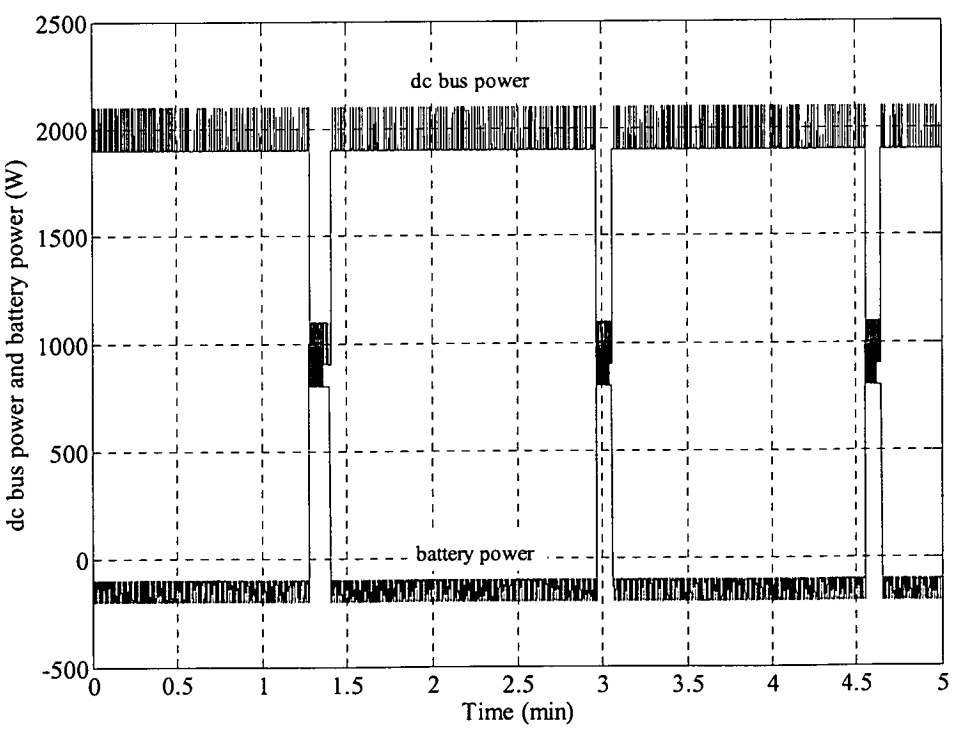

Fig. 4.21 dc-bus power and battery power.

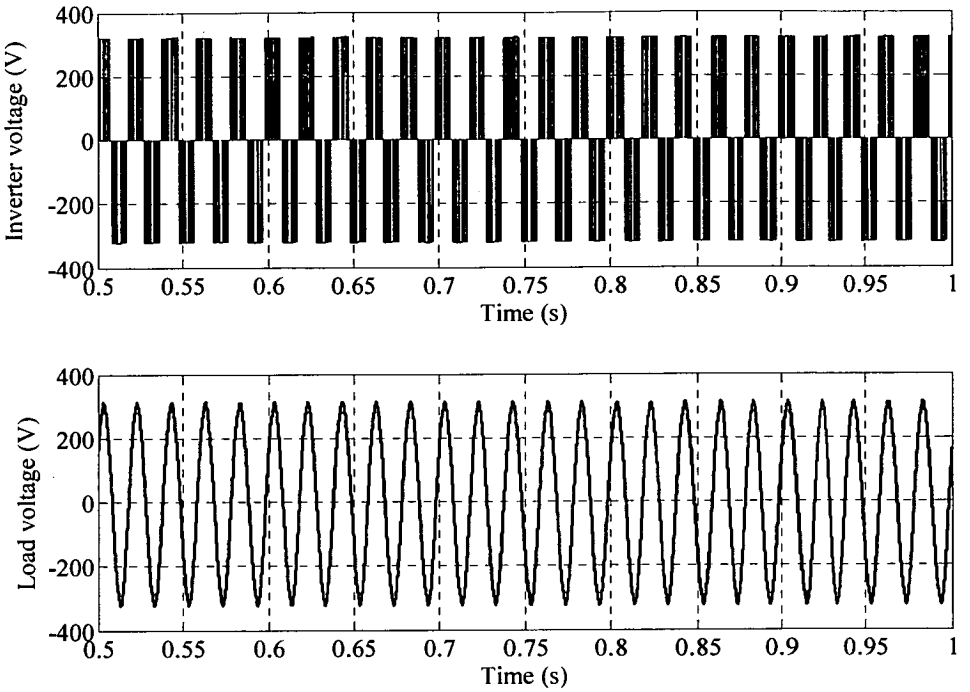

Fig. 4.22 Inverter output voltage and load voltage.

The system is designed for 2kW load, hence the PV module and the battery supplies that amount of power to the load. As can be seen from Fig. 4.21, the PV module is used to supply 2kW power to the load as well as to charge the battery. When the power level of the dc bus goes down from 2 kW to about 1kW, the battery supplies the necessary 1kW power to the load. This confirms the power transfer among the dc bus, battery and load.

The output voltage of the inverter and the load voltage are shown in Fig. 4.22. The inverter output provides a 230 V rms voltage with 50 Hz frequency while 2 kW, 3-phase load is fed by the PV system.

4.6 Conclusion

This chapter presents an efficient control scheme for versatile power transfer among the PV source, the storage battery and the load. A high efficiency bidirectional converter-based battery charger control algorithm is designed for the effective management of battery charging and discharging. The bidirectional converter

between the dc link and the battery ensures proper charging and discharging as well as secure control over the battery. The modes of operations of the battery charger are designed to make flexible management and to improve the reliability of the whole system through quick control incorporating the assessment of the dc link power and the battery state of charge. The supervision of the dc link power and the battery state-of-charge makes the control scheme well-organized to manage safely the battery charger. The modeling and simulation of the system under the proposed control strategy is done with the Simulink/Simpower dynamic software simulation system. Simulation results are provided to justify the proposed control algorithm. The simulated system performs well with a 3kW PV source, a boost-type dc-dc converter, a buck-boost type bidirectional converter, a battery bank and a PWM IGBT inverter to support a 2 kW load. The hysteresis current control method is used to control the dc-dc converter and vector control method is used to control the inverter. A novel control strategy is proposed as the bidirectional converter-based battery charge controller. Simulation study confirms the feasibility and effectiveness of the control strategy and shows the successful coordination of the versatile power transfer. The proposed control algorithm is able to supply the dc link power effectively either to the load or to the battery according to the requirements, as well as to take power from the battery and to protect the battery from overcharging, and thus ensures a long life and an efficient management system for the battery.

Chapter 5

Hardware Implementation and Experimental Evaluation of Current Mode Control of DC-DC Converter

5.1 Introduction

The employment of current mode control techniques for dc-dc converter controllers is investigated in Chapter 3 through MATLAB/Simulink software simulation. This chapter deals with the experimental investigation of the current mode control techniques for dc-dc converter controllers of photovoltaic power systems. Real time control of the dc-dc converter is experienced through the dSPACE DS1104 controller board. The controller consists of a real time processor, a controller board, a connector panel, and hardware-software interfacing systems.

Real time data are collected through the I/O interfacing connector panel and processed inside the real time processor (RTP). The real time application is downloaded and executed in the memory of the dSPACE board. Then the switching signals are fed back to the converter through the I/O interfacing connector panel. The ControlDesk installed in the host PC is the central tool for experimenting with dSPACE systems. In order to observe the behaviour of the real time application and to change application-specific parameters, the dSPACE experimentation tool ControlDesk is used. The real time interface (RTI) is the interface between the Simulink and the dSPACE platform [99].

In this chapter, firstly, data acquisition and digital signals processing are discussed in this chapter. The dSPACE DS1104 R&D controller board, real time implementation, and dSPACE-Simulink interfacing are discussed in the following subsections. In the next sections, hardware implementation, including of the voltage sensor, current sensor, and IGBT driver circuit are presented. Then, experimental components and experimental set up are presented. Finally, the experimental results and discussion are presented, followed by the conclusion.

5.2 Data Acquisition and Digital Signal Processing

Voltage and current from the electrical circuit are obtained by transducers and manipulated for generating control signals. The control signals then drive the IGBT switches of the converters. This data acquisition and signal processing involves sensing, signal conditioning, sampling and manipulating. Fig. 5.1 shows the data acquisition and signal conditioning systems as a block diagram. As this process involves both analog and digital data, there is both analog to digital (A/D) and digital to analog (D/A) conversion. Here the converter circuit, sensors, signal conditioning circuits, ADCH 1 and DACH 1 are implemented in the hardware. Conversely, the DS1104 ADC_C1, digital signal processor and DS1104 DAC_C1 are implemented in the software. The hardware part is a prototype photovoltaic power system and associated sensor circuits. The software part is built in the MATLAB/Simulink environment. The dSPACE controller system is used as the software-hardware interfacing medium. The dSPACE system consists of the DS1104 R&D controller board mounted within a PC, a breakout panel for connecting signal lines to the DS1104 board, and software tools for operating the DS1104 board through the MATLAB/Simulink block diagram.

Digital control of switch-mode power converters is becoming popular due to the availability of low cost, high performance DSP controllers with enhanced and integrated A/D converters and pulse width modulators. DSP based digital control allows flexibility of control, real-time hardware-software interfacing, high speed signal processing and quick modification facilities. Moreover, digital controllers are less susceptible to aging and environmental variations and have better noise immunity.

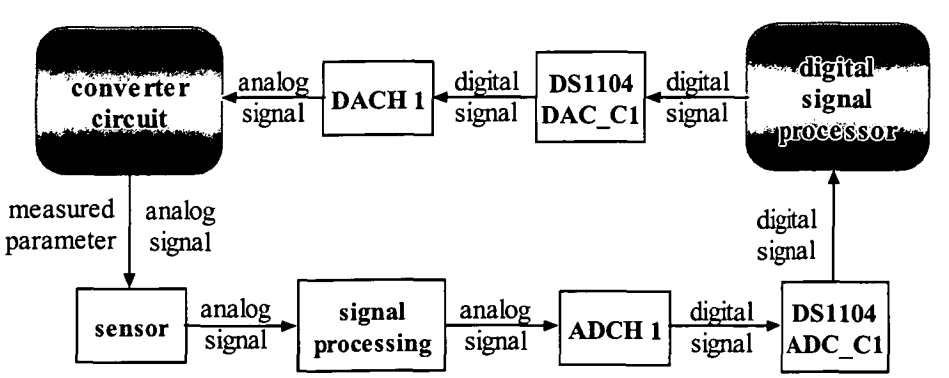

Fig. 5.1 Data acquisition and signal processing block diagram.

5.2.1 dSPACE DS1104 R&D Controller Board

A dSPACE DS1104 R&D controller board is used to obtain the data and to manipulate it to generate necessary control signals. The obtained signals from the circuits are processed inside the processor in digital form. The processor can be accessed from the host computer for on-line monitoring and parameter tuning. The dSPACE software first translates the MATLAB/Simulink block diagram into C code. Then it compiles the C code to form an executable file for the processor residing on the dSPACE DS1104 board. Afterwards, dSPACE software downloads the executable code to the processor of the dSPACE DS1104 board.

The dSPACE DS1104 has eight 16 bit D/A converters each with a output range of 10 V and can be the source or sink of up to 5mA. The output voltage of the D/A converter can be varied from -10V to +10V in 0.305 mV steps. The dSPACE DS1104 contains eight A/D channels – the first 4 channels share a single 16-bit a/D converter through an analog multiplexer, the remaining 4 channels each have a dedicated 12-bit A/D converter. Connections to the A/D and D/A converters are made using BNC connectors [100].

5.2.2 Real Time Implementation

The controllers are designed in the MATLAB/Simulink and are executed in real time using the dSPACE DS1104 DSP board. Once the controller has been built in Simulink block-set, machine codes are achieved that run on the DS1104 TMS320F240 DSP processor. While the experiment is running, the dSPACE DS1104 provides a mechanism that allows the user to change the controller parameter online. A dSPACE connector panel (CP1104) provides easy access to all input and output signals of the DS1104 board. All currents and voltages are measured using the sensors which will be input to the analog to digital conversion channel (ADCH). The output switching signals from the controller board come through the CP1104 and use the digital to analog conversion channel (DACH) [101].

5.2.3 Integrating dSPACE and Simulink

The dSPACE DS1104 DSP board forms the core of the closed loop system. Aside from the duties of controlling the operator interface, it performs the acquisition of the feedback signal, computes an error signal, delivers the error signal to the control algorithm, and executes the control algorithm to determine a control signal. The control algorithm is built within a Simulink environment combined with the RTI provided by dSPACE and is implemented by the main processor of the DS1104 board in real time [102].

Once the controller has been built in a Simulink block diagram, the designer can utilize the MATLAB real time workshop (RTW) routine that can automatically produce C code from the Simulink block diagram. The C code generated by the RTW is used with the real time hardware dSPACE DS1104 DSP-board for real time control. Then the interface between Simulink and the dSPACE DS1104 DSP-board allows the algorithm to be run on the hardware of the DS1104.

5.2.4 dSPACE Hardware-Software Interfacing

External input to the board (sensed voltage or current) –

Function	Signal	BNC connector	Nature of signal	Input	RTI block
Analog to digital conversion for the analog input channels	ADCH1	CP1	One 16 bit ADC with four multiplexed input signals	-10V to +10V	DS1104MUX_ADC
	ADCH2	CP2			
	ADCH3	CP3			
	ADCH4	CP4			
	ADCH5	CP5	Four 12-bit parallel ADCs with one input signal each		DS1104ADC_Cx
	ADCH6	CP6			
	ADCH7	CP7			
	ADCH8	CP8			

External output from the board (switching signals) –

Function	Signal	BNC connector	Nature of signal	Output	RTI block
Digital to analog conversion for the analog output channels	DACH1	CP9	8 parallel DAC channels	-10V to +10V -5mA to +5mA	DS1104DAC_Cx
	DACH2	CP10			
	DACH3	CP11			
	DACH4	CP12			
	DACH5	CP12			
	DACH6	CP14			
	DACH7	CP15			
	DACH8	CP16			

5.3 Hardware Implementation

5.3.1 Voltage Sensor and Conditioning Circuit

The voltage sensor circuits are designed to sense the output dc voltage of the dc-dc converter and feed it to the feedback controller. The details of the voltage sensor and conditioning circuits are shown in Fig. 5.2. The voltage is measured using a LEM LV-25P voltage transducer. The voltage to be sensed is fed through the input terminal of the transducer. A current proportional to the sensed voltage flows through the input resistor 47k. The current, flowing in the primary circuit, produces a current in the secondary side of the LV 25-P voltage transducer. The secondary current multiplied by the R is the output voltage of the sensor.

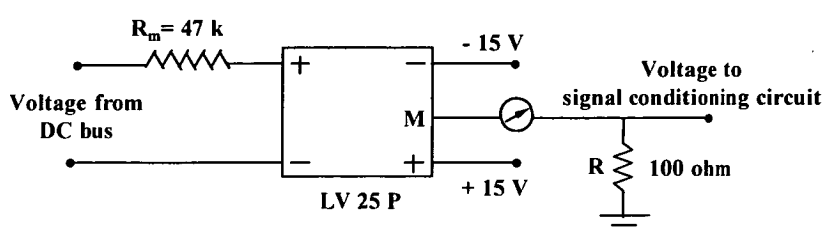

Fig. 5.2 Voltage sensor circuit.

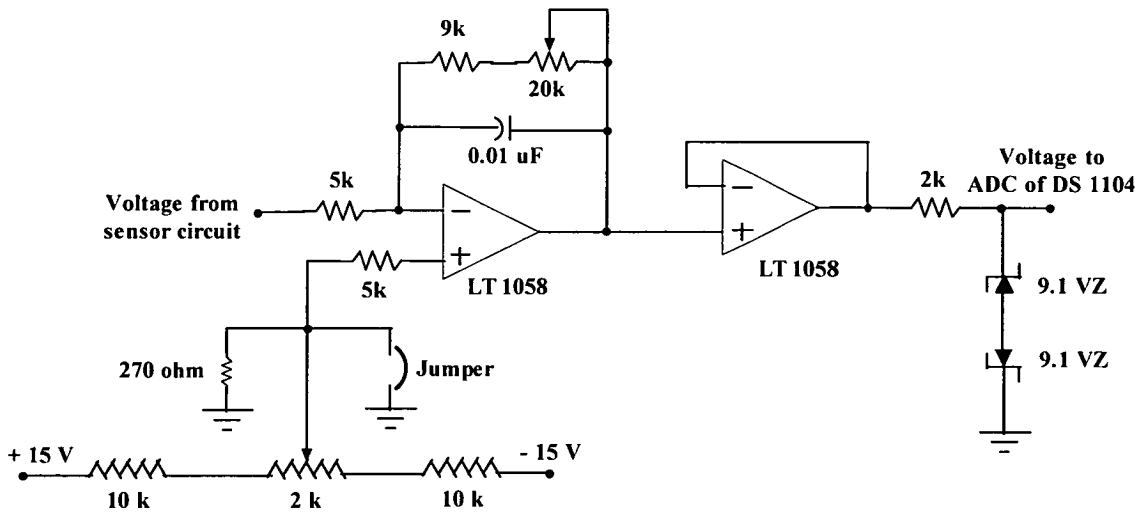

Fig. 5.3 Sensed voltage conditioning circuit.

The voltage conditioning circuit is shown in Fig. 5.3. The adjustment of the 20k potentiometer regulates the precision of the conditioning of the sensed signal. This is adjusted in such a way that the maximum voltage to be measured can give ±10V peak value. An LT1058 high speed op amp (operational amplifier) is used to process the sensed signals. The output of the voltage conditioning circuit is connected through the BNC connectors to the dSPACE connector panel CP1104. This signal is then connected to the DS1104ADC_C1 of the MATLAB/Simulink model.

5.3.2 Current Sensor and Conditioning Circuit

The current transducer LA 100-P/SP13 is used in the current sensor circuit. The basic principle of current sensing is based on the Hall-effect. The primary current produces magnetic flux which results in secondary voltage proportional to the primary current. This transducer uses galvanic isolation between the primary circuit and secondary circuit to measure currents. Fig. 5.4 shows the simple representation of the current transducer connection.

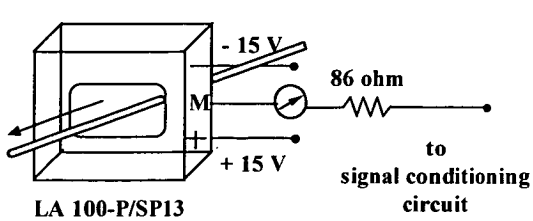

Fig. 5.4 Current sensor circuit.

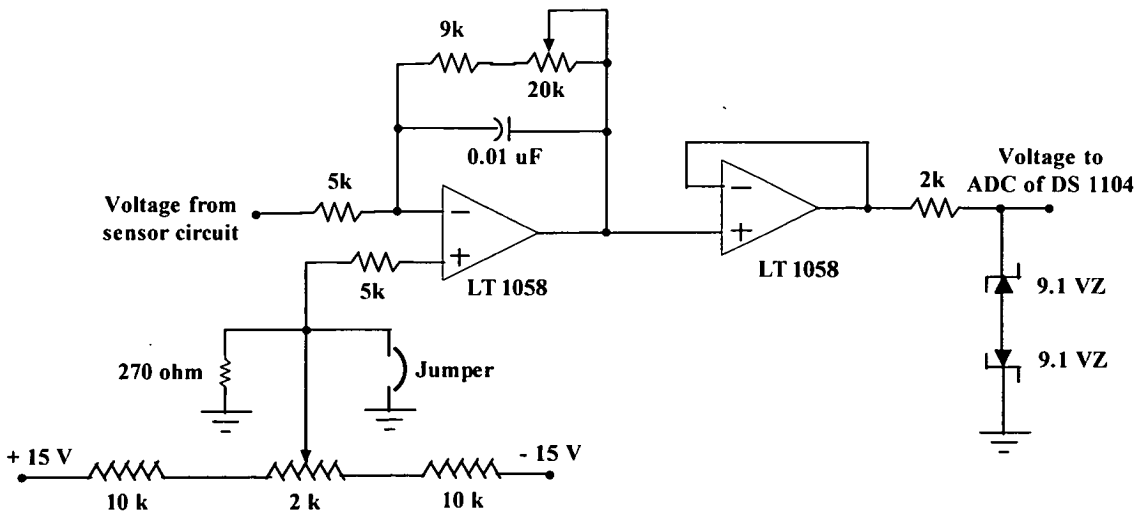

Fig. 5.5 Sensed current conditioning circuit.

The current conditioning circuit is shown in Fig. 5.5. This is almost the same as the voltage conditioning circuit. The output voltage signal obtained from the current transducer is fed to the dSPACE connector panel CP1104. This signal is then connected to the DS1104ADC_C2 of the MATLAB/Simulink model.

5.3.3 IGBT Driver Circuit

The Agilent HCPL3180 IGBT gate drive optocoupler is used as the gate drive circuit. The proper selection of gate resistance greatly affects the performance of the gate drive circuit. The connection of the IGBT gate drive circuit is shown in Fig. 5.6.

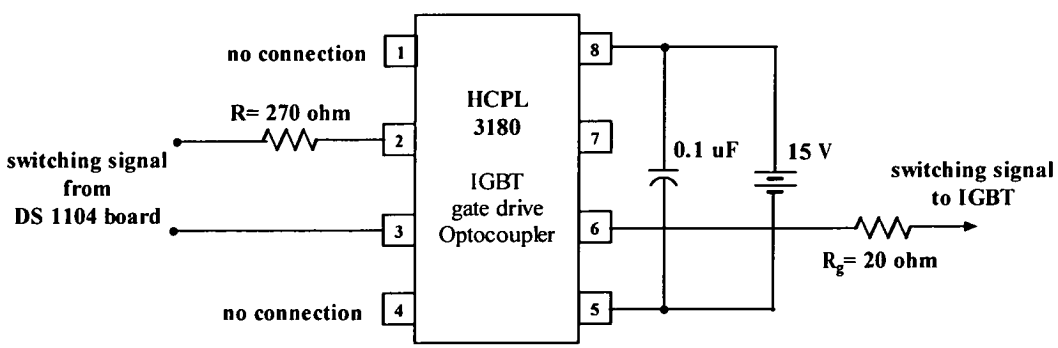

Fig. 5.6 Gate drive optocoupler circuit to process IGBT switching signal.

5.4 Experimental Components and Setup

5.4.1 BP-380 80W Photovoltaic Module

Two 80W photovoltaic modules are used as photovoltaic source. 36 polycrystalline cells are connected in series in each module. The nominal voltage is 12V. The voltage and current at maximum power point are 17.6V and 4.6A respectively. Fig. 5.7 shows the photovoltaic module used in the experiment.

5.4.2 Stafford Halogen Lamp

Two Stafford 500W work-lights are used for convenient illumination of the photovoltaic module. The light intensity can be tuned for experimental investigations. Fig. 5.8 shows the halogen lamp used in the experiment.

5.4.3 Voltage and Current Sensors, and IGBT Driver

The voltage sensor circuits, current sensor circuits and IGBT driver circuits are described in section 5.3. Figs. 5.9 and 5.10 show the voltage sensor circuit, current sensor circuit and IGBT gate drive optocoupler implemented in the breadboard.

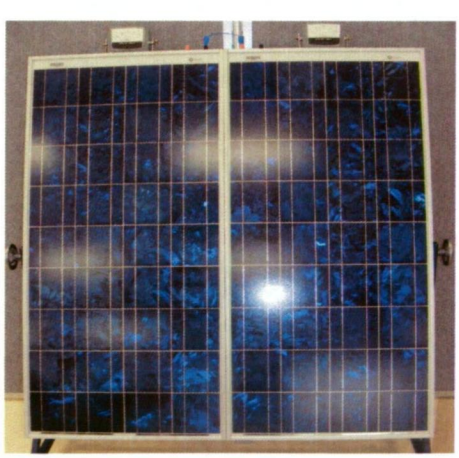

Fig. 5.7 Photovoltaic module.

Fig. 5.8 Halogen lamp.

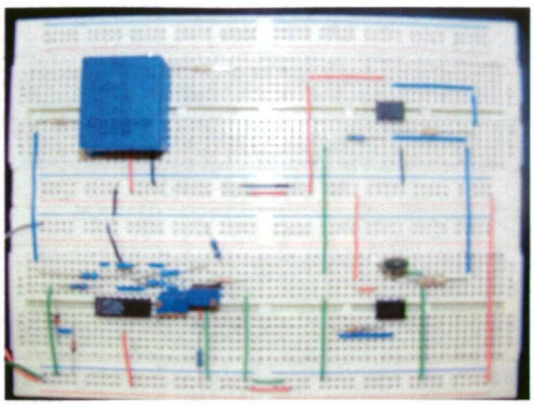

Fig. 5.9 Voltage sensor and IGBT driver.

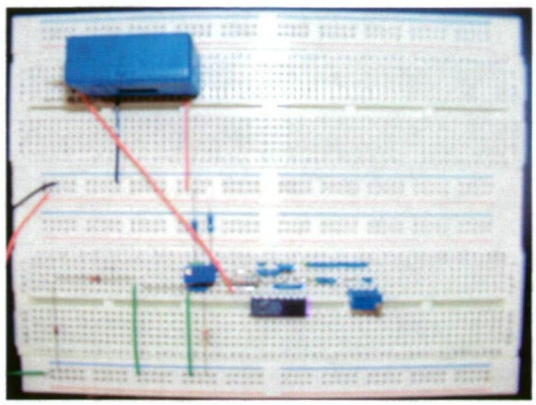

Fig. 5.10 Current sensor circuit.

5.4.4 IGBT

A Semikron SKM50GB063 D n-channel IGBT module is used as the switch. This IGBT is been chosen for high efficiency, fast switching and suitability for medium to high power applications.

5.4.5 Inductor, Capacitor and Diode

With the decrease in frequency the inductor and capacitor values are increased. If load current is increased, the capacitor value should be increased. The voltage ripple is increased with the decrease in capacitor value. The value of inductor and capacitor value has been defined by using the equations of the boost converter [103].

5.4.6 Operating Frequency

To handle high power, the frequency should be lower. But with the reduction of frequency the inductor and capacitor size is increased. The optimum value has been chosen to minimize power loss. The operating switching frequency was 10 kHz.

Fig. 5.11 CP1104 connector panel.

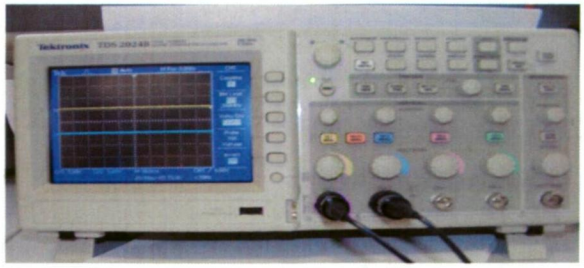

Fig. 5.12 Digital oscilloscope.

Fig. 5.13 Experimental setup for prototype photovoltaic power system.

5.5 Experimental Results and Discussion

5.5.1 PV Module Output Voltage and Current

The voltage and current obtained from the photovoltaic module is shown in Fig. 5.14. Certainly the voltage level and current level changes with the change in insolation. The voltage is about 12V and the current is 80mA.

5.5.2 Response of Voltage Sensor

The response of the voltage sensor circuit to changes in voltage is shown in Fig. 5.15. This voltage is fed back to the controller to generate the switching signals.

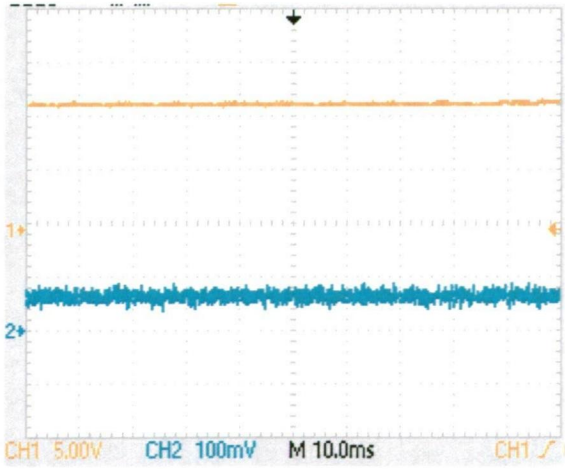

Fig. 5.14 PV module voltage and current.

5.5.3 Generation of Switching Pulses

Fig. 5.16 shows the switching pulses generated from the converter controller implemented in Simulink and downloaded in the dSPACE DS1104 controller board. The switching pulses are fed to the IGBT gate drive optocoupler. The output of the optocoupler circuit is also shown in Fig. 5.16.

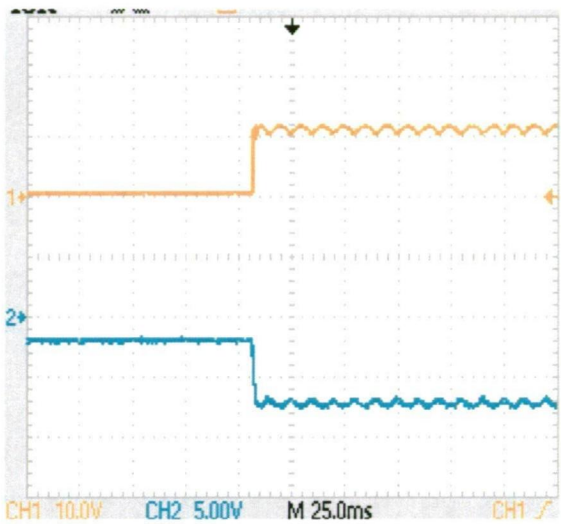

Fig. 5.15 Response of voltage sensor to change in voltage.

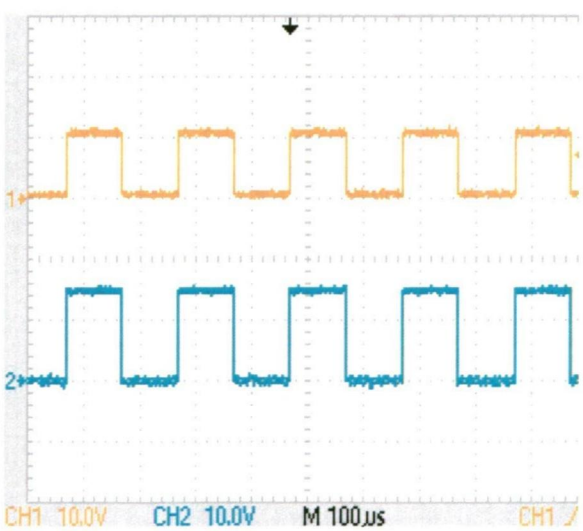

Fig. 5.16 Switching pulses (top) and IGBT gate driver output (bottom).

5.5.4 Output Voltage of the dc-dc Converter

Fig. 5.17 shows the output voltage of the boost converter. As can be seen from Fig. 5.17, the output voltage of the boost converter is about 25V, for an input voltage of about 12V.

5.5.5 Effect of Input Variations

The effect of input variations is shown in Fig. 5.18. The input voltage is suddenly changed in a step of 10 V, but the output voltage doesn't change instantly. As the power from the photovoltaic module disappears, the controllers are able to hold the output voltage level, for a certain time.

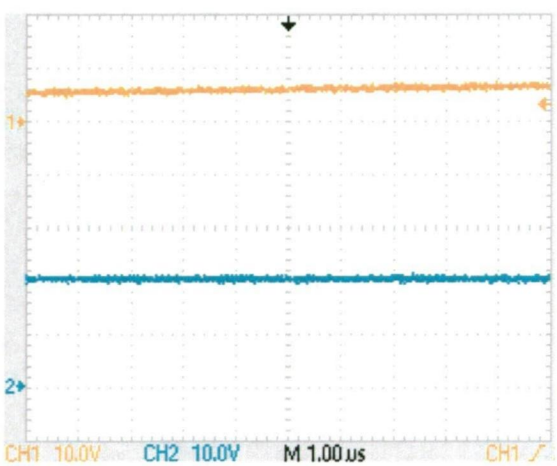

Fig. 5.17 Input (top) and output (bottom) voltage of the PV boost converter.

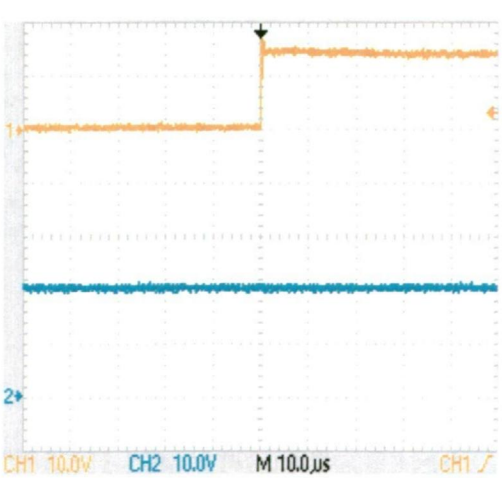

Fig. 5.18 Effect of input variations.

5.5.6 Effect of External Disturbances

External disturbance is a common phenomenon in photovoltaic power systems. A sudden disappearance of sunlight, due to cloud, usually happens. Fig. 5.19 shows the effect of external disturbance on the photovoltaic power system. As the power from the photovoltaic module disappears, the controllers are able to hold the output voltage level, for a certain time. So, the disappearance of photovoltaic power doesn't affect the load instantly.

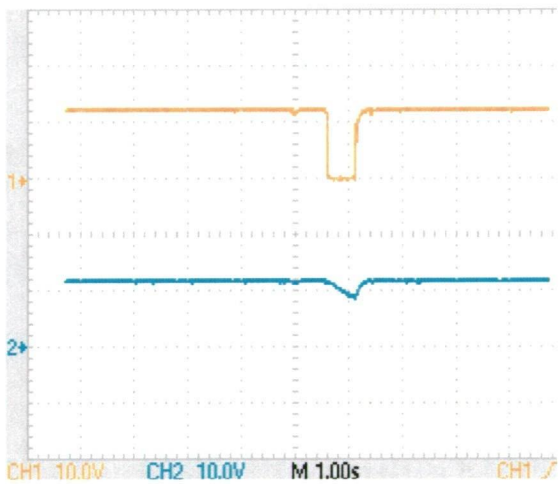

Fig. 5.19 Effect of external disturbances.

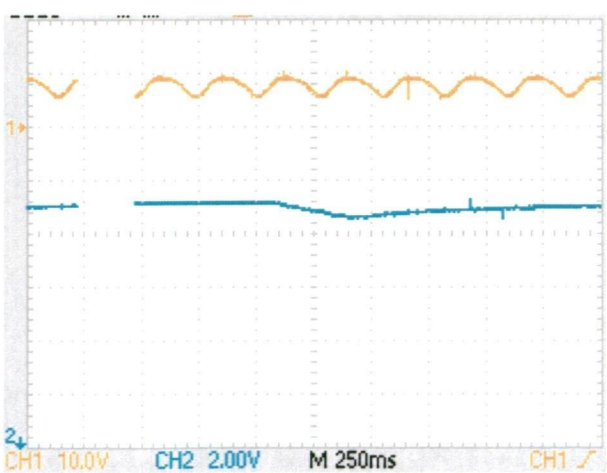

Fig. 5.20 Effect of load changes.

5.5.7 Effect of Load Changes

The effect of output change is shown in Fig. 5.20. The output is suddenly changes from 8kΩ to 45kΩ. At that time the change in output voltage appears as shown in Fig. 5.20. During the change in load, the voltage level goes down for a while and then recovers again. So, the change in load in a large extent also doesn't affect the output voltage level.

5.6 Conclusion

The experimental setup is implemented to investigate the performance of the current mode controller for the control of dc-dc converter in a photovoltaic power system. The response of the voltage and current sensor circuits, and IGBT gate drive optocoupler is presented. The performance of the current mode controller as a dc-dc converter controller in photovoltaic power system is presented considering input fluctuations, load variations and external disturbances. The experimental setup facilitates real time interface of the sensor circuits and switching pulses for the dc-dc converter. Noise free, high speed signal processing is performed inside the dSPACE DS1104 controller board.

CHAPTER 6

Conclusions and Suggestions for Future Research

6.1 Conclusions

Photovoltaic power system technology, as a sustainable energy source, is a potential solution for generating electrical power. However, large scale use of photovoltaic power systems lies in the employment of efficient and cost effective technologies in power electronic interfaces and control techniques. This thesis has focused on power electronic interfaces and control techniques of photovoltaic power systems. The ultimate goal was to find converter topologies and control techniques which are well-matched for employment in power electronic interfaces of photovoltaic power systems.

Improved maximum power point tracking of the photovoltaic module based on current mode control is presented in Chapter 2. The photovoltaic module current is directly proportional to the solar irradiation, and therefore, photovoltaic modules act as a current source. Hence, the current control method is employed in the maximum power point tracking technique. The inherent current source characteristic of the photovoltaic module is used to obtain a robust response during rapidly changing environmental conditions. The variable perturbation step size employed in the algorithm facilitates fast response and accurate holding of the maximum power point of the photovoltaic module. The correlation between the reference current and the change in photovoltaic power makes the algorithm appropriate in steady state condition as well as in transient state. The effect of irradiance change, perturbation step size, switching frequency and sampling rate on the improved maximum power point tracking are also assessed.

Employment of the current mode control of the switch-mode dc-dc converter for photovoltaic power applications is presented in Chapter 3. Average current control, current programmed control, hysteresis current control and nonlinear carrier control methods are addressed as the dc-dc converter controller considering input fluctuations and load variations of the photovoltaic power systems. The Dynamic responses of photovoltaic systems are investigated and harmonic analysis is performed. Performances of the above current controllers are examined through simulation and the results are presented. The results show that the selection of different current control techniques depends on the working conditions and the area of applications. A comparative assessment of the voltage mode control and four current mode control techniques of switch-mode converters for photovoltaic power application is also presented.

Control of battery storage with a bidirectional converter is presented in Chapter 4. This study focuses on the control of a battery management system for photovoltaic power applications with a high efficiency bidirectional converter. The proposed control strategy utilizes the dc bus power and battery state of charge for the charging and discharging of the battery with a bidirectional converter. The bidirectional converter includes fewer components and switches, has less switching losses with zero voltage switching, and has high gain buck-boost operations. A new control algorithm of charging-discharging control for the battery storage system is proposed. The complete photovoltaic power system with a boost dc to dc converter controller to regulate the dc link voltage, a bidirectional converter based battery charge controller, and an inverter with its associated vector mode controller is implemented in the Simulink/Simpower environment. The simulation results are presented and discussed to verify the validity of the proposed control algorithm.

Experimental evaluation of the dSPACE DS1104 based controller for photovoltaic power application is presented in Chapter 5. A 160W prototype photovoltaic power system with BP solar panel, sensors, IGBT gate driver and dc-dc converter is implemented. The controller is implemented in the dSPACE ControlDesk® and the hardware-software interface is experienced through the dSPACE DS1104 controller board and controller panel. The implementation of high speed, noise free, accurate

control of the dSPACE ControlDesk® verifies good performance of the current mode controller of the photovoltaic power system.

The thesis mainly studies the control of power electronic interfaces employed in photovoltaic power systems. The conclusions from this study can be summarized as follows.

- **Maximum Power Point Extraction**

An in-depth analysis of the maximum power point tracking on the photovoltaic module has been presented in this thesis. The current mode control technique is employed considering the current-source characteristics of the photovoltaic module. Variable step-size is used in the maximum power point tracking algorithm as the photovoltaic power is subject to change under rapidly changing solar irradiation. The effects of perturbation step size and sampling rate are analysed, which are vital design considerations for maximum power point tracking techniques.

- **Regulation of Photovoltaic Voltage**

Detailed analysis is performed for the boost converter and four current mode control techniques, namely average current control, current programmed control, hysteresis current control, and nonlinear carrier control. This study demonstrates the viability of the employment of current mode control for photovoltaic applications. Current mode control techniques are assessed through simulation to regulate the photovoltaic voltage, considering input variations, load changes, external disturbance, dynamic performance and inverter harmonics. The comparative assessment of current mode controls and voltage mode control are presented to support the superiority of current mode control in different aspects of applications.

- **Charging and Discharging of the Battery**

This study investigates appropriate system configuration, converter topology and control techniques for battery charging/discharging of photovoltaic power systems. A battery charging/discharging algorithm has been presented and verified through

simulation. Simulation results show that the battery charger can effectively coordinate power transfer among the photovoltaic module, battery and load.

6.2 Suggestions for Future Research

An interesting future project would be to integrate the maximum power point tracking technique with the dc-dc converter controller. The employment of the maximum power point technique within the converter controller will make it possible to combine the voltage regulation with the maximum power point extraction.

A further stage of this project could be the employment of the inverter controller. Effective coordination of the maximum power point tracking technique, dc-dc converter controller, battery charger controller and inverter controller would be a very promising field of research.

Another significant possibility for further research could be the experimental implementation of the whole system using the dSPACE DS1104 digital signal processor.

References

[1] Solar Generation V – 2008, Solar electricity for over one billion people and two million jobs by 2020, European Photovoltaic Industry Association. [Online]. Available: http://www.epia.org/fileadmin/EPIA_docs/documents/EPIA_SG_V_ENGLISH_FULL_Sept2008.pdf. [Accessed, Mar. 26, 2009]

[2] Solar Cell, from Wikipedia, the free encyclopedia. [Online]. Available: http://en.wikipedia.org/ wiki/ Solar_cell. [Accessed, Feb. 21, 2009]

[3] IEEE Std. 929-2000, *IEEE Recommended Practice for Utility Interface of Photovoltaic (PV) Systems*. [Accessed, Apr. 14, 2009]

[4] G. Walker, "Evaluating MPPT converter topologies using a Matlab PV model", *Australian Journal of Electrical & Electronics Engineering*, vol. 21, no.1, pp. 49-55, 2001.

[5] W. Xiao, N. Ozog, and W. G. Dunford, "Topology study of photovoltaic interface for maximum power point tracking", *IEEE Transactions on Industrial Electronics*, vol. 54, no. 3, pp. 1696-1704, Jun. 2007.

[6] G. Walker and P. C. Sernia, "Cascaded dc-dc converter connection of photovoltaic modules", *IEEE Transactions on Power Electronics*, vol. 19, no. 4, Jul. 2004.

[7] J. L. D. Gomez, E. G. Cervantes, P. N. Enjeti, and L. Palma, "Analysis and evaluation of a series-combined connected boost and buck boost dc-dc converter for photovoltaic application", *IEEE Applied Power Electronics Conference and Exposition*, Mar. 2006.

[8] K. Kobayashi, H. Matsuo, and Y. Sekine, "Novel solar-cell power supply system using a multiple-input dc-dc converter", *IEEE Transactions on Industrial Electronics*, vol. 53, no. 1, Feb. 2006.

[9] H. S. Chung, K. K. Tse, S. Y. R. Hui, C. M. Mok, and M. T. Ho, "A novel maximum power point tracking technique for solar panels using a Sepic or Cuk converter", *IEEE Transactions on Power Electronics*, vol. 18, no. 3, May 2003.

[10] J. P. Lee, B. D. Min, T. J. Kim, D. W. Yoo, and B. K. Lee, "A novel topology for photovoltaic series connected dc/dc converter with high efficiency under wide load range", *IEEE Power Electronics Specialists Conference,* pp. 152-155, Jun. 2007.

[11] S. B. Kjaer, J. K. Pedersen, and F. Blaabjerg, "A review of single-phase grid-connected inverters for photovoltaic modules", *IEEE Transactions on Industry Applications*, vol. 41, no. 5, Sep.-Oct. 2005.

[12] S. B. Kjaer, J. K. Pedersen, and F. Blaabjerg, "Power inverter topologies for photovoltaic modules-a review", *IEEE Industry Applications Conference*, vol. 2, pp. 782-788, 2002.

[13] D. C. Martins and R Demonti, "Grid connected PV system using two energy processing stages", *IEEE Photovoltaic Specialists Conference*, pp. 1649-1652, May 2002.

[14] L. R. Chen, N. Y. Chu, C. S. Wang, and R. H. Liang, "Design of a reflex-based bidirectional converter with the energy recovery function", *IEEE Transactions on Industrial Electronics*, vol. 55, no. 8, pp. 3022-3029, Aug. 2008.

[15] K. H. Edelmoser and F. A. Himmelstoss,"Bi-directional dc-to-dc converter for solar battery backup applications", *IEEE Power Electronics Specialists Conference*, 2004.

[16] C. G. Yoo, W. C. Lee, K. Lee, and I. Suh, "Current mode PWM controller for a 42V/14V bidirectional dc/dc converter", *IEEE Power Electronics Specialist Conference*, pp. 1-6, Jun. 2006.

[17] H. Matsuo and F. Kurokawa, "New solar cell power supply system using a boost type bidirectional dc-dc converter," *IEEE Transactions on Industrial Electronics*, vol. IE-31, no. 1, pp. 51-55, Feb. 1984.

[18] R. J. Wai and R. Y. Duan, "High-efficiency bidirectional converter for power sources with great voltage diversity," *IEEE Transactions on Power Electronics*, vol. 22, no. 5, pp. 1986-1996, Sep. 2007.

[19] L. Schuch, C. Rech, H. L. Hey, H. A. Grundling, H. Pinheiro, and J. R. Pinheiro, "Analysis and design of a new high-efficiency bidirectional integrated ZVT PWM converter for dc-bus and battery-bank interface," *IEEE Transactions on Industry Applications*, vol. 42, no. 5, pp. 1321-1332, Sep.-Oct. 2006.

[20] R. Faranda, S. Leva, and V. Maugeri, "MPPT techniques for PV systems: energetic and cost comparison", *IEEE Power and Energy Society General Meeting,* Jul. 2008.

[21] D. Dera, R. Teodorescu, J. Hantschel, and M. Knoll, "Optimized maximum power point tracker for fast-changing environmental conditions", *IEEE Transactions on Industrial Electronics*, vol. 55, no. 7, pp. 2629-2637, Jul. 2008.

[22] T. Esram and P. L. Chapman, "Comparison of photovoltaic array maximum power point tracking techniques", *IEEE Transactions on Energy Conversion*, vol. 22, no. 2, pp. 439-449, Jun. 2007.

[23] S. Jain, and V. Agarwal, "Comparison of the performance of maximum power point tracking schemes applied to single-stage grid-connected photovoltaic systems", *IET Journal of Electrical Power Application*, vol. 1, no. 5, pp. 753-762, Sep. 2007.

[24] N. Femia, D. Granozoi, G. Petrone, G. Spagnuolo, and M. Vitelli, "Predictive and adaptive MPPT perturb and observe method", *IEEE Transactions on Aerospace and Electronic Systems*, vol. 43, no. 3, pp. 934-950, Jul. 2007.

[25] G. M. S. Azevedo, M. C. Cavalcanti, K. C. Oliveira, F. A. S. Neves, and Z. D. Lins, "Evaluation of maximum power point tracking methods for grid connected photovoltaic systems", *IEEE Power Electronics Specialists Conference,* pp. 1456-1462, Jun. 2008.

[26] F. Liu, S. Duan, F. Liu, B. Liu, and Y. Kang, "A variable step size INC MPPT method for PV systems", *IEEE Transactions on Industrial Electronics*, vol. 55, no. 7, pp. 2622-2628, Jul. 2008.

[27] H. Cha and S. Lee, "Design and implementation of photovoltaic power conditioning system using a current based maximum power point tracking", *IEEE Industry Applications Society Annual Meeting,* Oct. 2008.

[28] K. H. Hussain, I. Muta, T. Hoshino, and M. Osakada, "Maximum photovoltaic power tracking: an algorithm for rapidly changing atmosphere conditions", *IEE Conference of Generation, Transmission and Distribution*, vol. 142, no. 1, pp. 59-64, Jan. 1995.

[29] T. Esram, J. W. Kimball, P. T. Krein, P. L. Chapman, and P. Midya, "Dynamic maximum power point tracking of photovoltaic arrays using ripple correlation control", *IEEE Transactions on Power Electronics*, vol. 21, no. 5, pp. 1282-1291, Sep. 2006.

[30] J. W. Kimball and P. T. Krein, "Discrete-time ripple correlation control for maximum power point tracking", *IEEE Transactions on Power Electronics*, vol. 23, no. 5, pp. 2353-2362, Sep. 2008.

[31] D. Casadei, G. Grandi, and C. Rossie, "Single-phase single-stage photovoltaic generation system based on a ripple correlation control maximum power point tracking", *IEEE Transactions on Energy Conversion*, vol. 21, no. 2, pp. 562-568, Jun. 2006.

[32] W. Xiao and W. G. Dunford, "A modified adaptive hill climbing MPPT method for photovoltaic power systems", *IEEE Power Electronics Specialists Conference*, pp. 1957-1963, 2004.

[33] S. Jain and V. Agarwal, "A new algorithm for rapid tracking of approximate maximum power point in photovoltaic systems", *IEEE Power Electronics Letters*, vol. 2, no. 1, pp. 16-19, Mar. 2004.

[34] K. Kobayashi, H. Matsuo, and Y. Sekine, "An excellent operating point tracker of the solar-cell power supply system", *IEEE Transactions on Industrial Electronics*, vol. 53, no. 2, pp. 495-499, Apr. 2006.

[35] H. Patel and V. Agarwal, "Maximum power point tracking scheme for PV systems operating under partially shaded conditions", *IEEE Transactions on Industrial Electronics*, vol. 55, no. 4, pp. 1689-1698, Apr. 2008.

[36] N. Femia, G. Petrone, G. Spagnuolo, and M. Vitelli, "Optimization of perturb and observe maximum power point tracking method", *IEEE Transactions on Power Electronics*, vol. 20, no. 4, pp. 963-973, Jul. 2005.

[37] L. Egiziano, N. Femia, G. Lisi, G. Petrone, G. Spagnuolo, and M. Vitelli, "Design and optimization of a maximum power point tracking controller for a PV battery charger", *IEEE Industrial Electronics Symposium,* pp. 2426-2431, Jun. 2007.

[38] N. Femia, G. Petrone, G. Spagnuolo, and M. Vitelli, "Optimizing duty-cycle perturbation of P&O MPPT technique", *IEEE Power Electronics Specialist Conference*, pp. 1939-1944, 2004.

[39] N. Femia, G. Petrone, G. Spagnuolo, and M. Vitelli, "Optimizing sampling rate of P&O MPPT technique", *IEEE Power Electronics Specialist Conference*, pp. 1945-1949, 2004.

[40] C. W. Tan, T. C. Green, and C. A. H. Aramburo, "A current-mode controlled maximum power point tracking converter for building integrated photovoltaics", *European Conference on Power Electronics and Applications*, Sep. 2007.

[41] M. A. S. Masoum, H. Dehbonei, and E. F. Fuchs, "Theoretical and experimental analyses of photovoltaic systems with voltage-and current-based maximum power-point pracking", *IEEE Transactions on Energy Conversion*, vol. 17, no. 4, pp. 514- 522, Dec. 2002.

[42] C. W. Tan, T. C. Green, and C. A. H. Aramburo, "An improved maximum power point tracking algorithm with current-mode control for photovoltaic applications", *International Conference on Power Electronics and Drives Systems,* pp. 489-484, 2005.

[43] R. Gules, J. D. P. Pacheco, H. L. Hey, and J. Imhoff, "A maximum power point tracking system with parallel connection for PV stand-alone applications", *IEEE Transactions on Industrial Electronics*, vol. 55, no. 7, pp. 2674-2683, Jul. 2008.

[44] R. Mammano, "Switching power supply topology: voltage mode vs. current mode". [Online]. Available:http://focus.ti.com./lit/an/slua119.pdf. [Accessed, May 6, 2008]

[45] B. Lynch, "Current-mode vs. voltage-mode control in synchronous buck converters". [Online]. Available: www.analogzone.com/pwrt0407.pdf. [Accessed, May 20, 2008]

[46] K. N. Hasan, M. E. Haque, M. Negnevitsky, and K. M. Muttaqi, "Performance analysis of VMC and CMCs of switch-mode converters for photovoltaic applications", *IEEE Industrial Electronics Conference*, pp. 315-320, Nov. 2008.

[47] K. N. Hasan, M. E. Haque, M. Negnevitsky, and K. M. Muttaqi, "Output quality evaluation of photovoltaic systems with different current control methods of switch-mode converters", *International Conference on Harmonics and Quality of Power*, Sep. – Oct. 2008.

[48] R. W. Erickson and D. Maksimovic, "Control of the current waveform", in *Fundamentals of Power Electronics*, 2nd ed., Kluwer Academic Publishers, 2001, pp. 648 – 663.

[49] J. Sun and M. Chen, "Nonlinear average current control using partial current measurement", *IEEE Transactions on Power Electronics*, vol. 23, no. 4, Jul. 2008.

[50] Z. Bing, X. Du, and J. Sun, "Generalization of a nonlinear average current control method for CCM and DCM operation", *IEEE Applied Power Electronics Conference and Exposition,* pp. 51 – 57, 2008.

[51] L. Dixon, "Average current mode control of switching power supplies". [Online]. Available: www.colorado.edu/~ecen5807/course_material/papers/ cpm/ dixon_1990.pdf. [Accessed, Mar. 20, 2008]

[52] F. J. Azcondo, C. Bracas, R. Casanueva, and D. Maksimovic, "Approaches to modelling converters with current programmed control", *IEEE Workshop on Power Electronics Education,* pp. 98 – 104, Jun. 2005.

[53] N. S. Choi and Li Yulong, "Current programmed control of three-phase PWM AC-AC buck-boost converter", *International Conference on Electrical Machines and Systems,* vol. 2, pp. 1146 – 1151, 2005.

[54] A. S. Lock and E. R. Da Silva, "Improved hysteresis current control of a single phase, three level, double PFC converter", *IEEE Power Electronics Specialists Conference,* pp. 1326 – 1330, 2007.

[55] L. Jian, D. Ningyi, and R. Jiangjun, "The analysis of hysteresis current control strategy of three-phase four-wire shunt APF based on the unified topology", *IEEE Industrial Electronics and Applications Conference,* pp. 575 – 580, 2007.

[56] Krismadinata, N. A. Rahim, and J. Selvaraj, "Implementation of hysteresis current control for single-phase grid connected inverter", *International Conference on Power Electronics and Drive Systems,* pp. 1097 – 1101, 2007.

[57] R. Zane and D. Maksimovic, "Nonlinear-carrier control for high-power-factor rectifiers based on up-down switching converters", *IEEE Transactions on Power Electronics,* vol. 13, no.2, pp. 213 – 221, Mar. 1998.

[58] N. Jayaram and D. Maksimovic, "Power factor correctors based on coupled-inductor Sepic and Cuk converters with nonlinear-carrier control", *Applied Power Electronics Conference and Exposition,* pp. 468 – 474, 1998.

[59] J. A. Gow and C. D. Manning, "Photovoltaic converter system suitable for use in small scale stand-alone or grid connected applications," *IEE Electrical Power Applications*, vol. 47, no. 6, pp. 535-543, 2000.

[60] M. P. Kajmierkowski, R. Krishnan, and F. Blaabjerg, "*Control in Power Electronics Selected Problems*". Academic Press, 2002

[61] M. H. Rashid, *Power Electronics Circuits, Devices, and Applications*, 3rd ed., Prentice Hall, 2004, p. 627.

[62] M. Hartman, "Inside current-mode control," National Semiconductor. [Online]. Available: www.national.com/ appinfo/ power/ files/ Power Designer _ 106.Pdf. [Accessed, Apr. 03, 2008]

[63] N. Mohan, T. M. Undeland, and W. P. Robbins, *Power Electronics Converters, Applications, and Design*, 2nd ed., Wiley, 1995, p. 340.

[64] H. M. Kojabadi, B. Yu, I. A. Gadoura, L. Chang, and M. Ghribi, "A novel DSP-based current-controlled PWM strategy for single phase grid connected inverters," *IEEE Transactions on Power Electronics*, vol. 21, no. 4, pp. 985-993, Jul. 2006.

[65] E. Rogers, "Understanding boost power stages in switch-mode power supplies", Texus Instruments Application Report, Mar. 1999.

[66] R. B. Ridley, "A new small-signal model for current-mode control", PhD dissertation, Ridley Engineering, 2008. [Accessed, Jan. 15, 2009]

[67] R. Zaitsu, "Voltage mode boost converter small signal control loop analysis using the TPS61030", Texas Instruments Application Report, May 2007

[68] PV module Simulink models. [Online]. Available: http://ece-www.colorado.edu/~ecen2060/matlab.html. [Accessed, Feb. 22, 2008]

[69] IEEE Standard 519-1992, *IEEE Recommended Practices and Requirements for Harmonic Control in Electrical Power Systems.*

[70] K. Agbossou, M. Kolhe, J. Hamelin, and T. K. Bose, "Performance of a stand-alone renewable energy system based on energy storage as hydrogen," *IEEE Transactions on Energy Conversion*, vol. 19, no. 3, pp. 633-640, Sep. 2004.

[71] M. E. Glavin, P. K. W. Chan, S. Armstrong, and W. G. Hurley, "A stand-alone photovoltaic supercapacitor battery hybrid energy storage system", *Power Electronics and Motion Control Conference*, pp. 1688-1695, 2008.

[72] S. C. Smith, P. K. Sen, and B. Kroposki, "Advancement of energy storage devices and applications in electrical power system", *IEEE Power and Energy Society General Meeting,* Jul. 2008.

[73] S. S. Choi, K. J. Tseng, D. M. Vilathgamuwa, and T. D. Nguyen, "Energy storage systems in distributed generation schemes", *IEEE Power and Energy Society General Meeting,* pp. 1-8, Jul. 2008.

[74] S. Faias, P. Santos, F. Matos, J. Sousa, and R. Castro, "Evaluation of energy storage devices for renewable energies integration: application to a Portuguese wind farm", *International Conference on European Electricity Market,* May 2008.

[75] Kusko and J. Dedad, "Stored energy – short-term and long-term energy storage methods for standby electric power systems", *IEEE Industry Applications Magazine*, pp. 66-72, Jul.-Aug. 2007.

[76] R. B. Schainker and M. Nakhamkin, "Compressed-air energy storage (CAES); overview, performance and cost data for 25 MW to 220 MW plants", *IEEE Transactions on Power Apparatus and Systems,* vol. PAS-104, no. 4, pp. 791-795, Apr. 1985.

[77] M. L. Lazarewicz and A. Rojas, "Grid frequency regulation by recycling electrical energy in flywheels", *IEEE Power Engineering Society General Meeting*, vol. 2, pp. 2038-2042, Jun. 2004.

[78] S. J. Chiang, K. T. Chang, and C. Y. Yen, "Residential photovoltaic energy storage system," *IEEE Transactions on Industrial Electronics*, vol. 45, pp. 385-394, Jun. 1998.

[79] V. M. Pacheco, L. C. Freitas, J. B. Vieira Jr., E. A. A. Coelho, and V. J. Farias, "Stand-alone photovoltaic energy storage system with maximum power point tracking", *IEEE Applied Power Electronics Conference and Exposition*, vol. 1, pp. 97-102, 2003.

[80] P. Thounthong, S. Rael, and B. Davit, "Control algorithm of fuel cell and batteries for distributed generation system," *IEEE Transactions on Energy Conversion*, vol. 23, no. 1, pp. 148-155, Mar. 2008.

[81] S. Duryea, S. Islam, and W. Lawrance. "A battery management system for stand-alone photovoltaic energy systems", *IEEE Industry Applications Magazine*, pp. 67-72, May – Jun. 2001.

[82] F. Boico, B. Lehman, and K. Shujaee, "Solar battery chargers for NiMH batteries," *IEEE Transactions on Power Electronics*, vol. 22, no. 5, pp. 1600-1609, Sep. 2007.

[83] H. Matsuo and F. Kurokawa, "New solar cell power supply system using a boost type bidirectional dc-dc converter," *IEEE Transactions on Industrial Electronics*, vol. IE-31, no. 1, pp. 51-55, Feb. 1984.

[84] Battery University. Com. [Online]. Available: http://www.batteryuniversity. Com/partone-24.

[85] F. S. D. Reis, J. C. D. Lima, V. M. Canalli, J. A. Pomilio, J. Sebatin, and J. Uceda, "Matching conducted EMI to international standards", *IEEE Power Electronics Specialists Conference*, Jun. 2002.

[86] F. Lacressonniere and B. Cassoret, "Converter used as a battery charger and a motor speed controller in an industrial truck", *European Conference on Power Electronics and Applications*, pp. P1-P7, 2005.

[87] R. Li, A. Pottharst, N. Frohleke, and J. Bocker, "Analysis and design of improved isolated full-bridge bi-directional dc-dc converter", *IEEE Power Electronics Specialist Conference*, pp. 521-526, 2004.

[88] H. Shiji, K. Harada, Y. Ishihara, T. Todaka, and G. Alzamora, "A zero-voltage switching bidirectional converter for PV systems", *IEEE International Telecommunication Energy Conference*, pp. 14-19, 2003.

[89] M. Fernaadez, A. Ruddell, N. Vast, J. Esteban, and F. Estela, "Development of a VRLA battery with improved separators and a charge controller for low cost photovoltaic and wind powered installations", *Journal of Power Sources*, vol. 95, no. 1-2, pp. 135-140, 2001.

[90] M. R. Patel, "*Wind and Solar Power Systems- design, analysis and operation*", 2nd Edition, CRC press, Taylor and Francis, 2006.

[91] M. Bhatt, W. G. Hurley, and W. H. Wölfle, "A new approach to intermittent charging of valve-regulated lead–acid batteries in standby applications", *IEEE Transactions on Industrial Electronics*, vol. 52, no. 5, Oct. 2005.

[92] S. Armstrong, M. E. Glavin, and W. G. Hurley, "Comparison of battery charging algorithms for stand alone photovoltaic systems", *IEEE Power Electronics Specialist Conference*, pp. 1469-1475, Jun. 2008.

[93] M. E. Glavin and W. G. Hurley, "Ultracapacitor/battery hybrid for solar energy storage", *International Universities Power Engineering Conference*, pp. 791-795, Sept. 2007.

[94] R. J. Wai and R. Y. Duan, "High-efficiency bidirectional converter for power sources with great voltage diversity," *IEEE Transactions on Power Electronics*, vol. 22, no. 5, pp. 1986-1996, Sep. 2007.

[95] F. Lasnier and T. G. Ang, *Photovoltaic Engineering Handbook*, Adam Hilger, 1990.

[96] Battery charger, from Wikipedia, the free encyclopedia. [Online]. Available: http://en.wikipedia.org/wiki/Battery_charger. [Accessed, May 2, 2009]

[97] PV battery, Solar PV electric. [Online]. Available: http://www.solardirect.com/pv/batteries/batteries.htm. [Accessed, May 9, 2009]

[98] R. A. Messenger and J. Ventre, *Photovoltaic Systems Engineering*, 2nd ed., CRC press, 2004.

[99] First Work Steps, dSPACE systems, dSPACE GmbH, Germany, Release 5.3 – Mar. 2007.

[100] ControlDesk Experiment Guide, dSPACE GmbH, Germany, Release 5.3 – Mar. 2007.

[101] Real-Time Interface Implementation Guide, dSPACE GmbH, Germany, Release 5.3 – Mar. 2007.

[102] DS1104 Hardware Installation and Configuration, dSPACE GmbH, Germany, Release 5.3 – Mar. 2007.

[103] Boost Switching Converter Design Equations. [Online]. Available: http://www.daycounter.com/LabBook/BoostConverter/Boost-Converter-Equations.phtml

[104] R. C. Campbell, "A Circuit-based Photovoltaic Array model for Power System Studies", *North American Power Symposium*, pp. 97-101, Sep.-Oct. 2007.

APPENDICES

Appendix A

Simulink Model of the Photovoltaic Module

A.1 Block Diagram Based Model

A Simulink model of the photovoltaic module based on MATLAB/ Simpower/ Simulink block is presented in Fig. A.1. This model takes solar irradiance profile and photovoltaic current as input and gives photovoltaic module voltage and power as the output. Fig. A.2 shows the internal blocks which makes the photovoltaic model [68].

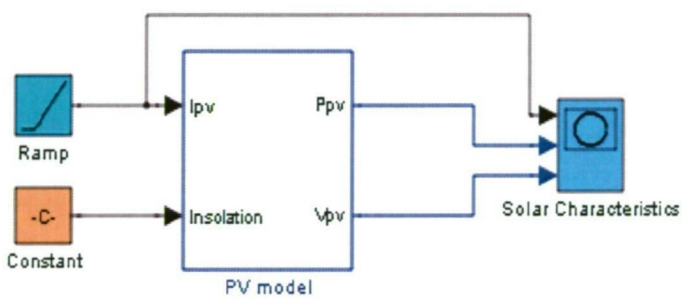

Fig. A.1 Simulink model of the photovoltaic module based on Simpower/Simulink functional block.

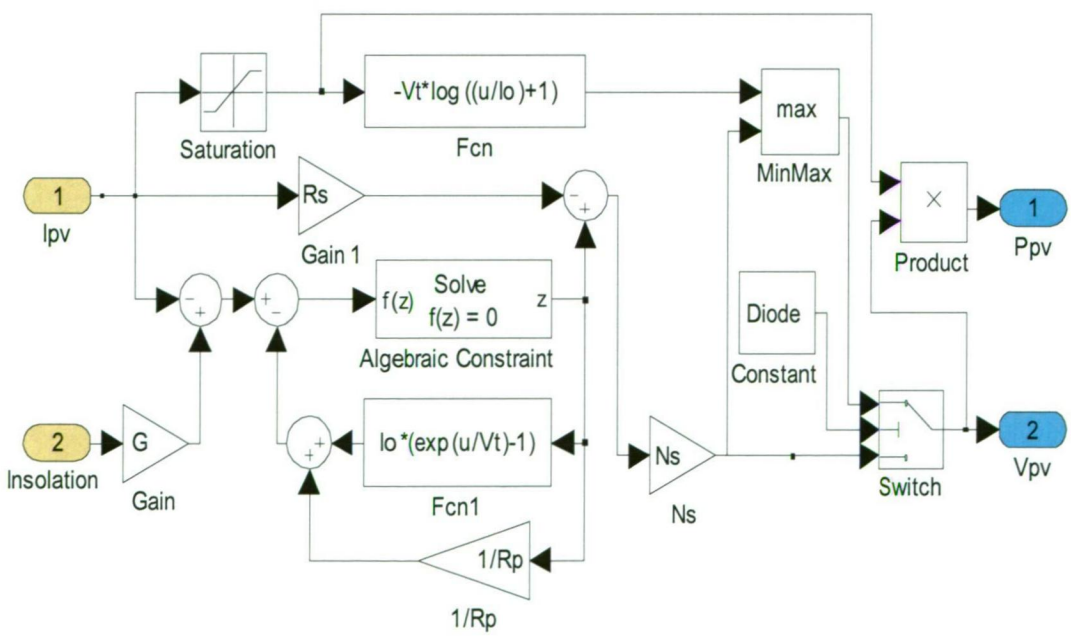

Fig. A.2 Simulink blocks used in building of model of photovoltaic module.

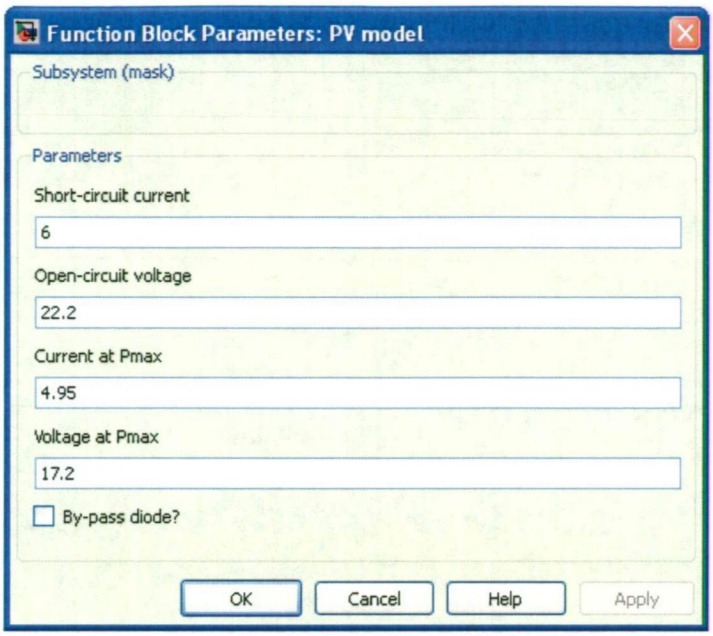

Fig. A.3 Functional block parameters of the Simulink model of the photovoltaic module.

Different parameters of the photovoltaic module based on the Simulink block diagram can be set in the model to obtain expected solar characteristics. For example, the short circuit current, open circuit voltage, current and voltage at maximum power point can be set in the model. Fig. A.3 shows the functional block parameters of the Simulink model of the photovoltaic module.

A.2 Circuit Based Model

A circuit based model of the photovoltaic module is presented in Fig. A.4. This electrical circuit model, based on the diode characteristics, is suitable for use in power electronic converters dynamic and transient behaviour studies [104]. To obtain a piecewise linear solar characteristics, the circuit is updated with some parallel resistors, as shown in Fig. A.5.

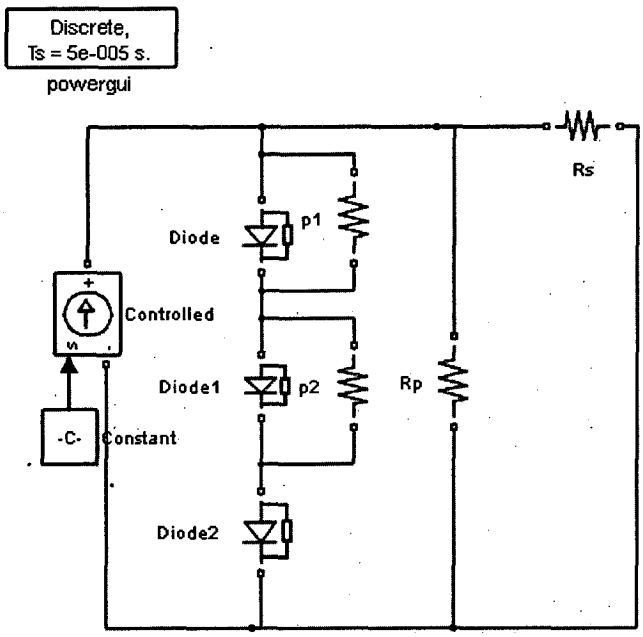

Fig. A.4 Basic Circuit-based model of photovoltaic module.

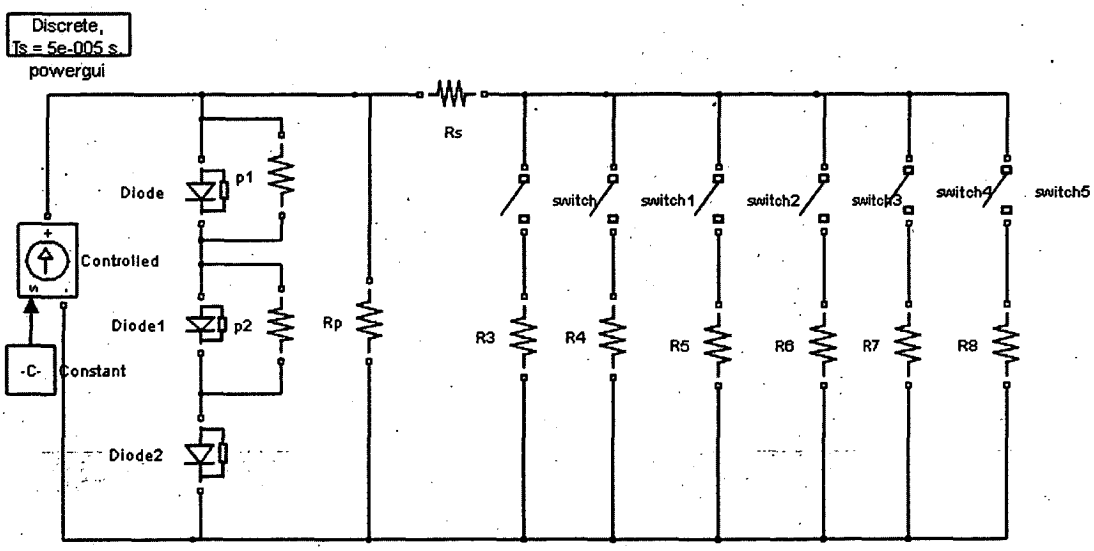

Fig. A.5 Updated circuit-based model of photovoltaic module.

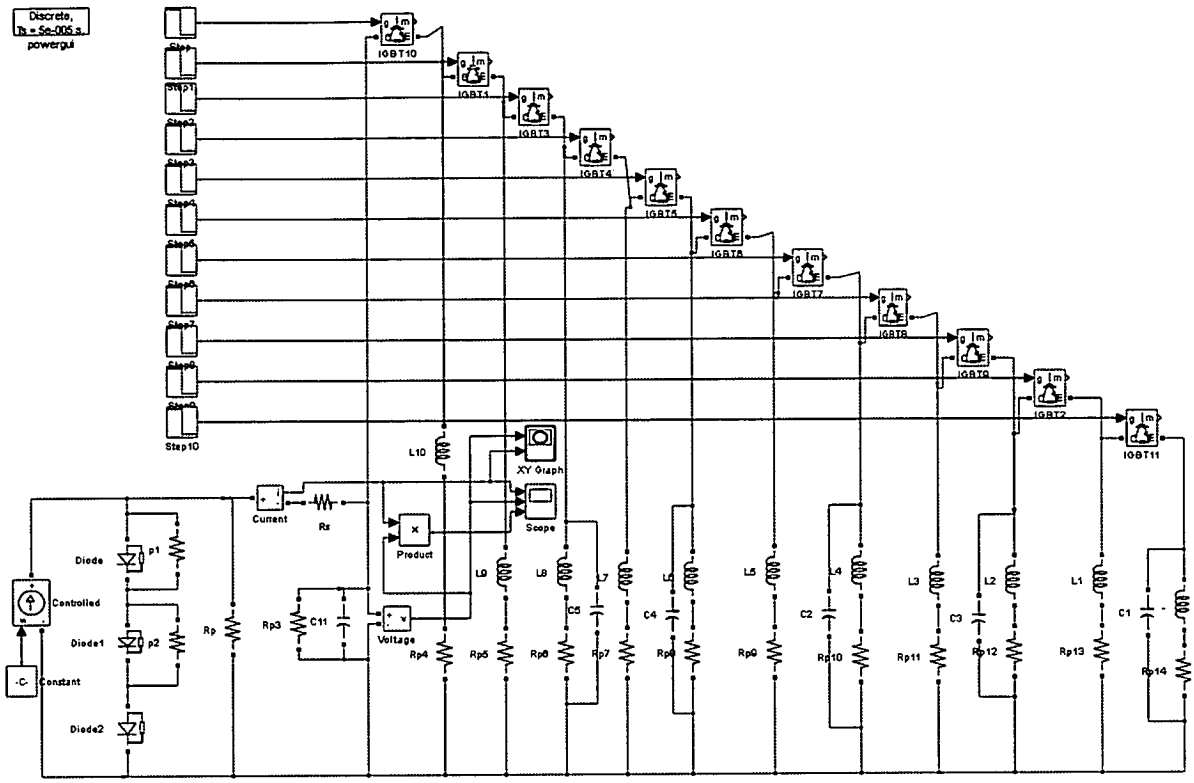

Fig. A.6 Circuit-based model of photovoltaic module for smooth wave-shape.

To obtain smooth solar characteristics, the circuit is further updated using sole parallel inductors and capacitors, as shown in Fig. A.6. The smooth solar characteristics are shown in Fig. A.7.

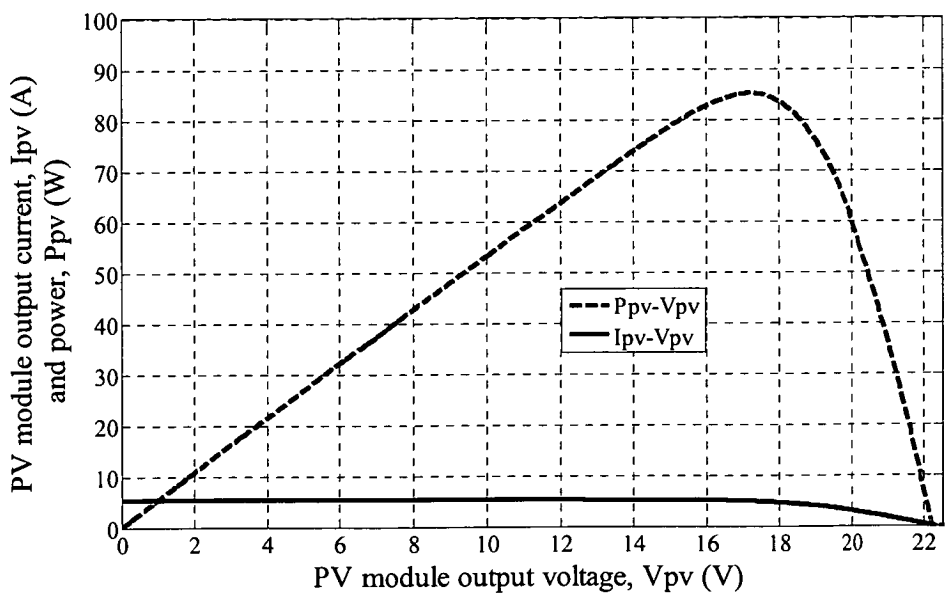

Fig. A.7 Current-voltage and power-voltage characteristics of the PV module at a constant temperature and a specified irradiance.

Appendix B

Simulink Model of the Current-Mode Controllers

B.1 Average Current Control

Fig. B.1 shows the block diagram of the average current control method implemented in the MATLAB/ Simpower/ Simulink system. The average current control method uses the input current and compares it with a reference voltage. A comparison of the voltage, which is proportional to the input current, with feedback voltage, produces an error signal to drive the controller and the PWM modulator.

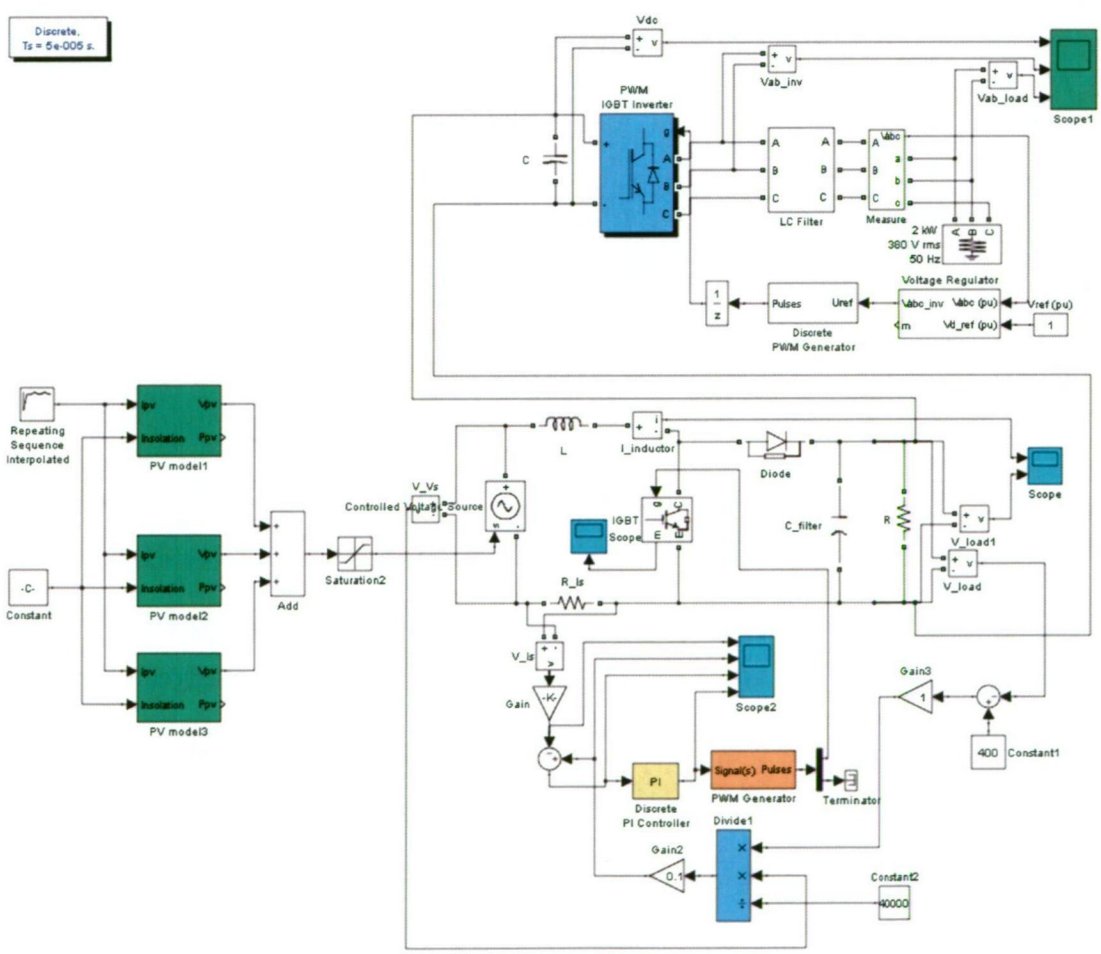

Fig. B.1 Simulink model of average current controller.

B.2 Current Programmed Control

The block diagram of the current programmed control implemented in the MATLAB/ Simpower/ Simulink system is shown in Fig. B.2. In this method, the converter switch current is measured and compared with the control current. The control current comes from the feedback loop. The comparator output drives a latch to pass the switching signal.

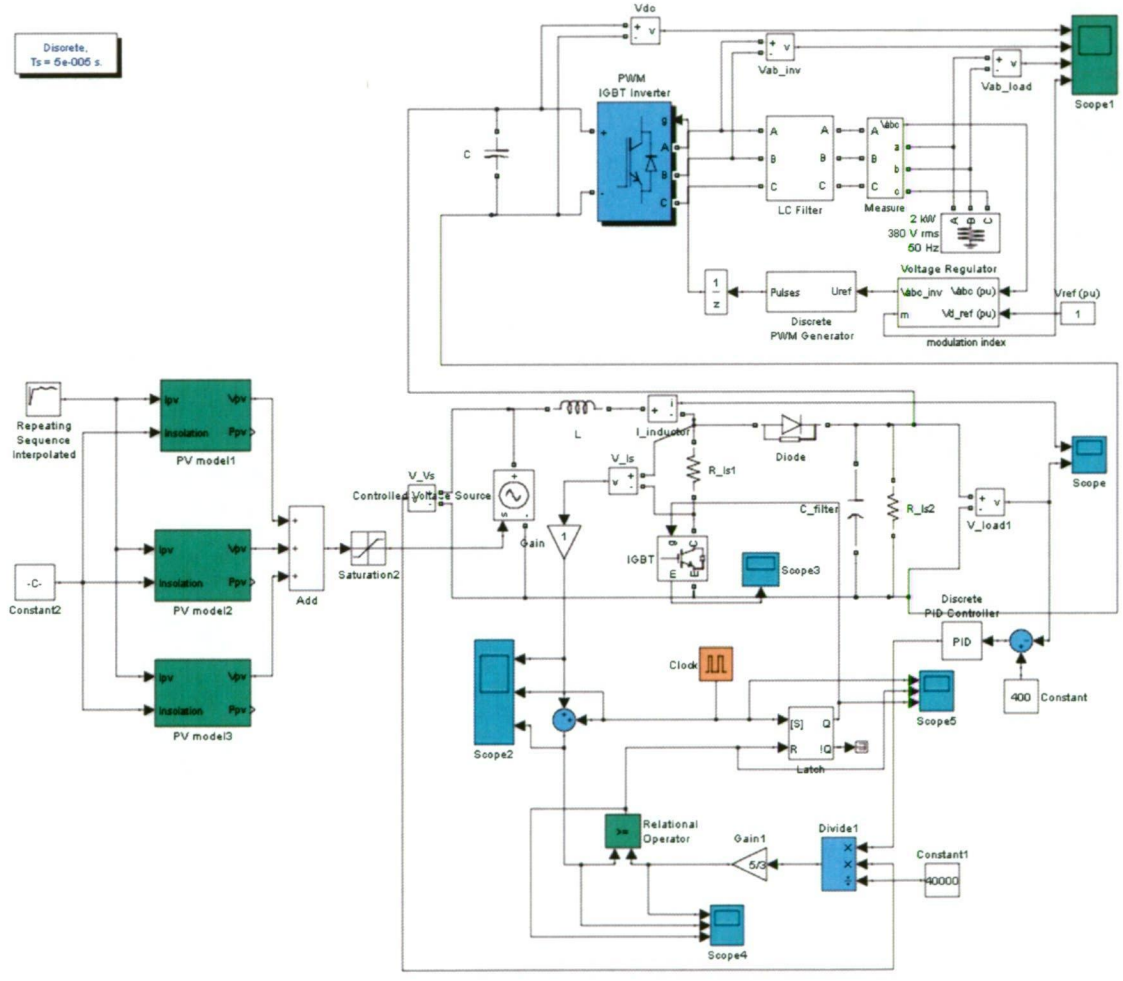

Fig. B.2 Simulink model of current programmed controller.

B.3 Hysteresis Current Control

Fig. B.3 shows the block diagram of the hysteresis current control method implemented in the MATLAB/ Simpower/ Simulink system. The hysteresis current control method operates at a variable frequency. The hysteretic controller provides the gating signal for switching on-off as necessary to maintain a waveform within a set limit. The switch is in either ON or OFF position according to the response of the zero current detectors (ZCD). The ZCD senses the inductor current.

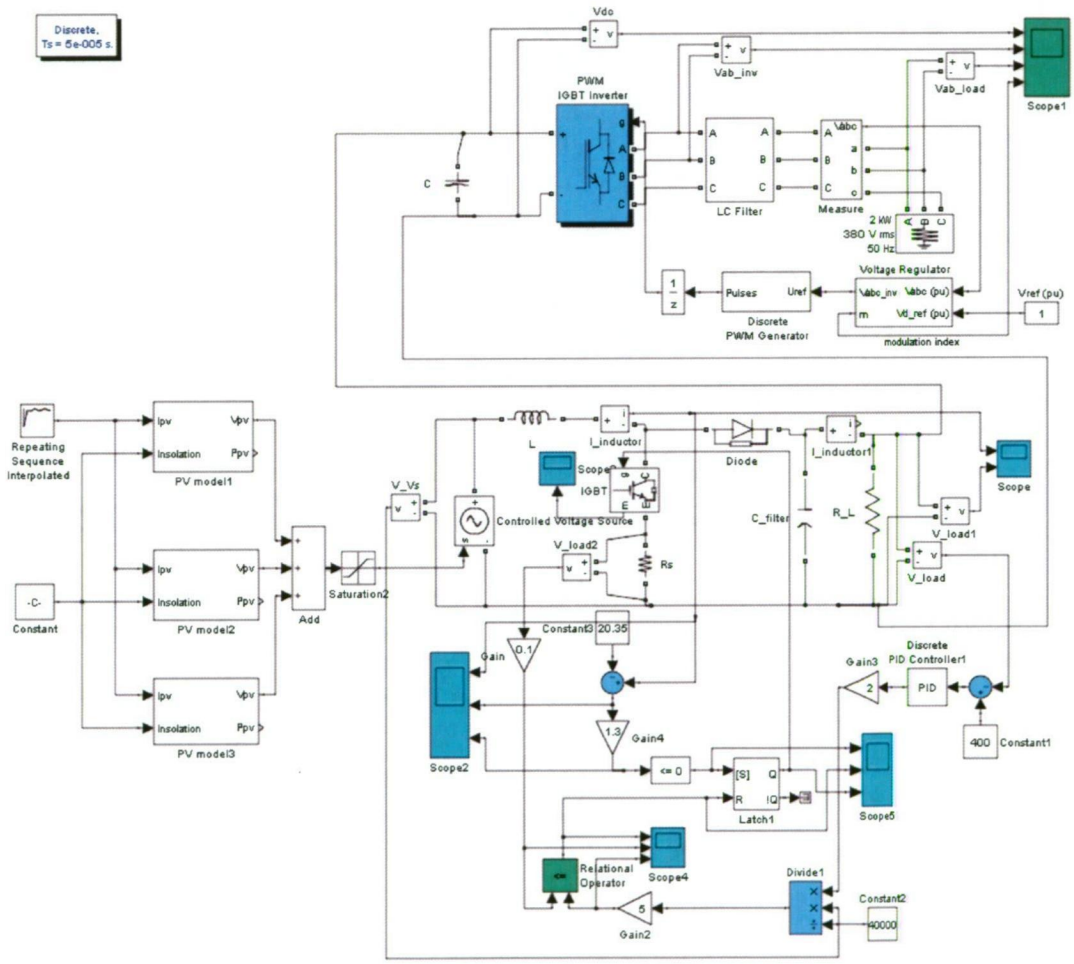

Fig. B.3 Simulink model of hysteresis current controller.

B.4 Nonlinear Carrier Control

The nonlinear carrier control method implemented in the MATLAB/ Simpower/ Simulink system is shown in Fig. B.4 as a block diagram. The nonlinear carrier control method uses a current transformer to obtain the switch current, which is then integrated. The output of the integrator is compared with the output of the nonlinear carrier generator. The carrier voltage is generated from the double integration of the feedback voltage. The output of the comparator then goes to the latch which generates gating pulses.

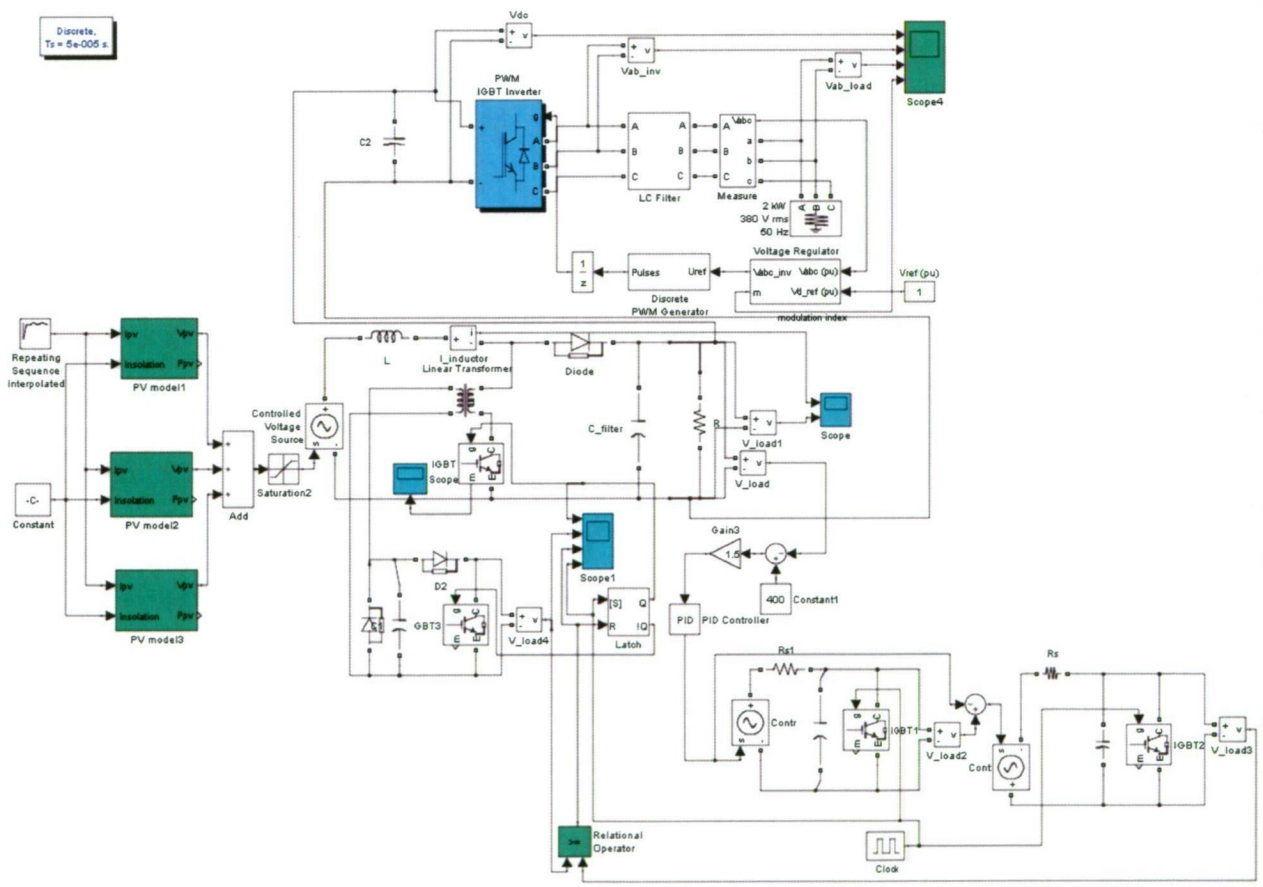

Fig. B.4 Simulink model of nonlinear carrier controller.

Appendix C

Hardware Data

C.1 Photovoltaic Module

In the crystalline silicon photovoltaic modules, used in the experiment, 36 cells are connected in series. Table C.1 presents the specification of the photovoltaic module.

Table C.1 Specification of the photovoltaic module

Model	BP-380J
Maximum power	80W
Nominal voltage	12V
Open circuit voltage	22.1V
Short circuit current	4.8A
Voltage at maximum power point	17.6V
Current at maximum power point	4.55A

C.2 Controller Board

The dSPACE DS1104 R&D (research and development) controller board provides real time interfacing facilities. Real time interface (RTI) provides Simulink blocks for graphical I/O configuration. The real time model is compiled, downloaded, and started automatically. Table C.2 shows the specification of the controller board.

Table C.2 Specification of the controller board

Model	DS1104	
Processor	MPC8240 processor with PPC 603e 64-bit floating point processor CPU click:250 MHz	
Memory	Global memory: 32 MB SDRAM Flash memory: 8MB	
Timer	32-bit down counter	
A/D converter	Channels	4 multiplexed, 4 parallel
	Resolution	Multiplexed 16-bit, parallel 12-bit
	Input voltage	±10V
	Conversion time	Multiplexed 2μs , parallel 800ns
	S/N ratio	Multiplexed >80dB, parallel >65dB
D/A converter	Channels	8 channels
	Resolution	16-bit
	Output range	±10V
	Settling time	10μs
	S/N ratio	>80dB

C.3 Voltage Transducer

The transducer is designed based on the Hall Effect, for the electronic measurements of dc, ac or pulsed voltage with a galvanic isolation between the primary circuit and the secondary circuit. A current proportional to the measured voltage is passed through an external resistance which has been calculated. Table C.3 presents the specification of the voltage transducer.

Table C.3 Specification of the voltage transducer

Model	LV 25-P
Supply voltage	+ terminal : +12V to +15 V - terminal : -12V to -15 V
Primary voltage measuring range	10V to 500V
Measuring resistance	30Ω to 350Ω
Primary nominal rms current	10mA
Secondary nominal rms current	25mA
Conversion ratio	2500:1000

C.4 Current Transducer

The transducer is designed based on the Hall Effect, for the electronic measurements of dc, ac or pulsed current with a galvanic isolation between the primary circuit and the secondary circuit. Table C.4 shows the specification of the current transducer.

Table C.4 Specification of the current transducer

Model	LA 100-P/SP13
Supply voltage	+ terminal : +12V to +15 V - terminal : -12V to -15 V
Primary current measuring range	0A to ±160A
Measuring resistance	10Ω to 95Ω
Primary nominal rms current	100A
Secondary nominal rms current	100mA
Conversion ratio	1:1000

C.5 IGBT Gate Drive Optocoupler

The IGBT gate drive optocoupler is suitable for high frequency driving of power IGBT and high performance dc/dc converter applications. Table C.5 presents the specification of the IGBT gate drive optocoupler.

Table C.5 Specification of the IGBT gate drive optocoupler

Model	Agilent HCPL-3180
Maximum switching speed	250 kHz
Minimum peak output current	2A
V_{cc} operating range	10V to 20V
Output voltage range	0V to V_{cc}